The University of Nottingham

Analysis of mechanical properties of woven textile composites as a function of textile geometry

by

Wout Ruijter, M.Sc.

Thesis submitted to the University of Nottingham

for the degree of Doctor of Philosophy

August 2008

Abstract

The topic of this thesis is mesoscale mechanics analysis of textile composites. The need for such analysis originates from the need to accurately predict structural performance of textile composite structures, which is known to vary as a function of textile geometry parameters.

Because of textile composites' suitability for use in large deformation forming methods, modelling of yarn geometries and their deformation mechanisms have seen much developments in recent years, in particular, the development of dedicated CAD modelling tools like TexGen.

The work in this thesis was started to devise automatic mechanics modelling of textile composite geometries, which was achieved by avoiding the generation of a mesh that follows yarn boundaries and instead assigns properties to integration points using textile querying implemented in TexGen.

The conceptual advantage is that in such a method any additional effects (like prestress, initial damage or voids) can be added without adding geometric complexity. The effect of spatial averaging on the convergence of relevant outputs is analysed and a case study on a simple plain weave textile is presented.

Good correlation of experimental and modelled strength was found and parametric studies on the textile geometry show that the range of strengths found in tests could be explained by the effects of geometric variables.

More importantly, a practical automatic link between TexGen and FE analysis is implemented and demonstrated to work.

Acknowledgements

The author wishes to thank his supervisors, Professor Andrew Long, Dr. Arthur Jones and Dr. Jon Crookston for their support during the course of this work. In particular the decision to release TexGen under the GNU General Public License was a decision that I continue to appreciate, and hopefully one that will allow us to cooperate freely in the future.

The Engineering and Physical Sciences Research Council is gratefully acknowledged for financially supporting this work.

I thank Geoff Tomlinson, Paul Johns and Roger Smith for helping me out in the making of tensile and microscopy specimens.

Much thanks is due to my colleagues in the ITRC office for making it such a great place to work, among others Jin, Sophie, Dhiren, Lee, Tom, Ben, Kevin, Paul, Richard and Andreas.

Working with Martin Sherburn on programming issues (or rather, seeing Martin work on programming issues) has been a joy, and his TexGen v3 has been essential to this work.

Finally, I want to thank my friends for their support in writing times, in particular Pete, Richard, Marlon and Jovita, and of course Merijn, Kees and Wil.

Contents

Nomenclature

$\mathbf{b}$	Body force
$\mathbf{C}$	Material stiffness matrix
$\mathbf{u}$	Displacement vector
$V_{f,dr}$	Relative dropoff of the in-yarn volume fraction towards the side of the yarn
$d\delta v$	Derivative of Lagrange shape function
ϵ	Error measure
f_f	Limiting height of yarn near model bounds (flattening of yarn)
$\mathbf{F}$	Force vector
ν_{ij}	Composite ij Poisson's ratio
δv	Shape function
γ	Shear deformation
τ	Shear stress
γ_x	Relative phase shift in $x-$direction between 2 layers of textile
γ_y	Relative phase shift in $y-$direction between 2 layers of textile
$\mathbf{K}$	Stiffness matrix
ε	Strain
σ	Stress
$\mathbf{t}$	Traction
V_f	Fibre volume fraction, percentage of composite volume taken up by fibres

V_m Matrix volume fraction, percentage of composite volume taken up by matrix material

V_y Yarn volume fraction, i.e. the fraction of a textile RVE that is taken up by the yarn domain

$V_{y,f}$ Intra-yarn fibre volume fraction, percentage of impregnated yarn volume taken up by fibres

E_m Young's modulus of the matrix material

E_{ii} Composite Young's modulus in the $ii-$direction

G_{ij} Composite shear modulus in the $ij-$plane

$S_{11,Cd}$ Delamination strength of fibre reinforced UD composite

$S_{11,Cf}$ Strength of fibre reinforced UD composite, based on fiber microbuckling

$S_{11,Cr}$ Strength of fibre reinforced UD composite, in compression loading, based on rule of mixtures

$S_{11,T}$ Strength of fibre reinforced UD composite, in tension loading

$S_{22,C}$ Transverse strength of fibre reinforced UD composite in compression

$S_{22,T}$ Transverse strength of fibre reinforced UD composite in tension

$S_{f,T}$ Strength of fibre in tension loading

AMR Adaptive mesh refinement

TexGen Geometric textile modelling software, based on the work of Francois Robitaille, version 2 and 3 are written by Martin Sherburn at the University of Nottingham. Version 3 is licensed under the GPL

API Application Programming Interface

BEM Boundary Element Method

DOF Degree Of Freedom, in displacement based

FEM Finite Element Method

fibre_area Sum of the cross section area of the filaments in a yarn

FMM Fast Multipole Method, a clustering method used to improve scaling of BEM simulations.

height Height of the unit cell

hgap Horizontal gap between yarns within a layer of textile

NCF Non-crimp fabric

Petsc Portable, Extensible Toolkit for Scientific Computation

RVE Representative Volume Element

vgap Vertical gap between yarns within a layer of textile

Chapter 1

Introduction

This thesis is concerned with the analysis of mechanical properties of textile composites. Textile composites have been used as structural materials for several decades, and have seen a rapid increase in use in the last 10 years.

Composites in general come in various classes, differing by the type of reinforcement and binding material (matrix). Reinforcement types are continuous fibres, chopped fibres or other particles of various materials (common fibre materials are carbon, glass or aramid), matrix types can be plastics, metals or ceramics. Textile composites are a subclass of continuous fibre composites, where fibres come in bundles and are woven, braided or stitched together.

Traditionally, composites were based on unidirectional material. Mechanically (at least for fibre direction loading) this is the best way to use such materials as it fully exploits the anisotropic properties. However, the preimpregnated material (pre-preg) is very fragile, and therefore hard to process correctly. Parts made out of unidirectional composite generally involve a lot of manual labour which can make them costly and slow to manufacture.

Textile composites represent a large improvement in manufacturability and multi-directional strength which is obtained at a (small) reduction in single-direction stiffness and strength properties. In addition, textile composites generally fail in a more gradual manner (and absorb more energy during failure) than laminated UD composites. Because of this, textile composites are often used in the following applications:

- Crash structures
- Top layer as impact protection for an underlying UD structure
- Doubly curved parts

- Resin infused parts

Examples of such components were traditionally found in aerospace and defence industries, but are currently also common in automotive, sports equipment and wind energy.

Since textiles, unlike unidirectional plies of fibres, do not disintegrate when stretched, draped or infused with resin, they are used in manufacturing processes that involve high deformation (diaphragm forming, rubber stamping) or in resin infusion moulding.

Failure behaviour in composites is expressed in terms of failure modes or failure mechanisms. These terms indicate what happens inside the material when the macroscopic material gets overloaded and begins to break. Because textile composites have intricate internal geometry, many things can happen internally once a composite is damaged. For instance: damage can progress along a yarn; a crack can go through the resin material and might be stopped by a yarn; fibres can pull out or break; and yarns can split along their length. Generally, a combination of these phenomena occurs.

Engineering structures are generally designed to withstand (or transfer) loading and are optimised to do so with a minimal amount of material. Such optimisation puts much emphasis on accurate knowledge of material properties as well as measures of property variation based on the natural variation of manufacturing and environment related parameters. In current design practice this is true to such an extent that variability can be considered as a material property in its own right since it influences safety factors and therefore design weight and cost.

Because of this, the first reason for modelling composite mechanics at the meso-scale (i.e. the scale of fibre bundles of yarns) is to find out how strongly the material properties are influenced by internal variables (yarn shape, inter-yarn spacing, filament content, filament spread etc.).

Another reason for modelling these materials in detail is that material properties are input to FEA tools which require full sets of strength and stiffness data. Such datasets can not be practically obtained using mechanical testing due to the following reasons:

- For some terms no practical testing methods are available, for example: through thickness tensile strength
- When testing a piece of material longitudinally until it fails, the *same piece* of material can not also be tested transversely
- Some tests are dominated by clamp/edge conditions
- Tests cannot be linked to geometric measurements of the *same piece* of material because it cannot be both a microscopy and a tensile specimen

In summary, modelling is used to understand composite properties and their variation as a function of manufacturing and constituent parameters. This knowledge can then be used to optimise the manufacturing process or increase confidence in designs made with the material.

The analysis of textile composites is commonly put as a multiscale problem, which (since the advent of nano fillers) consists of four different length scales. These length scales are referred to as macro (component), meso (textile), micro (fibre) and nano (filler), where the current thesis is concerned with effects on the meso scale. However, particular attention in the methodology is paid to the cases where there is no scale separation[1], since such cases represent particular challenges in the design of textile composite structures (bolt and rivet connections, bondlines etc).

The thesis explores a particular combination of analysis methods that allows fully automated analysis of textile composites which is robust to varying levels of complexity in the textile. The composite modeller uses the TexGen geometric modelling package, basic micromechanics analysis to analyse yarn properties and an empirical damage model. The key component is the use of Adaptive Mesh Refinement to arrive at computationally efficient meshes for the composite structure. This circumvents the use of conformal mesh generators which reduce robustness of the modelling strategy.

The thesis is built up as follows:

- Literature on textile composite analysis is reviewed in Chapter 2
- The building blocks of the presented analysis method are described in Chapter 3.
- Numerical and analytical behaviour of the method are presented in Chapter 4. This chapter focuses on convergence behaviour of the devised methods for representative problems. It also analyses an example textile using both conformal (tetrahedral) and AMR meshes.
- Micrographs of textile composite material are used as a basis for a parametric textile model which is then analysed and compared to mechanical testing of specimens in Chapter 5. Several single variable parametric studies are included, as well as some relevant combinations.
- In Chapter 6 the pitfalls and limitations of the presented methods are discussed. Conclusions are drawn regarding the use of it, and recommendations regarding future use and development of the methods are given.

[1] Geometric or strain field features are not small compared to the length of the repeating textile structure.

Chapter 2

Literature review

In this chapter current and historical literature on the analysis of textile composites is discussed with the aims of obtaining a broad view of the field as well as outlining the gaps in literature that serve as the research area of this thesis.

This thesis was initiated with the particular goal of eliminating the problem of mesh generation for mesoscale analysis of composites. Therefore the focus of this literature review is on various representations of the mesoscale geometry and mechanics problems of textile composites.

Other aspects, which are either used for demonstrating and validating the method (damage modelling, experimental methods) or describe the context in which this work fits (multi- and macroscale modelling of composite structures) are referenced but not discussed in detail.

It is noted here that the work in this thesis builds on the work done by Jon Crookston which also relates to the interaction of geometric modelling of textile reinforcement and solution of the mechanics problem. His thesis [1] and a subsequent review paper [2] contain a more extensive literature review on the state of the art with regards to macroscale damage modelling and geometric modelling in the context of forming processes.

The current work can be seen as a generalisation of the Grid Average method proposed in the same work.

This chapter will proceed with a brief outline of the history of analysis methods, linking the development of modelling methods with advances in materials and manufacturing.

2.1 Background

Analysis techniques for composites have been a topic of research since the initiation of the theory of elasticity (which is covered by Timoshenko in [3]).

The earliest application of this theory for microscale composites was to analyse inclusions of one material in another and report stress concentration factors for such basic multiphase materials. At the macro-scale the anisotropic form of Hooke's Law allowed the analysis of anisotropic materials. These two capabilities of elasticity theory are the basis on which multiscale modelling of composites is founded. These methods were applicable to some extent to particle reinforced composites and single layers of fibre reinforced composites.

The advent of continuous fibre reinforced composites and their performance in weight critical structures caused a great surge in the development of modelling techniques for these materials. Micromechanics models were expanded from elastostatics on materials with cylindrical inclusions to include microbuckling and debonding of the fibre-matrix interface (a host of such methods were packaged in the ICAN program developed by NASA [4]).

Because these materials came in the form of preimpregnated layers of fibres that were stacked to form a composite product much accuracy was gained in describing the effects relating to interacting layers of fibres. Describing stiffness of multilayer laminates was done using the averaging technique that is now referred to as Classical Laminate Theory (CLT). This method is described extensively in [5] and still is the basis of many composite design methodologies as well as the formulation of some layered elements in commercially available finite element software packages [6–8].

However, the use of UD pre-preg based composites is still restricted to high-end applications (e.g. aerospace, defence, Formula 1), mainly because of the labour cost associated to these materials. For applications where higher volume and lower cost are important (automotive, naval, wind energy) other options are used which have greater ease of handling (draping) and allow the use of resin infusion processes. Among these materials are textile composites, stitched unidirectional (or non-crimp) fabrics but also chopped or random fibre composites.

The focus in the present work is on woven or braided textile composites, non-crimp fabrics are not explicitly covered here but could be analysed in the same manner, while chopped or random fibre composites are not addressed.

The advantages of textile composites are not just apparent in handling of the material but also in increased delamination and crack propagation resistance, something that

is loosely attributed to "crack stopping mechanisms" that are added to the material through giving it a non-trivial meso-structure.

It is this meso-structure that is the focus of the current work. The modelling difficulty that comes with such a meso-structure is due to the following attributes:

- Yarn geometries are geometrically intricate
- Yarns have internal fibre distributions which are not necessarily trivial
- Length scales are not necessarily separable[1]

The level of accuracy needed in the analysis of each of the length scales in order to obtain an accurate structural solution is an open question, the answer to which will be different for different materials and different analyses (for example, in permeability analysis the yarn's internal geometry can be neglected whereas it is of key importance in elastostatics). A schematic figure showing different levels of intricacy in modelling a plain woven textile is given in Figure 2.1, reprinted from [9].

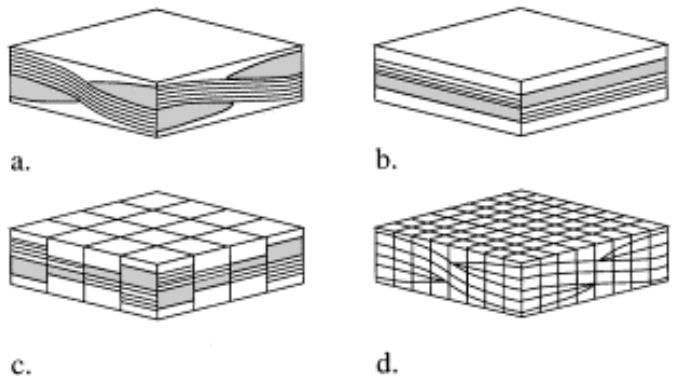

Figure 2.1: Stiffness analysis of orthogonal WF laminates (a) Repeating element of a plain WF lamina. (b) Analytical approximation using CLT. (c) Micromechanics approach (d) finite element analysis. Figure taken from Hofstee and Van Keulen [9]

2.2 Textile geometry modelling

Geometric descriptions of textiles were initially based on analytical functions or combinations of arcs and straight lines [10]. This line of work has been more extensively

[1] One of the basic assumptions of "classical" multiscale analysis is that the representative volume element (RVE) of the lower scale is sufficiently small that the gradient of the higher scale solution (in the case of elastostatics the gradient of the displacement field) can be assumed constant

referenced in Sherburn's work [11] on textile geometry modelling. In the 40's to 60's the formulations have become more sophisticated, both in the modelling of the yarn path, taking into account bending of yarns, and in modelling of the the cross section, moving from circular to elliptical and lenticular cross sections.

Some of the more advanced analytical models known to date are the models presented by Hofstee and Van Keulen [12–14]. These models have variable cross section and allow deformation mechanisms of yarn paths like twisting and compaction as shown in Figure 2.2. These geometric descriptions were used in the analysis of thermoplastic based composites, the models were geometrically advanced but used to obtain input for analytical models rather than for 3D mesh generation.

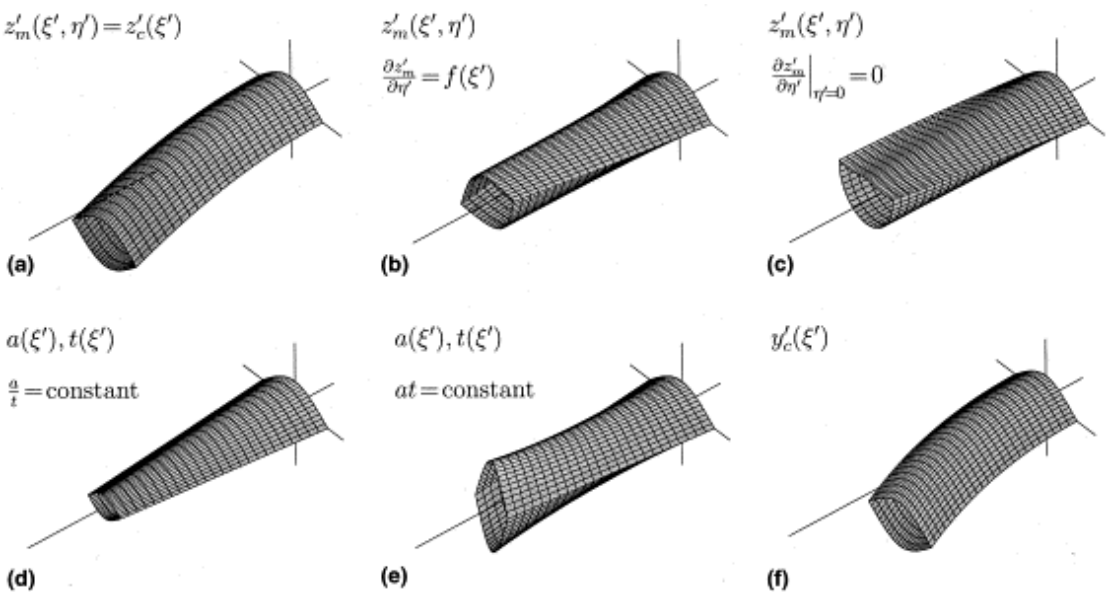

(a) Fibre bundle configurations; (a) undulated (out-of-plane), (b) twisted, (c) with curved horizontal midplane, (d) compacted, (e) pinched, (f) undulated (in-plane).

Figure 2.2: Fibre bundle deformation modes as modelled in the work of Hofstee and Van Keulen (Figure reproduced from [14]).

There are some commercial programs that allow geometric textile modelling, notably TechText CAD [15, 16] and Scotweave [17]. These packages contain comprehensive libraries of textiles, but they are not aimed at 3D mesh generation or any other than geometric analysis (digital prototyping) of a textile.

Mesoscale analysis requires the generation of a 3D mesh from a textile geometric model.

Whitcomb and coworkers were among the initiators of geometry descriptions designed for use with numerical analysis (see [18–20]). Whitcomb used basic domains which had known and scalable mesh patterns; a sequence of such patterns could be used to obtain

meshes for various (2D) weave patterns, resulting in FE models that are topologically similar to the models presented in Figure 2.1(d).

Recent textile geometry formulations have moved away from a mesh basis towards a CAD based formulation. Improvements include:

1. Interference correction of yarns to allow generation of more tightly packed and more realistic yarn patterns.
2. Formulation of yarn cross sections that allow consistent yarns (constant fibre area), regardless of yarn shape and surface.
3. Flexible implementation of textiles, allowing fully variable stitching patterns and yarn cross sections.

Several textile modelling suites have been developed by different research groups, the two most prominent and general purpose implementations known to the author at the time of writing are WiseTex (Lomov et al, KU Leuven, see [21]) and TexGen (Long et al, University of Nottingham, see [22]).

2.2.1 Validation and geometry measurements

There are a number of methods for obtaining 2D and 3D images of (slices of) a textile composite. The methods that are being reviewed here are optical microscopy and micro CT scanning.

Microscopy

Microscopy is commonly used to obtain cross section images of a cured composite material. It has the advantage (over examining the dry textile) that any geometry changes caused by the forming of the fabric or resin addition are present and the actual internal geometry of the material is obtained. Microscopy is used by Potluri and coworkers [23] for plain woven composites (see Figure 2.3), with focus on the impact of forming on the geometry (shear, compression and tension on dry textile). This work falls in a programme of work covering shear deformation of textiles as well (see [24–27]). In [28] microscopy is used to measure the internal geometry of non-crimp fabrics .

μCT scanning

μCT scanning is a 3D method that has gained interest recently and can be used to obtain geometric data for dry fabrics with medium to high accuracy, a comparison of

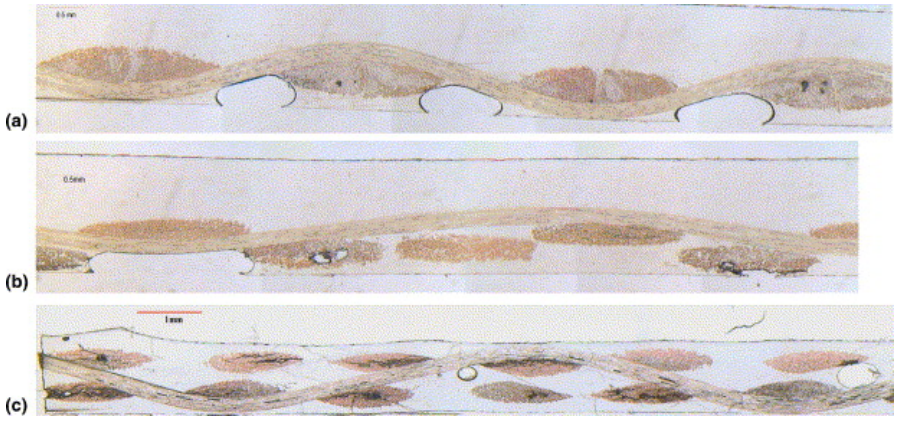

Figure 2.3: Cross section micrographs from Potluri et al [23], showing a plain weave structure in Figure **a**, a five-harness satin weave in Figure **b** and a 3D weave in **c**.

this method to microscopy (analysing 3D warp-interlaced fabrics) is given by Desplentere et al [29]. The method has also been used in conjunction with the TexGen modeller by Sherburn [11], an example of the images obtained is given in Figure 2.4.

2.3 Mesoscale mechanics of textile composites

2.3.1 Mesh generation

Textile composites mesomechanics modelling is a field in which the geometrical modelling and mechanics solution are very much connected. The reason for this is the fact that yarns alternate between being in- and out of contact with each other, which results in a geometric problem that is dominated by geometric regions with high aspect ratios.

It is likely that the shape of these local features plays a role in the stress intensity factors they give rise to, which in turn dominates the stress level at which the onset of damage occurs. At the same time, the presence of such highly localised and geometrically intricate features poses a problem in numerical modelling, in particular in the generation of meshes that allow capture of the local physics.

Broadly, this problem is addressed in the following "schools of thought":

- The inter-yarn domains are neglected and the yarn domains are assumed to be fully connected. An example of a mesh resulting from this method is shown in Figure 2.1. This method is popular since it allows representation of relatively complex textiles with relatively few elements. It is also fully robust, in fact, textile

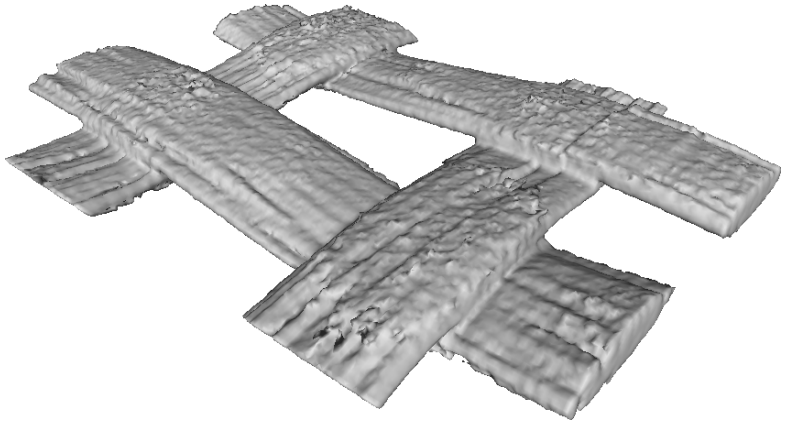

(a) Chomarat 150TB μCT reconstruction

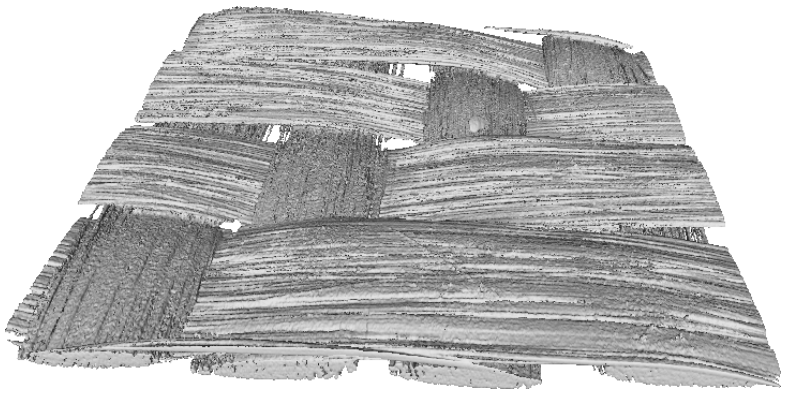

(b) Chomarat 800S4-F1 μCT reconstruction

Figure 2.4: μCT images reproduced from Sherburn's thesis [11].

models can be made by coupling standardized meshes, without having to consider geometry modelling.

The method was proposed by Whitcomb and coworkers who have used it to implement a global-local substructuring method in [19, 20] which has been expanded to a full multiscale mechanics model (see [18], the models on the different scales are shown in Figure 2.5). The method was used in combination with a stiffness degradation method based on the model proposed by Blackketter [30].

Potluri et al used the method in a series of studies with particular focus on textiles which have undergone deformation in forming or handling, in [31] on woven textile composites and [26] on braided preform based composite tubes.

Other uses with focus on forming are documented by Hofstee et al in [12] which focuses on the geometry of sheared thermoplastic plain woven composites as a preparation for analytical models as described in [9].

- Modification of the inter-yarn domains such that they can be dealt with by mesh-

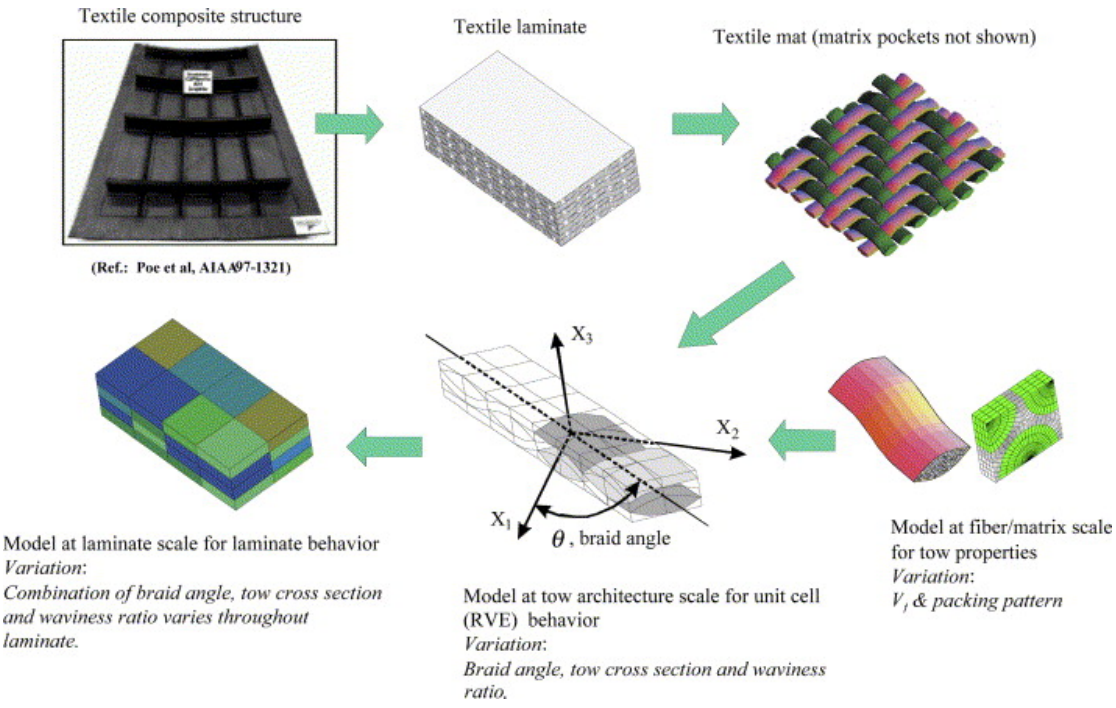

Figure 2.5: The 3D modelling strategy as used by Tang and Whitcomb et al. for the analysis of braided composites (Figure reproduced from [18]).

generators; this can be seen in the work of Quek and Waas et al [32–36] where it is applied to 2D braided composites.

This method is also used in the work of Zako et al [37] on damage analysis of woven textile composites, which provides a qualitative comparison of the damage predicted using the FE model and the damage seen in the tensile experiment (see Figure 2.6). This is an example of a case where the problem does not really exist because of the low V_f in the textile at hand.

A more general formulation for this strategy is found in the work by Lomov, Verpoest and coworkers, where it fits in a fully general and comprehensive modelling framework for textile composites. It is this generality that dictates the use of a dedicated CAD modeller (WiseTex), which is demonstrated to work well for woven fabrics [38], multiply stitched fabrics [39] and braided fabrics [40]. The methods have been extensively validated, most recently using optical strain measurements [41]. Strategic papers are written laying out the geometric modelling method [42] as well as the embedding of this method into mesoscale mechanics and computational homogenisation [43]. Of particular interest, in light of the current thesis, is the work on use of continuum damage mechanics to represent physically realistic crack propagation in brittle materials. This was initiated based on the finding that

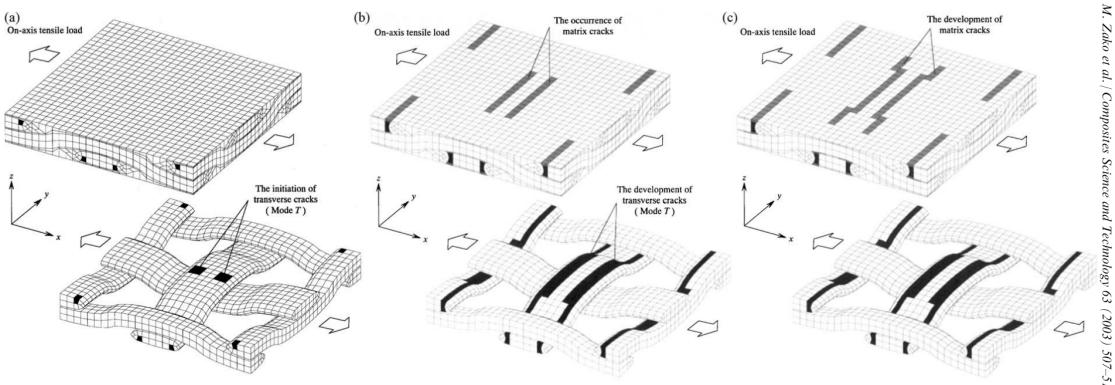

M. Zako et al. / Composites Science and Technology 63 (2003) 507–516

Fig. 5. Damage development in plain woven fabric composite under on-axis tensile load (a) $\varepsilon = 1.01\%$, (b) $\varepsilon = 1.14\%$, (c) $\varepsilon = 2.01\%$.

Figure 2.6: Damage predictions made by Zako et al in [37]. This fabric has a fibre volume fraction of 22% meaning that a realistic V_f can be modelled without any special treatment to the yarn shape to ensure the geometry can be meshed.

CDM damage regions tend to propagate across yarns [44] whereas experimental evidence shows that damage tends to propagate along yarns in the form of a split or mesoscale crack (a finding reported by Lomov and Ivanov in [45]). In [46] this problem is isolated and although an improvement was made to the CDM algorithm, no satisfactory qualitative result was reached. It was suggested that CDM is not adequate for the modelling of mesoscale cracks.

- Avoid conformal mesh generation and use structured meshes where elements have averaged properties. Mapping of the elastic properties based on geometry is used to represent the textile architecture. In terms of methodology this method is similar to methods in medical science where bone marrow is scanned using Micro CT imaging and the resulting 3D voxels are used to contruct a mesh for computational analysis [47]. In the work of Crookston [1] this method is used focussing on 2D weaves, where the interface between traversing yarns was modelled using layered solid elements. The work of Gowayed and Yi [48] focusses on some of the numerical issues arising from having mixed material elements containing strongly anisotropic materials.

  The current work is heavily based on the work by Kim and Swan [49, 50] which is more extensively reviewed in the context of adaptive mesh refinement in section 2.3.2.

- Generation of conformal meshes for the separate domains where the yarn is subsequently tied or embedded into the matrix mesh using constraint equations. The binary model is one such method [51], where the yarns are implemented as line

elements. Approaches where the yarns are approached as solid elements have also been reported (for example by Zako et al [37]). Iarve et al [52] have used this method and have found good correlation of predicted local strain predictions with experiments.

In addition, there are a number of more far-reaching idealisations that neglect the effect of yarn cross section shape altogether and focus on particular aspects of the textile structure.

- The Mosaic model by Bogdanovich et al [53] which focuses (within a schematic representation of the textile) on accurate representation of the yarn interface stresses using Bernstein polynomial based finite elements.
- The binary model (see the work of Cox et al [51, 54]) wherein the yarns are represented by line elements rather than separate solids.
- The method of inclusions was used by Huysmans [55] in conjunction with WiseTex software.

These methods were devised especially to deal efficiently with the geometric problem posed by 3D weaves, in particular, the weaving architecture and possible variations in the weaving pattern.

All these models, and in particular the binary model can deal efficiently with textile domains much larger than the size of a typical repetitive volume element (RVE) or unit cell, something which is essential in investigating the effects of local fibre architecture distortions (no periodicity can be assumed). Through being able to model these larger domains, it overlaps in its capability with macroscale modelling.

However, in generating the schematic representations of the textile weave patterns local parametric information *within* a weave pattern is lost. In particular, yarn shape, inter-yarn domain shape, yarn path shape and in-yarn V_f distribution and their local effects are neglected.

2.3.2 Adaptive mesh refinement

The subject of adaptive mesh refinement (AMR) originates from the desire to obtain the best representation of highest possible solution accuracy for a given CPU effort. The reasoning behind it can be formulated loosely as “concentrate computational resolution in areas where it contributes most to the solution accuracy”.

In Figure 2.7 an example is given of a typical adaptively refined mesh. In this case the 2D Laplace equation is solved on an L-shaped cavity with Dirichlet boundary conditions.

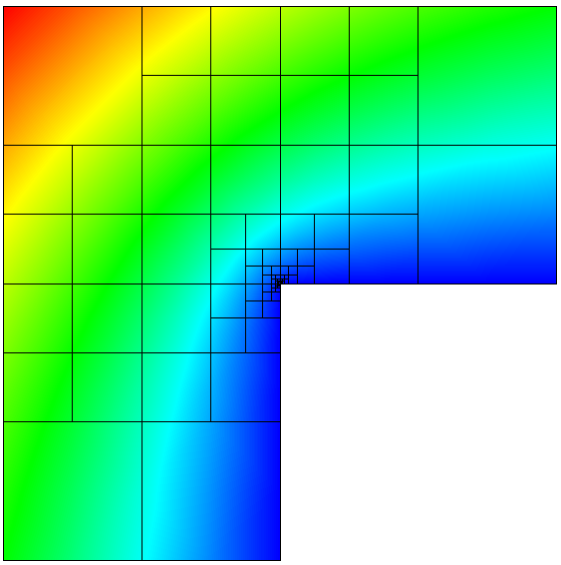

Figure 2.7: Solution of the Laplace equation in an L-shaped cavity using AMR. Figure obtained from example problems distributed with the LibMesh Finite Element library [56].

Great increases in accuracy were obtained in fields like fluid mechanics and astrophysics.

To date, there are very few known applications of AMR in the analysis of textile composite materials. The only known study was done by Kim and Swan [49]. This study is quite elaborate in the analysis of the effects of the use of different refinement criteria, as well as in ways to deal with (or avoid) the problem of "hanging nodes" (see [50]).

The rate of convergence between different refinement strategies (uniform, material boundary based and error estimation based) were compared and the following conclusions were drawn:

- Voxel/pixel based meshing has a (slightly) higher associated CPU cost than full tetrahedral conformal meshing for the textile under consideration.
- The method can be used in a fully automatic manner.
- A constrained-selective mesh refinement scheme converges more rapidly than uniform refinement. The constraint refers to the mismatch in refinement level between two adjacent elements.
- Adaptive mesh refinement schemes based on error estimators were tried and found to converge only when starting from a sufficient refinement level.

- There is complexity related to dealing with periodicity of RVEs that have undergone refinement.
- The solution can be improved when using the refined mesh as a basis for tetrahedral mesh generation [50].

The method was presented in the context of analysing a plain woven textile geometry with an analytical yarn path description and elliptical yarn cross section. In addition, material properties were geometrically averaged and subsequently attributed to the entire voxel in a symmetric manner.

Although the study was detailed on the numerical aspects it was based on highly idealised textile structures.

2.3.3 Damage modelling in composites

Macroscale damage modelling

Modelling of damage in composites is a topic that has been approached from many angles in literature. The approaches to damage modelling which are used in the composites manufacturing industry are those which can be directly related to test data on the macroscale.

The most commonly used way of predicting failure in laminate composites is the Tsai-Wu criterion [57], which can relate a stress state to a failure envelope and as such gives a measure of how far the local material is removed from being damaged. This is the widest available damage measure available to composites engineers and it is available in a multitude of commercial finite element analysis packages. For laminates consisting of unidirectional plies, the body of experimental data available is large and a comprehensive comparative study of (macroscale) failure models for multiaxial in-plane loading has been executed, this study is known as the World Wide Failure Exercise (WWFE). The work of the WWFE has been carried out in three stages (prediction, experiments and comparisons) and was reported between 1998 and 2004 resulting in a set of recommendations to designers and researchers in the field [58].

Key models that were found to work well were the Puck [59, 60] and LaRC [61] criteria, which can be seen as expansions of the Tsai-Wu criterion, particularly the inclusion of models to account for microscale compressive failure modes like microbuckling.

These criteria apply to UD laminates and stitched fabrics, but are reliant on the accuracy of the multidirectional strength data available for the laminate at hand.

Macroscale laminate models are applicable to the current work because the yarn material in a mesoscale RVE can be seen as a unidirectional composite in its own right.

Mesoscale damage modelling

For common high-performance woven composites damage is accumulated throughout the composite starting with cracking of the transverse yarns along the fibres, where the fibres are acting as a stress raiser rather than a reinforcement. Subsequently a host of mechanisms can manifest themselves, depending on the textile structure and loading, as well as the characteristics of the matrix material, in particular, whether it acts as a brittle material or has plastic properties.

In solid mechanics of concrete, and also of brittle metals, failure of a solid is well represented by analysis of crack propagation, assuming that damage exists on the same length scale as the modelled problem. In composite materials (as in plastics) this is not generally the case, and even in the case that there is a mesoscale crack, it is likely to coexist with a host of other damage, present on a smaller length scale.

Because it is numerically prohibitive to devise a scheme in which the smaller scale fracture mechanics problem would have to be solved, damage mechanics in composites generally starts out with the assumptions of continuum damage mechanics (CDM). This approach records and analyses the effects of damage by using degraded properties in regions where the material has been found to be damaged.

One of the earliest applications of CDM to composite materials was documented by Blackketter et al and used to analyse plain woven textiles [30]. In that work an orthotropic failure criterion was used in conjunction with brittle knockdown of the stiffness properties to a marginal residual value (large enough to allow the FE analysis to progress).

Similar methods were used by a number of people for different purposes: Takeda et al used a maximum strain criterion and degradation for prediction of progressive failure in woven textile composites at cryogenic temperatures [62]. Whitcomb et al used the method to investigate the effects of fibre architecture and stacking in woven composites [19, 63].

Recent use of CDM is reported in [46] where the problem of transverse tow damage patterns developing non-parallel to the yarns is addressed.

2.3.4 Geometric nonlinearity

The treatment of geometric nonlinearity in the analysis of textile composites is particularly important when modelling thermoplastics or any situation relating to the forming processes of composites. This falls outside of the scope of this thesis where the glass-polyester laminates typically fail at a strain of 2.5% in on-axis experiments and up to 12% in bias direction experiments. Carbon based composites with non-thermoplastic matrix systems fail at lower strains. The effects of geometric nonlinearity in the range of strains displayed in on-axis experiments would be small.

For the state of the art on thermoplastic forming modelling dealing specifically with nonlinear analysis of highly anisotropic materials the reader is referred to the work of Akkerman and ten Thije [64].

2.4 Multiscale modelling

The field of computational homogenisation is concerned with solving problems which are non-trivial on multiple scales.

There are a number of studies reporting multi-scale modelling of particulate composites using AMR on the microscale, the reader is referred to the work of Zohdi et al [65]. On the multiscale modelling of granular metals the work of Geers et al can be examined, in particular for dealing with second order homogenisation schemes [66] (i.e. homogenisation extended to the case where the macromaterial is in bending).

These studies have the common theme that they do not have to deal explicitly with the presence of a meso-structure. All of these methods are based on automatic modelling of the microscale, which in Zohdi's case was achieved by using AMR .

A general approach to the analysis of textile composites in a full multiscale manner has been taken in the work by Fish et al [67],[68] and [69]. Fish outlines the formulation of the multiscale model and solves the case where all levels are represented by FE models. FE models (especially on the meso-scale) are simplified to obtain the robustness needed in an automated multiscale analysis. The results are presented regarding stiffness and onset of damage which are validated using component testing.

More recently, Tang and Whitcomb have used a similar multiscale method to investigate progressive failure of composites based on 2x2 braided mats. As is discussed in section 2.3.1 a fully robust method for analysis of mesoscale models is obtained through assuming lenticular yarn shapes and full connectivity between connecting yarns (see Figure 2.5).

2.5 Numerical aspects

Because finite element analysis of textile composites is numerically involved and comparisons between different models or strategies are attempted that often involve different implementations altogether, it is appropriate to review briefly the state of FE analysis software that is available. Although this review can by no means be exhaustive, it is intended to help in reading the implementation sections of this thesis.

The development of finite element analysis software was initially driven in a manner analogous to the development of composite materials, originating from the low-volume high-performance oriented industries. From the sixties onwards (since the invention of Fortran and microprocessors) the implementation of numerical algorithms was greatly accelerated. Early finite element programs were developed to facilitate the design of aircraft and automotive structures (Nastran, see [7]), nuclear facilities (Ansys, see [6]) and civil structures (Abaqus, see [8]). These were the main commercial analysis codes and have since converged in the sense that all are now general purpose codes with extensive multiphysics capabilities as well as integrated graphical pre- and postprocessing and more or less advanced methods for mesh generation.

Since the advent of object oriented programming languages the modular design of software has become much easier, reducing the development cost of new software. This has resulted in a host of new FE packages, often aimed to scale well in distributed memory environments. Since the "traditional" finite element packages have been developed in times where the top-spec computers were shared-memory machines it is on this aspect that new codes can surpass them in performance on new clustered hardware. This is generally done by building upon openly available general software components for aspects of FE analysis such as graph partitioning (ParMETIS, see [70]), processor communication (MPICH, see [71]) and sparse systems solvers (Petsc, see [72]). Examples of extensive and general finite element libraries which are built on top of these components are DealII [73] and LibMesh [56].

Work closely related to the topic of the current thesis is the work of Adams who used a scalable multigrid solver to solve microscale voxel models of bone marrow comprised of $\approx 5e8$DOF on several thousands of processors.

2.6 Conclusions

The literature on the topic of composite mesoscale mechanics modelling has been reviewed. Focus was placed on various approaches concerning the representation of yarn

geometry inside mechanics models. It was found that there are general and robust methods of analysis that can represent complex textile reinforcement over large (sub-component) geometries. Such methods operate on schematised representations of the textile ignoring the effects of local yarn geometric details.

On the other hand there are detailed modelling approaches, the most modern of which are based on textile-oriented CAD modelling (WiseTex and TexGen). These models deal with the textile geometry directly through use of a mesh generator, which sometimes requires the adjustment of yarn geometry to achieve a mesheable geometry description. The fact that textile geometries are not by definition mesheable is a problem which can be dealt with in this manner, but the introduction of yarn-shape modifications for the benefit of mesh algorithms is undesirable in the case where the effect of the yarn shape is the subject of investigation.

In addition, there are some fully robust methods available for arriving at numerical models for textile composites which don't require modification of the yarn shape, these models either use spatial averaging of material properties or domain superposition, both of which work on the premiss that the meshing problems of the full RVE domain and the yarn domains are easy to deal with compared to the matrix-only domain.

Methods based on material property averaging were reported to converge in terms of stiffness upon mesh refinement. Such mesh refinement can be done more efficiently using adaptive mesh refinement.

The combination of AMR and property averaging has not been used in conjunction with fully general (CAD based) textile geometry formulations, in particular, the variation of intra yarn fibre volume fraction has not been taken into account.

Of the cited studies on AMR and textile composites, none exploited the fact that AMR meshes are well suited for partitioning and solution on parallel computers, which is demonstrated in particular in fluid mechanics applications.

This thesis describes the implementation of a mesoscale finite element approach based on AMR and TexGen in order to demonstrate that a method is obtained that a) converges upon mesh refinement b) can deal with arbitrary textile geometry c) can operate automatically, making it suitable for extensive parametric analysis and as a tool in multiscale analysis d) allows dealing with property-affecting field variables (damage, orientation, local fibre volume fraction) in a unified manner.

The review also touched upon damage mechanics and a damage model is implemented in the current method, however, the damage model used in this thesis follows the a simple simplified orthotropic maximum stress criterion for the yarns and the Bauwens

[74] stress criterion is used to detect onset of damage in the neat resin regions.

The choices for damage models are based predominantly on simplicity, suitability for glassy polymers and the knowledge that only bias direction and axial tensile testing are among the validation cases in the current study (this avoids the need to use more complex failure criteria commonly used to predict compressive failure). In addition, the problems pertaining to the representation of mesoscale cracks using continuum damage mechanics methods are noted, but since a considerably less brittle matrix material is used in the current validation cases it is deemed outside of the scope of the current work. It is also noted that Kim and Swan [50] have suggested a hybrid approach where the voxel-meshes are used as a basis for meshing with tri-quadratic tetrahedrons and have shown that this increases the rate of convergence for their problems. This approach is not used here because the approach is not seen to have any conceptual benefit for the case where the inter-yarn region is very narrow. I.e. one would either end up with very large aspect ratio tetrahedrons or a similar number of elements that a free mesh generator would use to fill the space.

In general, the base method is used in this thesis, noted approaches for improvement could be:

- H-P refinement, as opposed to H-refinement as implemented currently
- The use of a functionally graded material (polynomial interpolation of the material properties) to describe the local material for mixed-material elements

Chapter 3

Methodology

In this chapter different aspects of the modelling strategy are explained in detail. It is appropriate at this stage to look at the proposal that started this PhD project. The project was aimed at tackling the meshing problem in textile composite analysis (as outlined in the literature review, section 2.3) by using the Boundary Element Method (BEM, for an introduction to the topic, see [75]) in order to represent the matrix domain. BEM would lift the (volume) meshing limitation because the solution of a BEM problem only requires a boundary discretisation of the domain.

The first year of the PhD work was spent evaluating a hybrid approach in which the matrix domain was defined using BEM and the yarns using FEM. Although this work is not formally reported (it was reported in [76]) there were a number of conclusions drawn that lead to the design of the current modelling strategy:

- BEM, when not using Fast Multipole Method[1] (FMM, see for example [77]), has prohibitively high CPU and memory demands.
- Coupling of BEM to FEM is feasible (see for example [78]), but very hard to optimize due to the differences in system matrices associated to the two methods (again, not assuming FMM), BEM results in dense system matrices and FEM in sparse or banded systems. This would be a drawback since having a standard matrix structure means that free solver software such as Petsc [72] can be used without further modification.
- The inclusion of an inhomogeneous continuum, such as a matrix domain containing local damage, is very complicated in BEM (the introduction of crack surfaces by

[1] FMM is a hierarchical clustering method analogous to octree in graphics rendering and multigrid in FEA, taking the influence from "far away" nodes into account in a bundled manner, rather than directly.

contrast is fairly straightforward, in effect, the boundaries of the crack don't differ conceptually from the domain boundaries).

It was decided that a BEM based solution would require too much mathematical and algorithm development to form a feasible strategy for solving the problem at hand, and an alternative route to solve the same problem was devised.

The use of adaptive mesh refinement was chosen as strategy since it was certain that it would result in a robust analysis method (as was shown by Kim and Swan [50]) which was a key requirement considering the scope of the parametric problem at hand. In addition the application of AMR to realistic textile models would be novel, in particular in attempting to analyse progressive failure. Besides that the following developments in analysis software and hardware influenced the decision to use AMR:

- The multi-scale problem being solved has an analogous hierarchic structure to an AMR grid. This suggests that AMR has the potential to bridge the scales without the use of an explicit coupling/homogenisation step.
- AMR grids are easy to partition (since they are hierarchical), making the resulting FE system easier to solve on distributed memory systems.
- Several high performance Finite Element software libraries are available which are specifically written to support AMR (in particular, LibMesh [56] and Deal II [73]).
- Internal state variables such as damage, fibre volume fraction, or yarn orientation can be dealt with independently from the element formulation (i.e. they can be attributed to nodes, elements, or gauss points), allowing modularity of the resulting code.

The analysis data flow in a mesomechanics analysis based on AMR is shown in Figure 3.1, where other essential components are a *geometric model*, a *micromechanics model* and a *damage model*.

The present chapter is structured as follows:

- Textile geometry modelling based on TexGen is introduced in section 3.1.
- Aspects of Finite Element modelling are described from section 3.2 onwards.
  - The element formulation used in FE analysis is given in section 3.2.
  - Micromechanics formulae used in micro-meso homogenisation are given in 3.2.2.

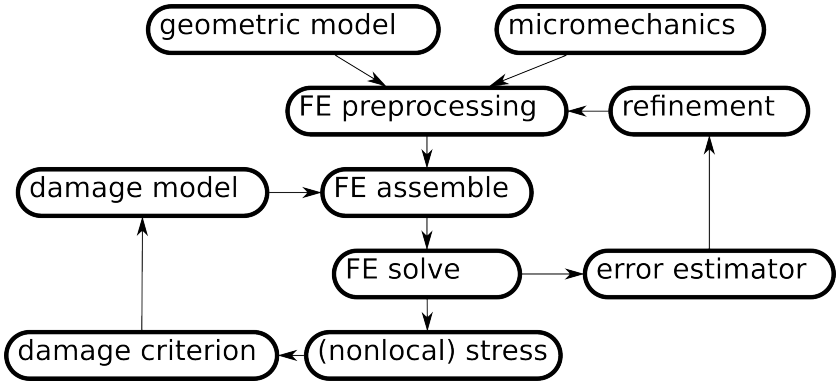

Figure 3.1: Connectivity of the different analysis modules in the program flow of an FE analysis using AMR and a continuum damage model, in this case preprocessing refers to the lookup of gauss point data in the textile structure.

  - The details of the damage model used to describe material behaviour post damage initiation is given in section 3.2.3.
  - The adaptive mesh refinement (AMR) scheme is described in section 3.2.4.
  - Various sets of boundary conditions used in the remainder of the thesis are presented in 3.2.5.

- Closed form micromechanics equations used to efficiently describe yarn mechanics are described in section 3.2.2.

- A parametric textile model is defined in section 3.3 which is used in the remainder of this thesis to provide a compact parametric description of a textile composite structure.

3.1 Geometric modelling of textile composites

3.1.1 TexGen

Geometric modelling of the textile is performed using the TexGen geometric modelling package. TexGen is a development effort of the composites group at the University of Nottingham that has been initiated by the textile compaction work of Francois Robitaille [79] and of which Martin Sherburn has been the main developer. TexGen forms the basis of applications in predictive modelling of resin infusion [80], heat transfer and textile mechanics , as well as textile composite mechanics [81]. Recently the package has been subject to a complete redesign and rewrite to improve it on the following key aspects:

- Modular design:
  By pursuing a modular design it allows for easier contribution of programmers with knowledge of only one specific aspect of textile modelling, as well as allowing compilation of only parts of the program (e.g. leaving out the renderer on platforms that don't have graphics). A schematic overview of the texgen design is given in Figure 3.2.

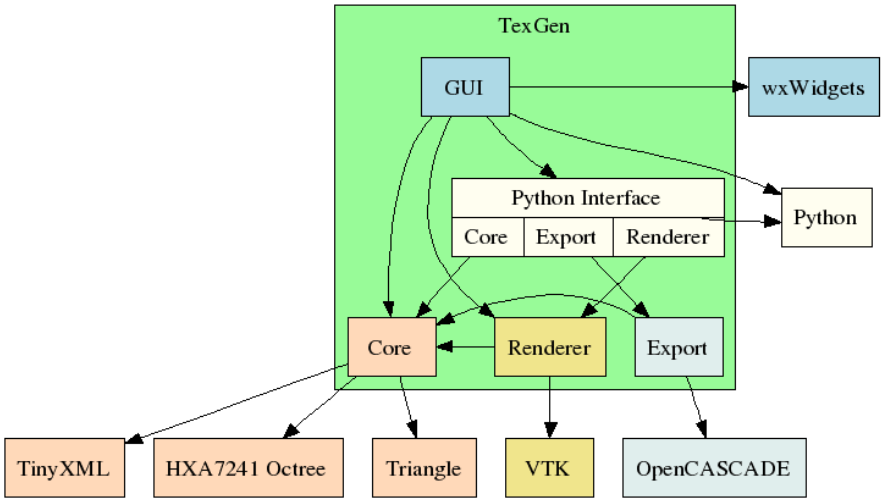

Figure 3.2: TexGen modules and their connection with external packages, reproduced from the online documentation for TexGen v3 [22].

- Platform independence:
  All dependencies are well maintained open source packages that are available on at least a variety of modern linux and windows operating systems, setup is made easy through the use of the cmake build system. The code itself is written in standard C++.

- Accessibility:
  The textile models are accessible through the graphical user interface, through python scripting and through the C++ API.
- Open source distribution:
  The code is released under the GNU General Public License [82].
- XML based file format:
  An xml format for textiles is defined that reflects the hierarchic structure in which textiles are defined within TexGen . Use of an xml format makes it easy to parse TexGen textile files in other applications and allows extension.

Many of the algorithms that are used to arrive at a realistically compacted textile geometry are based on Sherburn's work on fibre compaction, which is most extensively documented in his thesis [11].

The modular design of TexGen and the existence of a scripting interface are key to the current work, source contribution to the TexGen modelling package in the context of this thesis has been the ability to allow variable fibre density across yarn cross sections and the ability to have consistent fibre area along yarns.

In addition a number of benchmark tests and parametric (scripted) textile models have been written (see section 3.3).

3.1.2 Yarn path representation

Within TexGen the yarn path is represented by a b-spline with an arbitrary number of control points. The undulation pattern of the textile acts as the basis, but a number of points can be added in between so that a path of arbitrary complexity can be described. Figure 3.3 shows the control points displayed in a TexGen model of a plain weave.

3.1.3 Yarn cross section representation

The yarn cross section is represented in a TexGen model as a 2D polyline. This polyline can be obtained from a base yarn shape (elliptical or lenticular, see Figure 3.4(a) 3.4(b)), after which it can be modified (e.g. by a compaction algorithm). The polyline representing the yarn cross section can consist of an arbitrary number of points (see Figure 3.4(d)), and an arbitrary number of cross sections can be defined along the yarn at parametric locations along the yarn path.

The main aspect of the yarn cross section representation is the kind of deformation it

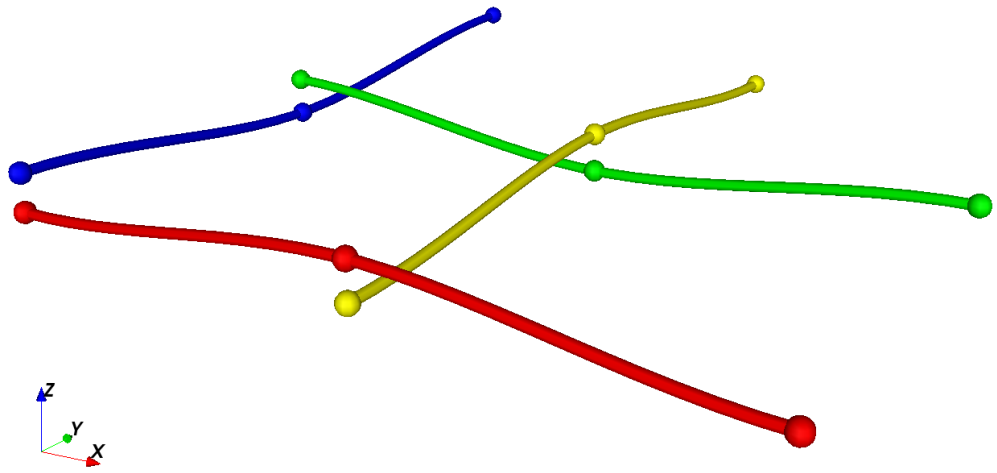

Figure 3.3: TexGen model showing the control points defining the yarn path splines for a plain weave textile structure

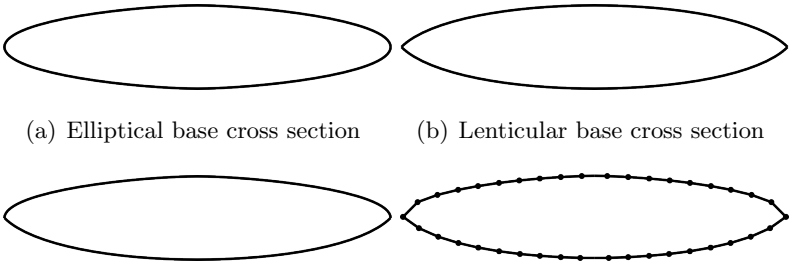

(a) Elliptical base cross section

(b) Lenticular base cross section

(c) Combined elliptical (top) and lenticular (bottom) cross section

(d) Polyline representation of the yarn section shown in Figure 3.4(c)

Figure 3.4: Yarn geometries

allows. There are a number of mechanisms that trigger cross section deformation in real life, and there are a number of ways to represent this inside the geometric model.

The relevant causes of yarn deformation are:

- Yarn manufacturing
- Yarn processing into a textile (contact with the weaving/braiding machine, contact with other yarns)
- Preforming (stacking, handling, compacting etc.)
- (Pre-) Impregnation (addition of resin to dry fibre)
- Curing (chemical and thermal shrinkage effects)

The combination of these processes results in a yarn shape that can be monitored using microscopy.

Since there is only geometric data of yarn geometry in the finished composite (this is further explored in the chapter 5.2) it is hard to attribute deformations to stages in the production process. Extensive numerical studies on the effects of forming on yarn geometry in dry textiles have been performed by Martin Sherburn and are documented in his PhD thesis [11]. However, even when taking dry textile deformation into account, the effects of the remaining processes needed to arrive at the actual composite (liquid resin infusion and curing) remain unresolved.

It is assumed here that the origin of yarn shape deformations is not important to the mechanical properties as long as the final shape can be described to satisfactory accuracy. So far, in geometric models, the challenge has been to find non-intersecting yarn descriptions that take up a sufficiently high fraction of the RVE (i.e. have a high V_y).

Since $V_f = V_y V_{yf}$ and local strength is very strongly dependent on V_{yf} (the fibre volume fraction within the yarn), the following holds for models that are normalised by V_f; the more realistic the value of V_y, the more realistic is the model (see section 3.2.2 on micromechanics for a detailed analysis of this issue).

The physical reasons that in a composite V_y is higher than obtained by extruding a constant cross section along a yarn path are the processing mechanisms mentioned above. TexGen implements a number of mechanisms (see Figure 3.5) that are used to modify yarn cross sections from the base shape in geometric interference correction or compaction iterations. Note that these deformation mechanisms do not represent restrictions of the yarn description in TexGen; rather, they are the deformation modes taken into account in the interference correction scheme as implemented in TexGen at the time of writing.

The methods used here to perform interference correction can be classified as geometry based interference correction, as opposed to mechanically based methods (which require the solution of a structural mechanics problem representing dry yarn contact).

Mechanically based interference correction is used to generate deformed textile meshes in work by Sherburn [11] and Lomov [43], and is known to generate realistic textile packings. The reasons that this was not pursued in this work are:

- Implementation would be cumbersome (the feedback from dry textile modelling to a deformed TexGen textile was not implemented when the work for this thesis was done).
- Resulting textile geometries are not conceptually more difficult to deal with in

AMR, hence the functionality could be added at a later stage without consequences to the solution methods.

- Robustness of this preprocessing step is unknown; in particular, not all compaction algorithms always converge.
- The resulting deformed textile is no longer parametric, which makes interpretation of results of parameter sensitivity data more complicated. I.e. an increase in inter-yarn gap on the initial textile does not necessarily result in an increase of the same parameter in the textile structure after a forming simulation.

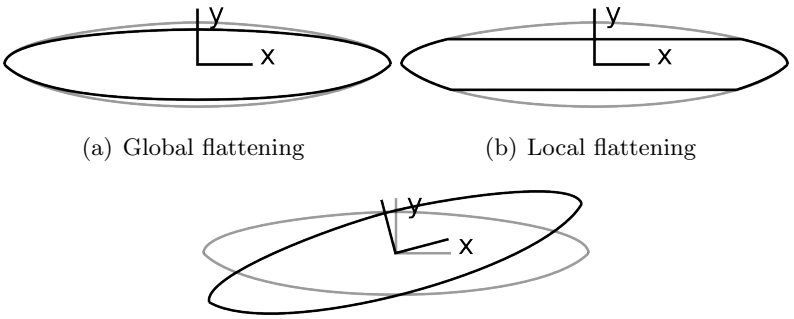

(a) Global flattening (b) Local flattening

(c) Yarn twisting

Figure 3.5: Yarn cross section deformation mechanisms shown in local (yarn cross section) coordinate system.

3.1.4 Fibre content modelling

Textile composites are assumed to consist of yarns which contain a fixed number of continuous fibres along the length of the yarn. Since the yarns are modelled as a continuum this condition cannot be imposed directly but only in the average sense. This introduces the assumptions that filaments are incompressible and do not vary significantly in cross sectional area along their length. Additionally the manner in which fibers are distributed within the cross section is assumed to be constant along the yarn path (constant and quadratic distributions are used through this thesis). In Figure 3.5 yarn deformation mechanisms are given. Since most of the deformation mechanisms affect the cross sectional area of the yarn, the local volume fraction has to be modified to satisfy the constant fibre area assumption. In the current implementation the distribution of fibres in the bundle as well as the total fibre area per yarn (A_y) are kept constant, meaning that the distribution is scaled such that

$$\int_{x=-w/2}^{x=w/2} V_f(x)h(x)dx = A_y \tag{3.1.1}$$

where w is the width of the yarn, $V_f(x)$ is the volume fraction distribution (linear and quadratic distributions are used), $h(x)$ is the height of the yarn and A_y is the summed fibre area across the cross section. The numerical implementation of this relation, considering that the cross section is represented by a polyline, is given as:

$$\sum_{i=0}^{i=n-1} V_{f,i} \frac{h_i + h_{i+1}}{2} dx_i = A_y \tag{3.1.2}$$

The theoretical maximum local fibre content is $\frac{\pi}{2\sqrt{3}} = 0.9069$ for a hexagonal packing and $\frac{\pi}{4} = 0.7854$ for a square packing, therefore any local values computed must be lower than 0.9069 in order to be realistic[2].

It can be seen in Equations 3.1.1 and 3.1.2 that only x direction dependence is taken into account in the current work. This is due to the fact that the work is based on 2D weaves with tows that have a high aspect ratio (slender shape). More general formulations based on both x and y location on the cross section of the tow can be used (for example in 3D weaves), but these are not currently implemented in TexGen.

3.1.5 Local point querying of a textile model

The key functionality of TexGen relating to this thesis is that it allows (efficient) querying of the geometric model for local textile information on the aspects outlined in the previous sections (local yarn orientation, position within the cross section, and local fibre volume fraction). It is this functionality that forms the interface between geometric and numerical analysis (an example of how this is used in practice from C++ is given in Appendix B).

The algorithms used to do this lookup efficiently for millions (depending on the problem) of material sampling points are based on octree partitioning of the domain.

The procedure consists of 3 steps (ignoring any algorithms for performance enhancement):

1. Locate the point on the yarn path using iterative search (position found to user set tolerance)
2. Construct interpolated cross section
3. Locate point on the cross section exactly for the cross section at hand (up to machine precision)

[2] Higher values can exist theoretically when assuming non-equally sized filament cross sections, however, geometric analysis shows that assuming any other scenario than perfect alignment will result in substantially lower V_f values (see [11]).

This shows that an additional approximation is introduced when performing point lookup within the textile, but that the level of error introduced by making it can be set by the user. From practical experience it is gathered that using point lookup with a tolerance that is small compared to element size (or integration point spacing) never causes lookup runtimes to approach FE assembly or solve runtimes.

3.1.6 Summary of geometric modelling

The geometric modelling strategy employed in this thesis is designed for the following key objectives:

- Full flexibility in modelling textile structures
- Computational efficiency in querying textile internal geometry
- Facilitating parametric textile modelling

The following approximations are used and controlled with either internal or user settings:

- The yarn path is a spline, the number of control points can be adjusted.
- Yarn section circumference is approximated by a polyline, for which the number of points can be varied.
- Yarns sections allow 1D variation of $V_{y,f}$; this assumes yarns to have constant $V_{y,f}$ through thickness. Currently only constant, linear and quadratic variations are implemented. The 1D variation is relative to the yarn section local x coordinate as depicted in Figure 3.5.
- Fibre area is enforced to be constant along the yarn path, independent of yarn deformation.
- A geometry based compaction algorithm is employed to obtain a realistic V_y, this algorithm operates on the following variables:
  - yarn control point location
  - yarn section twist
  - yarn section compaction.
- Geometry querying introduces a tolerance in the cross-section lookup along the yarn.

3.2 FEM modelling

The equations for modelling small-strain elastostatics have been implemented in C++ in order to allow the author to use the LibMesh Finite Element library for handling mesh refinement and solution whilst allowing a direct interface with the TexGen API. The FEM formulation given below is also used in [83] and results for single elements have been compared with results from both ABAQUS and Calculix and shown to match to machine precision.

3.2.1 FE formulation

In small-strain elastostatics an attempt is made to solve the equation of equilibrium:

$$\nabla \cdot \sigma + \mathbf{b} = 0 \text{ in } \Omega \tag{3.2.1}$$

where σ is the stress tensor, $\mathbf{b}$ are the bodyforces and ∇ the gradient operator. The material behaviour is described by generalised Hooke's law:

$$\sigma = \mathbf{C} : \varepsilon \ , \varepsilon = \nabla_s \mathbf{u} \tag{3.2.2}$$

where ε is the strain tensor, ∇_s is the symmetric gradient operator and $\mathbf{u}$ is the displacement vector.

When it is decided to solve this system using the Finite Element Method a weak form of the equilibrium equations is constructed. This is done by multiplying by a trial function δv and integrating.

$$\underbrace{\int_\Omega \nabla_s \delta v : \sigma d\Omega}_{internal\ stress} = \underbrace{\int_\Omega \delta v \cdot \mathbf{b} d\Omega}_{body\ forces} + \underbrace{\int_\Gamma \delta v \cdot \mathbf{t} d\Gamma}_{boundary\ tractions} \qquad \forall\ \delta v \in \mathcal{H}^1_E(\Omega) \tag{3.2.3}$$

At this point the trial function is still arbitrary. According to Galerkin's method a specific trial function is chosen that matches the interpolation function used for the geometry. From this, the classical finite element formulation that is suited for numerical solution is obtained:

$$\mathbf{K}\mathbf{u} = \mathbf{F} \tag{3.2.4}$$

where $\mathbf{K}$ is the global stiffness matrix, $\mathbf{u}$ are the displacements and $\mathbf{F}$ the nodal forces. In this system $\mathbf{K}$ is a banded matrix with a bandwidth dependent on the element connectivity (in case of a structured hexahedral mesh with 3 DOFs per node the bandwidth is 81).

The stiffness matrix and forces are computed using the following relation:

$$\mathbf{K} = \int_{\Omega} B^T D B d\Omega \tag{3.2.5}$$

$$\mathbf{F} = \int_{\Gamma} N\mathbf{t} d\Gamma + \int_{\Omega} N\mathbf{b} d\Omega \tag{3.2.6}$$

where N is the vector of Lagrange shape functions, B the matrix containing shape function derivatives and D the material stiffness tensor, the engineering equivalent of $\mathbf{C}$ as defined in the generalized Hooke's law (Equation 3.2.2).

Hooke's law is written for an orthotropic material in the following manner:

$$\begin{bmatrix} \sigma_{11} \\ \sigma_{22} \\ \sigma_{33} \\ \sigma_{23} \\ \sigma_{31} \\ \sigma_{12} \end{bmatrix} = \begin{bmatrix} E_1(1-\nu_{23}\nu_{23})\psi & E_2(\nu_{12}+\nu_{13}\nu_{32})\psi & E_3(\nu_{13}+\nu_{12}\nu_{23})\psi & 0 & 0 & 0 \\ & E_2(1-\nu_{31}\nu_{13})\psi & E_3(\nu_{23}+\nu_{13}\nu_{21})\psi & 0 & 0 & 0 \\ & & E_3(1-\nu_{12}\nu_{21})\psi & 0 & 0 & 0 \\ & & & 2G_{23} & 0 & 0 \\ & S & & & 2G_{31} & 0 \\ & & & & & 2G_{12} \end{bmatrix} \begin{bmatrix} \varepsilon_{11} \\ \varepsilon_{22} \\ \varepsilon_{33} \\ \varepsilon_{23} \\ \varepsilon_{31} \\ \varepsilon_{12} \end{bmatrix} \tag{3.2.7}$$

where

$$\psi = \frac{1}{(1-\nu_{12}\nu_{21}-\nu_{23}\nu_{32}-\nu_{13}\nu_{31}-2\nu_{12}\nu_{23}\nu_{31})}$$

where E_i are Young's moduli of the effective yarn medium in local yarn coordinates, ν_{ij} the Poisson's ratios and G_{ij} the shear moduli.

This formulation is used to describe the yarn properties. In order to describe the matrix properties the law is simplified using the knowledge that all directional properties are equal (the material only requires an elastic modulus and Poisson's ratio to define its behaviour).

Since the yarn material is aligned according to the yarn path coordinates, Equation 3.2.7 describes its behaviour in an undulating coordinate system that does not coincide with the coordinate system in which displacements are being calculated. In order to transform this behaviour into global coordinates the following transformation is applied to the stiffness tensor. In order to stay close to the implementation this particular

operation is more conveniently written in terms of the full stiffness tensor.

$$D_{ijkl} = R_{im}R_{jn}R_{ko}R_{lp}D'_{mnop} \tag{3.2.8}$$

where D_{ijkl} and D'_{ijkl} are the stiffness tensors in global coordinates and local coordinates respectively. The transformation matrix R_{ij} contains the direction cosines $R_{ij} = \cos(x'_i, x_j)$, where x_i and x'_i are the direction axes in global and local coordinates.

3.2.2 Micromechanics

The composites considered in this thesis are based on fibrous yarns which are regarded as homogeneous solids within mesoscale mechanics models.

In this work, homogenisation of the properties of impregnated yarns is done through the use of micromechanics models. There are a variety of different micromechanics models available, which vary with respect to the following aspects:

- Analytical or numerical representation of the microscale geometric and structural problem
- Assumptions regarding fibre packing order, being either square, hexagonal or random

Because the mesoscale FE solution is much faster when using closed form expressions for the microscale material behaviour (compared to, for example, microscale FE models) it was decided to use the models implemented in ICAN (see Murthy and Chamis [4]).

These models were set up to analyse properties of plies of unidirectional continuous fibre composite. They are relevant to the current models because the yarns in a textile based composite are essentially unidirectional continuous fibre composites.

Additionally these models provide strength predictions as well as full sets of stiffness terms. The major uncertainty arising from the use of such models is that they have not been validated for the 3D stress states for which they are being used, but this is also true for many numerical models. Thorough analysis of the validity of micromechanics models is outside of the scope of the current work.

ICAN models

In this work the micromechanics models implemented in ICAN are used [4, 84] which are reiterated here for the reader's convenience. The coordinate system used in these equations is given in Figure 3.6. The models are based on a hexagonal packing of filaments.

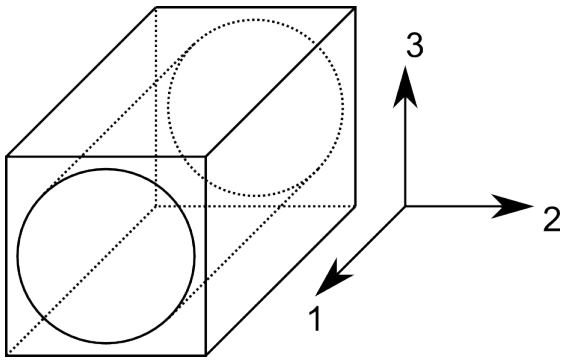

Figure 3.6: Local fibre coordinate system used in the formulation of ICAN models. The 2-direction refers to second in-plane direction in UD laminates, in this case the 2-direction holds parallel to the local x-direction in yarn cross section coordinates (see Figure 3.5).

Elastic constants are given by the following equations:

$$E_{11} = V_f E_{f,11} + (1 - V_f) E_m \tag{3.2.9}$$

$$E_{22} = E_{33} = \frac{E_m}{1 - \sqrt{V_f}\left(1 - \frac{E_m}{E_{f,22}}\right)} \tag{3.2.10}$$

$$G_{13} = G_{12} = \frac{G_m}{1 - \sqrt{V_f}\left(1 - \frac{G_m}{G_{f,12}}\right)} \tag{3.2.11}$$

$$G_{23} = \frac{G_m}{1 - V_f\left(1 - \frac{G_m}{G_{f,23}}\right)} \tag{3.2.12}$$

$$\nu_{12} = \nu_{13} = \nu_m + V_f\left(\nu_{f,12} - \nu_m\right) \tag{3.2.13}$$

$$\nu_{23} = V_f \nu_{f,23} + V_m\left(2\nu_m - \frac{\nu_{12}}{E_{11}} E_{22}\right) \tag{3.2.14}$$

These models are commonly used for the prediction of mechanical properties of unidirectional composites. As such they include a set of strength predictions which correspond to different failure mechanisms (here the delamination strength $S_{11,Cd}$ is reproduced as stated in the ICAN manual, even though delamination would constitute a failure in the 12 plane or 3 direction, it is assumed to hold as a predictor of delamination based on

fibre direction stress).

$$S_{11,T} = S_{f,T}\left(V_f + V_m\frac{E_m}{E_{f,11}}\right) \tag{3.2.15}$$

$$S_{11,Cr} = S_{f,C}\left(V_f + V_m\frac{E_m}{E_{f,11}}\right) \tag{3.2.16}$$

$$S_{11,Cd} = (13S_{12} + S_{m,C}) \tag{3.2.17}$$

$$S_{11,Cf} = \frac{F_2 G_m}{1 - V_f\left(1 - \frac{G_m}{G_{f,12}}\right)} \tag{3.2.18}$$

$$S_{22,T} = S_{m,T}\left(\frac{Fc}{Dn}\right) \tag{3.2.19}$$

$$S_{22,C} = \frac{S_{m,C}}{Dn} \tag{3.2.20}$$

$$S_{12} = \frac{\left(F_1 - 1 + \frac{G_m}{G_{f,12}}\right) F_2 G_{12} S_{m,S}}{G_m F_1} Fc \tag{3.2.21}$$

Where subscript Cr indicates the rule-of-mixtures compressive result, Cd the delamination strength and Cf the fibre microbuckling strength. Fc takes the value of 1 for all fibre types under consideration. The terms F_1, F_2 and D_n are defined as follows:

$$F_1 = \sqrt{\frac{\pi}{4V_f}} \tag{3.2.22}$$

$$F_2 = 1 - \sqrt{\frac{4V_f}{\pi V_m}} \tag{3.2.23}$$

$$Dn = \left[1 - \sqrt{V_f}\left(1 - \frac{E_m}{E_{f,22}}\right)\right]\sqrt{1 + \varphi(\varphi - 1) + \frac{1}{3}(\varphi - 1)^2} \tag{3.2.24}$$

$$\tag{3.2.25}$$

where φ is defined as:

$$\varphi = \frac{F_1 - \frac{E_m}{E_{f,22}\left[1 - \sqrt{V_f}\left(1 - \frac{E_m}{E_{f,22}}\right)\right]}}{F_1 - 1} \tag{3.2.26}$$

The microbuckling results relate to buckling of a microstructural beam, supported by an elastic medium. It can be seen as an upper bound on the buckling strength since fibres are assumed to be straight. This is noted here but not thought to be of great influence for the results in this thesis since the results are mainly generated for the tension loadcases.

Strength behaviour as a function of local volume fraction The strength behaviour as a function of local volume fraction strongly influences the results in the

present thesis. In Figure 3.7 this relation is illustrated for the quantities given in Equations 3.2.15 to 3.2.21. It can be seen that upper and lower bound values in transverse strength can be a factor of 5 apart when varying V_f between 0.5 and 0.75 (which is a realistic range of $V_{y,f}$ to exist in a textile model).

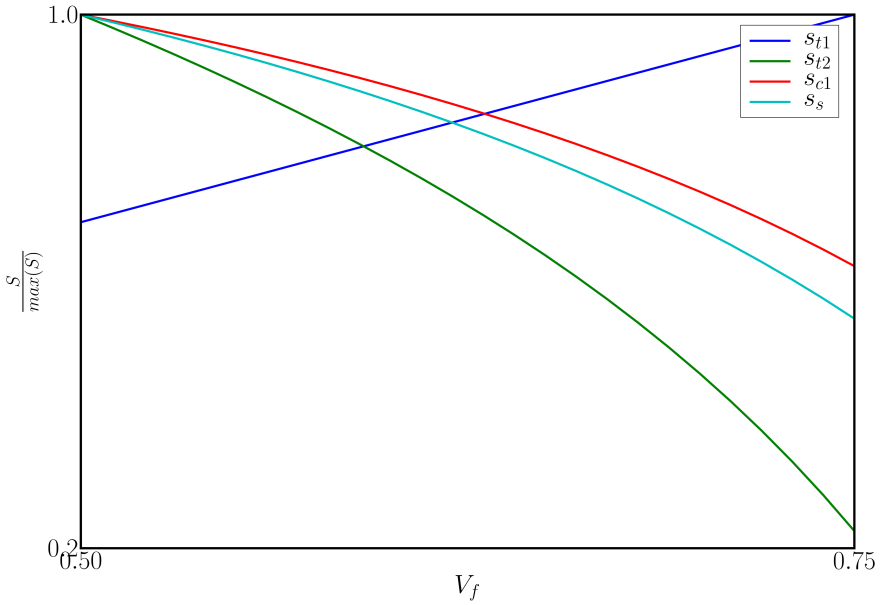

Figure 3.7: Normalised strengths as a function of volume fraction according to the ICAN strength models (as given in 3.2.21).

This represents the physical/geometric phenomenon of a load being transferred through an increasingly thin resin layer, leading to a nonlinearly increasing stress intensity factor with increasing average fibre volume fraction.

It is noted here that these models don't represent the state of the art in composite strength modelling, but rather a simple framework to scale damage initiation predictions based on local fibre volume fraction. More advanced strength predictors or interpolated composite strength values obtained from a database of experimental results could be used in the place of these formulae.

3.2.3 Damage modelling

Damage modelling consists of two stages; the detection of damage initiation, and the modification of the local material behaviour to reflect the damaged state. In the case of textile composites the added complication is that the impregnated yarns behave like a (sub)composite in their own right (a unidirectional composite).

Because most of the high-performance applications of composite materials involve brittle materials the prediction of initial damage is an important capability because it represents a conservative design limit.

Failure criteria

Section 3.2.2 lays out how directional yarn strengths are derived from constituent properties. Failure criteria provide a way to integrate single directional strengths and a multiaxial stress state into an estimate of how far away the local material is from failing.

In this case the damage parameter D is the measure in which the relevant stress or strain criterion is violated, for the matrix behaviour this is the Bauwens criterion (see 3.2.27, reproduced here from [85]).

$$D = \sqrt{2}\frac{\sigma_{yc} - \sigma_{yt}}{\sigma_{yc} + \sigma_{yt}}(\sigma_1 + \sigma_2 + \sigma_3) + \left[(\sigma_1 - \sigma_2)^2 + (\sigma_2 - \sigma_3)^2 + (\sigma_3 - \sigma_1)^2\right]^{1/2} \\ 2\sqrt{2}\frac{\sigma_{yc}\sigma_{yt}}{(\sigma_{yc} + \sigma_{yt})} \quad (3.2.27)$$

where σ_i the principal stresses and σ_{yc}, σ_{yt} are the yield stress in compression and tension respectively (S_C, S_T in Table E.1).

The yarn damage criterion is evaluated in the yarn coordinate system. Since the yarn is assumed to be orthotropic the 2- and 3- direction of the yarn coordinate system are oriented arbitrarily orthogonal to the 1 direction. Here 3 damage variables are introduced, where D_1 indicates fibre direction damage, D_2 is transverse shear damage and D_3 transverse damage.

$$D_{11} = \frac{\sigma_{11}}{S_{11,t}} \tag{3.2.28}$$

$$D_{12} = \frac{-\sigma_{11}}{S_{11,c}} \tag{3.2.29}$$

$$D_{31} = \frac{\max(\sigma_2, \sigma_3)}{S_{22,t}} \tag{3.2.30}$$

$$D_{32} = \frac{-\min(\sigma_2, \sigma_3)}{S_{22,c}} \tag{3.2.31}$$

and

$$D_1 = \max(D_{11}, D_{12}) \tag{3.2.32}$$

$$D_2 = \frac{\sqrt{(\sigma_{12}^2 + \sigma_{13}^2)}}{S_{12}} \tag{3.2.33}$$

$$D_3 = \max(D_{31}, D_{32}) \tag{3.2.34}$$

where σ_{11} is the stress in the fibre direction, σ_{12}, σ_{13} are shear stresses and σ_2 and σ_3 are the transverse principal stresses, i.e. rotated such that $\sigma_{23} = 0$).

A damage model for use in FE analysis

Since the use of brittle material models (step degradation of properties) as used by Blackketter et al. [30] was found to be unsuccessful for materials that fail in a non-brittle fashion and absorb energy during failure, a phenomenological stiffness degradation law is used to describe the local stiffness. This relation stems from the need to allow for failure mechanisms such as crazing, yielding or crack propagation which make the material macroscopically non-brittle (see Tijssens et al [86]) because the resin used in the experiments exhibits such behaviour.

The following relation (Equation 3.2.36) is used for the stiffness of the matrix material and for the transverse stiffnesses of the yarn material.

$$P = \left(1 - \frac{1}{\exp(-c_1 \cdot D + c_2)}\right) \tag{3.2.35}$$

$$E_d = E \max(P, 0.0001) \tag{3.2.36}$$

Where P is the penalty or knockdown factor, E_d is the modulus of the damaged material, E is the modulus of the undamaged material, constants c_1 and c_2 are set to $c_1 = 8, c_2 = 13$.

The behaviour of this knockdown method is shown in Figure 3.8. In order to be able to solve elastostatics problems containing fully damaged material a minimum knockdown of 0.001 is used.

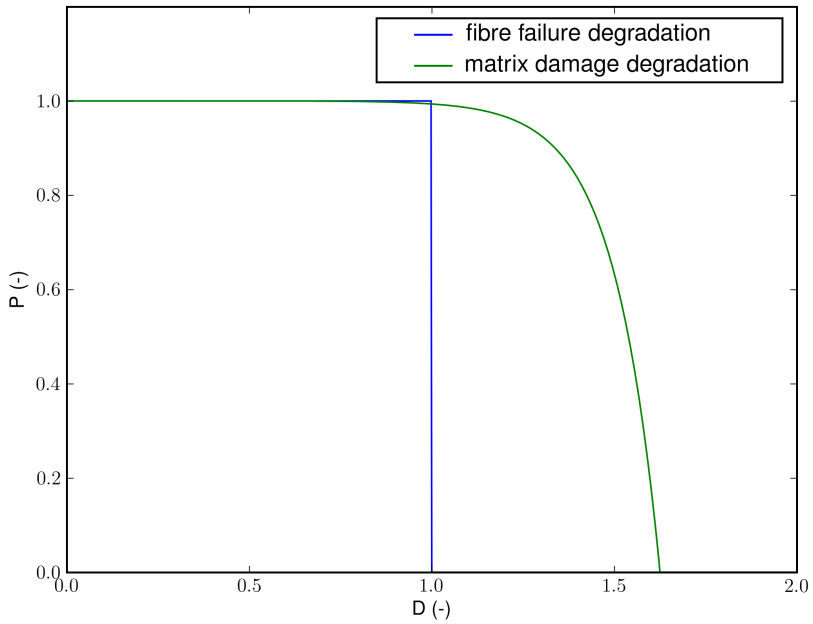

Figure 3.8: Stiffness knockdown factor P as a factor of damage variable D as given in Equation 3.2.36 (matrix damage and transverse yarn damage) and Equation 3.2.37 for longitudinal yarn damage.

This degradation law is also used to degrade the transverse and shear properties of the yarns (i.e. it degrades the matrix properties feeding into micromechanics as a function of D_2 and D_3 according to Equation 3.2.36). With respect to the fibre direction damage parameter D_1 brittle degradation is used, as described in Equation 3.2.37.

$$P = \begin{cases} 1 & , \quad D_1 <= 1 \\ 0.001 & , \quad D_1 > 1 \end{cases} \tag{3.2.37}$$

The introduction of gradual degradation according to 3.2.36 causes the model to absorb energy. When using local stress the amount of energy absorbed in the FEA model is related to the mesh size. In order to obtain mesh-independence of the damage behaviour a nonlocal stress measure is introduced.

Nonlocal stress

Mesh dependency of results is a common phenomenon in FE analysis, it is particularly apparent in the analysis of a problem that posesses a singularity in its analytical form. Common problems showing singular behaviour are crack propagation problems where explicit crack tips are modelled. The singularity that is handled in the current approach originates from using a lenticular yarn shape.

The most common circumvention of this problem is the use of a nonlocal stress measure. A nonlocal stress measure is computed from the grid solution but is a weighted average over a geometric domain, where the size of this domain is chosen to be independent of mesh size.

It is used here to see if a consistent peak stress value (which dictates the load level at which damage initiates) can be obtained at lower computational cost.

The nonlocal stress $\sigma_{nl}(\mathbf{x_i})$ is obtained from the local stresses $\sigma_l(\mathbf{x})$ using a weighting function $f(\mathbf{x})$ according to Equation 3.2.38.

$$\begin{aligned} \sigma_{nl}(\mathbf{x_i}) &= \frac{\int \sigma_l(\mathbf{x}) f(\mathbf{x}) dV}{\int f(\mathbf{x}) dV} \\ f(\mathbf{x}) &= \frac{1}{1 - (\frac{\varphi|\mathbf{x}-\mathbf{x_i}|}{\gamma})^2} \end{aligned} \tag{3.2.38}$$

Where γ is the nonlocal feature size[3] and φ a weight factor indicating the dropoff strength of the weight function.

In the present implementation only stresses in the same material are taken into account. For example, when looking at stress at a location within a yarn, the nonlocal stress is computed from contributions of local stresses in the same yarn.

[3] In chapter 5 this feature size was set to half the tow width of a typical textile (2.8mm, it was not varied further during the study), note that if this length is large the influence of remote contributions have marginal weights anyway.

3.2.4 Adaptive mesh refinement

Finite Element models of the textile are generated using Adaptive Mesh Refinement (AMR) on a simple hexahedral mesh as opposed to using a CAD driven mesh generator, a method resulting in similar meshes was devised by Kim and Swan [50]. The rationale behind developing such a method is to circumvent the difficulties that arise when trying to mesh realistic textile geometries. The touching yarns tend to generate high aspect ratio geometries which are either unmeshable or generate such fine meshes that they are impossible to solve on current hardware. The procedure in the current method is as follows:

1. Generate coarse mesh (of hexahedral elements)
2. Solve
3. Estimate error for all cells
4. Refine cells with highest error
5. Back to 2 to solve the refined mesh problem

The error estimator used is a Kelly error estimator [87] which uses the sum of discontinuities in computed strain over element boundaries as a measure for the discretisation error. Without modification this results in refinement around stiffness jumps, as are introduced by the multiphase character of the composite (see Figure 3.9).

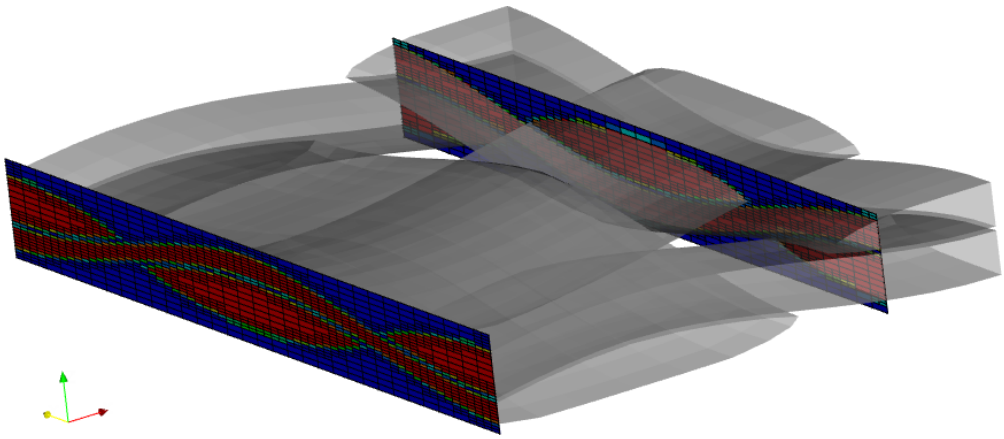

Figure 3.9: Grid refinement (slices of a 3D mesh) following tow boundaries in a plain weave textile geometry

To reduce implementation time the LibMesh [56] finite element library was used. This library was selected (over similar tools like Deal.ii [73]) because it supports a wide range

of element types. Both libraries interface to common solver libraries (like PETSc[72]) and contain implementations of various error estimators. The textile is queried for orientation and local V_f data at each of the stages of refinement, this is implemented by linking directly to the TexGen library.

3.2.5 Boundary conditions

Two different approaches are taken with regards to boundary conditions.

1. In the AMR based work relating to physical experiments on small specimens simple displacement boundary conditions are used which are implemented using a penalty method. The remaining edges are left free. The reason for doing so is primarily to simplify implementation. For details on how to implement periodicity in conjunction with AMR the reader is referred to [49]. A secondary reason for using simple boundary conditions is that verification is performed using specimens which are small compared to the RVE size. This means that (free) edge effects do play a role and therefore should be present in the model. It is for this reason that plain weave analyses are based on a full wavelength of axial yarn rather than the smallest possible RVE, so that all potential regions of interest are contained at least once away from the boundaries.

2. In the analyses for 2D and 3D stiffness evaluation 1st order periodic boundary conditions are used. Section 3.2.6 describes the use of 1st order periodicity in FE analyses with regular meshes.

In order to describe periodicity for RVEs in bending loadcases 2nd order homogenisation is needed. This is outside the scope of the current work and the reader is referred to [66].

3.2.6 Periodic boundary conditions

Because the unit cell models discussed here are to be used in a higher level model under the assumption that the higher level medium is continuous, it must be ensured that the model boundaries deform in such a way that the deformed shape remains repeatable and continuous.

This is done by implementing so-called periodic boundary conditions. Enforcing such a condition is done by replacing the t'th equation (relating to the t'th DOF) corresponding to a row in the equation system

$$K_{ti}u_i + K_{tj}u_j + K_{tt}u_t \cdots = F_t \tag{3.2.39}$$

with an Equation of shape

$$-u_m + u_t = \lambda \tag{3.2.40}$$

where u_i, u_j are the displacements of nodes connected by elements to u_t and λ is a forcing term that can be used to apply global longitudinal or shear deformation to the unit cell. u_m typically relates to a node on the opposite face of the unit cell and the creation of such an equation makes u_t a slave DOF.

If $\lambda = 0$ it can be seen that Equation 3.2.40 results in $u_t = u_m$, meaning that the two opposite sides move in the same manner. In order to enable the representation of load-driven experiments and periodic Poisson's effects λ has to be a DOF rather than a predetermined constant. When implementing periodic boundary conditions in commercial finite element codes this is generally achieved by creating a node that is separate from the structure and of which the DOF are used in the constraint equations binding the opposing faces of the unit cell. The resulting general equation used to implement periodic boundary conditions on a nodal level is:

$$-u_m + u_t + u_{side} = 0 \tag{3.2.41}$$

The use of periodic boundary conditions is apparent when considering unbalanced (single layer) textile composites. In this case the undulation pattern gives rise to periodic wavy patterns as shown in Figure 3.10. In these cases the assumption of straight sides constrains this motion and results in an overestimation of the stiffness. The difference between the two scenarios becomes smaller for more layers of textile.

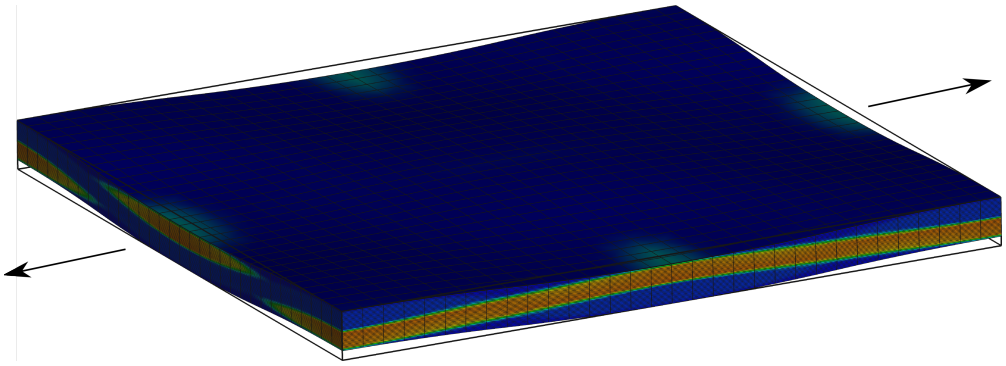

(a) Periodic deformation of a plain weave based composite in tension loading

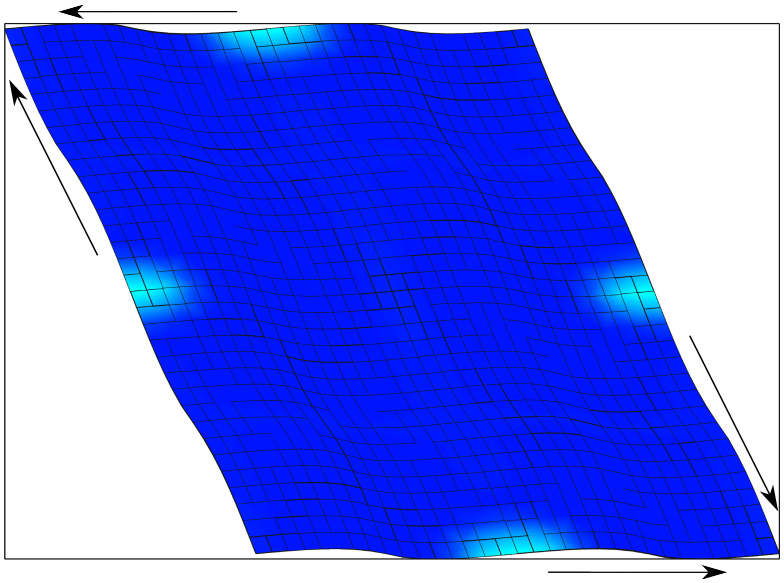

(b) Periodic deformation of a plain weave based composite in simple shear loading

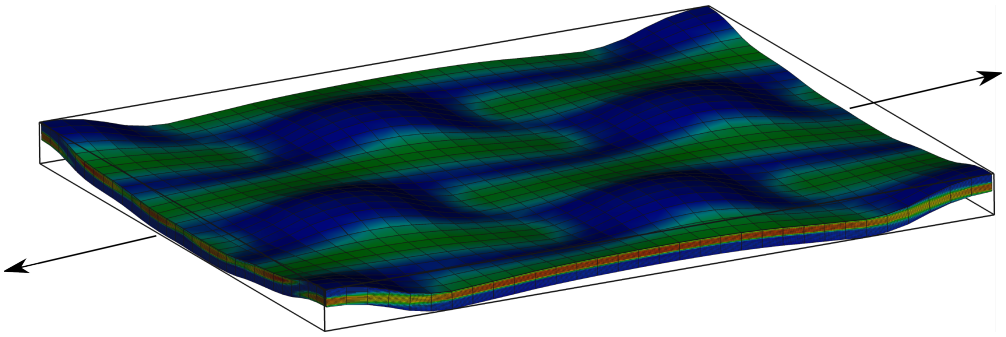

(c) Periodic deformation of a five harness satin weave based composite in tension loading

Figure 3.10: Periodic deformation (and σ_{11} contours) of unbalanced woven textile based composites in tensile loading. Model built up using texgen material sampling and uniform mesh refinement. The implementation is given in Appendix C.

3.2.7 Stiffness averaging

The numerical problem under consideration contains both continuous variations of local properties (intra yarn $V_{y,f}$) and discrete boundaries between materials (yarn-matrix interface). In addition spatial points can have associated time (or load step) dependent data such as damage.

Two methods for assigning averaged properties to elements spanning multiple materials are used in this thesis:

1. In the AMR related analyses the material is associated to quadrature points, since the method is coupled to a damage model which operates on non-averaged material properties. It is noted here that the order of quadrature can be varied arbitrarily and need not match the order of the element. It is also noted that single elements used in this manner can have nonuniform properties.

2. For the purpose of numerical benchmarking an alternative implementation was devised which follows the work of Kim and Swan more closely and uses arbitrary subdivisions of cells to perform material sampling.

   The material sampling points are distributed such that parametric coordinates are given by Equation 3.2.42

   $$x_i = \frac{1}{2n} + \frac{i}{n} \tag{3.2.42}$$

   where x_i the i'th location in parametric cell coordinates (in the $[0, 1]$ range) and n the number of points in the scheme (where i from 0 to $n - 1$).

   Using this sampling method the inhomogeneity that can exist in the gauss point sampling method is lost (i.e. an averaged stiffness is attributed to the whole element). The implementation for this method is given in Appendix B.

The assumption is that an increase in the number of material sampling points will converge the stiffness solution, where the uniform sampling method in 2D can be used to explore how many points are need to reach a fully converged solution.

3.3 Parametric textile modelling

The aim of the current modelling methodology is to provide a robust analysis tool that can deal with challenging textile geometries without manual intervention.

In this thesis the main focus is on 2D weaves in general and plain woven textiles in particular. A parameterisation of such textiles is defined that allows easy generation of geometric models for parameter studies. The geometric variables for a few textiles are given in Figure 3.11.

These are examples of the textiles on which variations are studied in Chapter 5. A textile model is permissible (it can be analysed using FE) when local $V_f < 0.906$ and there is no intersection between yarns. The parameters are given in Table 3.1. The model is implemented using the TexGen python interface (see Appendix C.3).

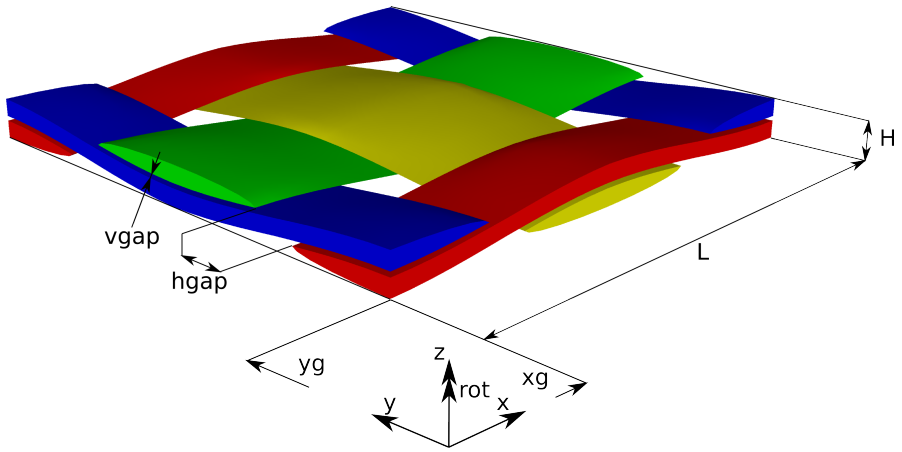

(a)

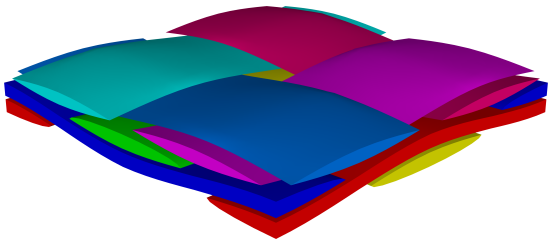

(b) Two layer nested version of 3.11(a)

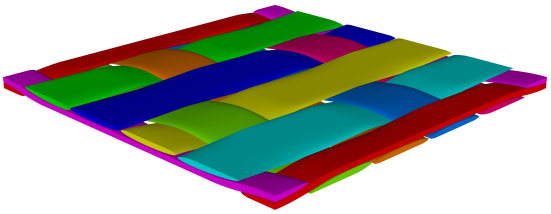

(c) Five harness satin weave

Figure 3.11: Examples of textiles described using the parametric representation of a 2D weave as given in Table 3.1.

	Units	Figs. 3.11(a), 3.11(b)	3.11(c)	description
length	mm	6	2	Unit cell length
γ_x	λ	[0,0.25]	[0]	Shift in undulation pattern in $x-$direction
γ_y	λ	[0,0.25]	[0]	Shift in undulation pattern in $y-$direction
h_n	$height$	0.75	0	Relative offset between layers in thickness direction, $h_n < 1.0$ means that the textile is nested
numlayer	$-$	{1,2}	1	Number of layers in the textile
vgap	mm	0.07	0.01	Vertical gap between yarns
hgap	mm	0.5	0.02	Horizontal gap between yarns
height	mm	0.5	0.2	Height of the unit cell
fibre_area	mm^2	0.35	0.04	Sum of the cross section area of the filaments in a yarn
$V_{f,dr}$	$-$	1	0.9	Relative dropoff of the in-yarn volume fraction towards the side of the yarn
f_f	mm	0.14	0.025	Limiting height of yarn near model bounds (flattening of yarn)
rot	πrad	[0,0]	[0]	Rotation of the layer
domainsize	length	[1,1]	[2.5,2.5]	Size of the domain
weavestyle		"plain"	"5satin"	Weave style

Table 3.1: Parameterisation for 2D woven textiles, examples of which are displayed in Figure 3.11, numbers in [] indicate values that apply to different layers, numbers in {} apply to different models. λ indicates the weave wave length.

Chapter 4

Numerical results

In this chapter the behaviour of the methods presented in Chapter 3 is analysed. The focus of the current thesis is on developing a method for automatically analysing textile composite mesoscale problems.

The methods introduced in this thesis can produce arbitrary meshes and relate them to arbitrary textile structures that reside in the same geometric space via the TexGen API. The problem posed by this is choosing how to construct a mesh such that it efficiently captures the physics of the underlying problem, the number of strategies that can be used to do this is large, and performance is likely dependent on the problem at hand. Since a full parametric examination of this problem does not lie within the scope of this thesis, it is attempted to provide insight in the convergence of various global (stiffness) and local (stress and strain) quantities as a function of the two main variables that can be used to increase performance: mesh refinement and material sampling. Because it conceivable that convergence of all terms in the 3D analyses can't be achieved on current hardware, a 2D problem is constructed that contains the same issues of aspect ratio and locally varying fibre volume fraction. The 2D problem represents a slice of the 3D textile and is used to gain insight in the number of DOF needed to obtain convergence in local and global terms.

The same problem is analysed using 3D models. A larger set of problems was generated parametrically and outputs are tabulated in Appendix E.

In addition, a tetrahedral mesh of a plain weave textile is set up and the solutions on the tetrahedral and AMR grids are compared.

Modelled problems in this chapter represent an E-glass polyester (see Appendix E) plain weave composite according to the baseline textile parametrically defined in Figure 3.11(a) and used in Chapter 5, Table 5.2.

4.1 Convergence of stiffness terms

It is known from the work of Kim and Swan that uniform refinement of a structured FE mesh results in convergence of the RVE stiffness terms. The study here is set up to investigate at what level of mesh refinement convergence can be expected for typical textile structure. In addition it is used to investigate whether the intra-cell material sampling rate can be used to improve the rate of convergence.

The material sampling scheme that is used refines uniformly according to the 1D scheme given in Equation 3.2.42. As an example the resulting 3^3 scheme is shown in figure 4.1.

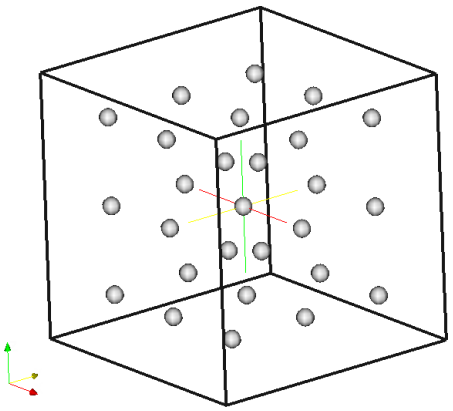

Figure 4.1: Rendering of 3^3 uniform material sampling points in a hexahedron.

4.1.1 2D convergence of stiffness

In order to obtain an upper bound for the level of mesh refinement required a 2D model is constructed that represents a 2D slice of the 3D model of a plain weave textile (see Figure 3.11(a)). The 2D model is obtained by sampling at the plane $y = 3.$ and assuming strain to be 0 in the $y-$direction. Mesh refinement is uniform in this case.

Figure 4.2 shows the convergence of stiffnesses and Poisson's ratio in the case of a 2D model with 11^2 material sampling and fairly large inter-yarn spacing. It can be seen here that the level of grid refinement needed to obtain converged solutions for all terms (in 2D) is quite substantial, and corresponds to a 3D scenario of more than 1M DOF (considering that convergence for all terms to within 1% happens at about 10^4 nodes, see Figure 4.2). Figure 4.2 shows that the in-plane moduli converge rapidly, and that the out-of-plane and shear results converge much slower. This can be easily understood when considering that these moduli are dominated by the weak inter-yarn resin layer

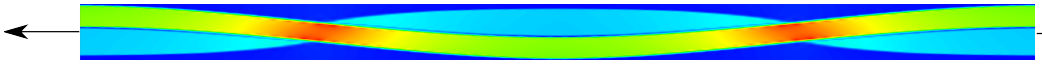

(a) 2D solution at $y = 3$ after 6 cycles of uniform refinement, the mesh shows $||\sigma||$

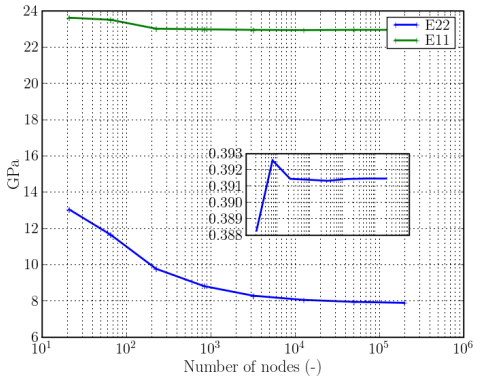

(b) E_{11} and E_{22} (out of plane) moduli

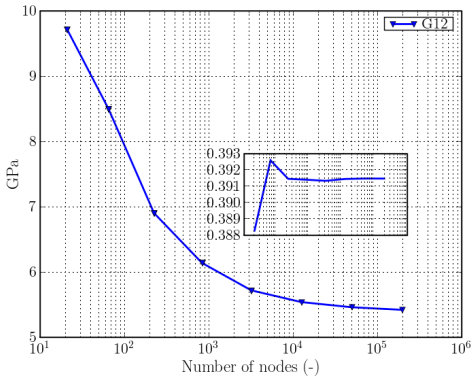

(c) Shear modulus

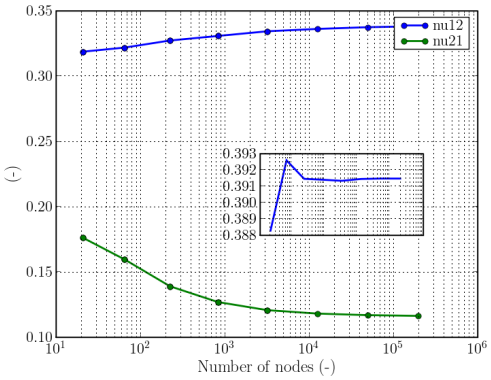

(d) Poisson's ratios

Figure 4.2: Convergence of elastic property predictions for a 2D slice from a textile shown in Figure 3.11 at $y = 3$ with 11^2 sampled material property averaging. The inset graph shows the convergence of V_f on the slice.

that is not explicitly represented until after about 6 levels of refinement.

For comparison, the 3D stiffness terms converge as shown in 4.3 for the reference textile given in Table 5.2 analysed with 1 and 6 internal sampling points, these plots are extracted from the data given in Appendix E.2.

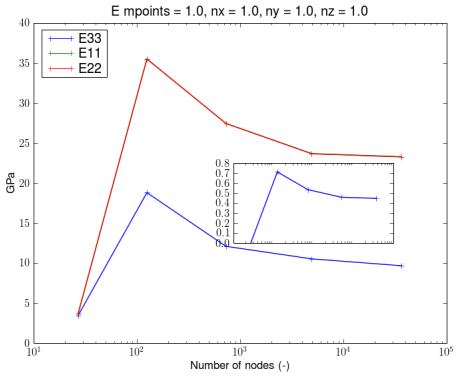

(a) $E-$moduli as a function of mesh refinement using 1^3 sampling, note that $E_{11} = E_{22}$

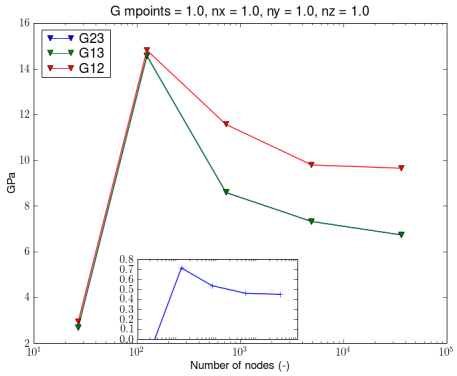

(b) $G-$moduli as a function of mesh refinement using 1^3 sampling

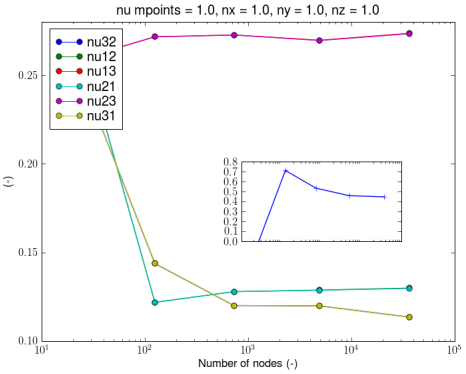

(c) ν as a function of mesh refinement using 1^3 sampling

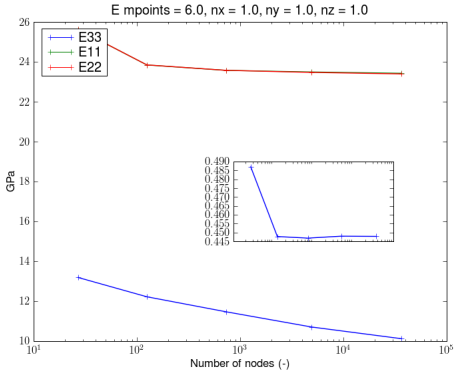

(d) $E-$moduli as a function of mesh refinement using 6^3 sampling

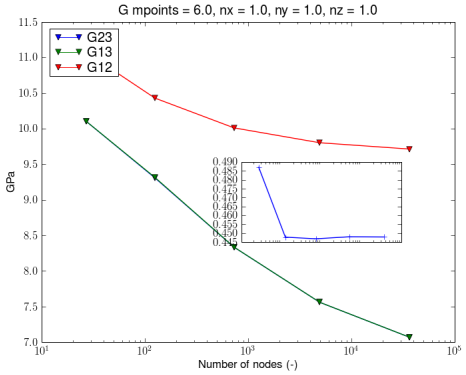

(e) $G-$moduli as a function of mesh refinement using 6^3 sampling

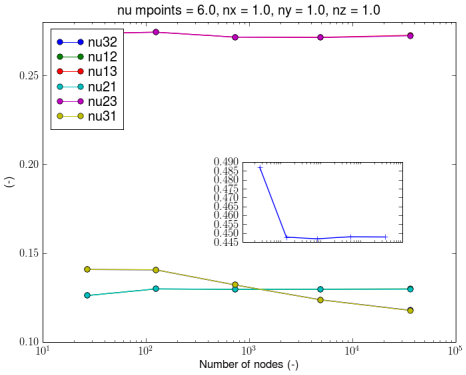

(f) ν as a function of mesh refinement using 6^3 sampling

Figure 4.3: Convergence of elastic property predictions for a 3D unit cell as shown in Figure 3.11 using 1^3 and 6^3 sampling to obtain averaged material properties. The inset graph shows the convergence of V_f in the RVE.

4.1.2 2D convergence of stress and strain

In addition to stiffness terms, local stress and strain values are also of importance, since they are used as inputs to the damage model. It is known that the domains contain sharp shapes around which stress and strain terms converge slowly if at all. When considering the micrographs presented in Chapter 5 it can be seen that with the filament size at hand, the element size is small compared to the microscale features (which would mean that any substructuring or computational homogenisation approach in these regions would remove the singularity). Because in the next chapter variable studies are done which vary the intra-yarn fibre volume fraction $V_{y,f}$ comparisons are made here between two scenarios with different $V_{y,f}$. In Figure 4.4 the scenario of $V_{f,dr} = 1$ is presented, showing poor convergence of both maximum stress and strain values. In both Figure 4.4 and Figure 4.5 a 2D slice is given, subject to loading in the $x-$direction. The slice is taken in between traversing yarns, at the location where two lenticular shapes meet $y = 2..$

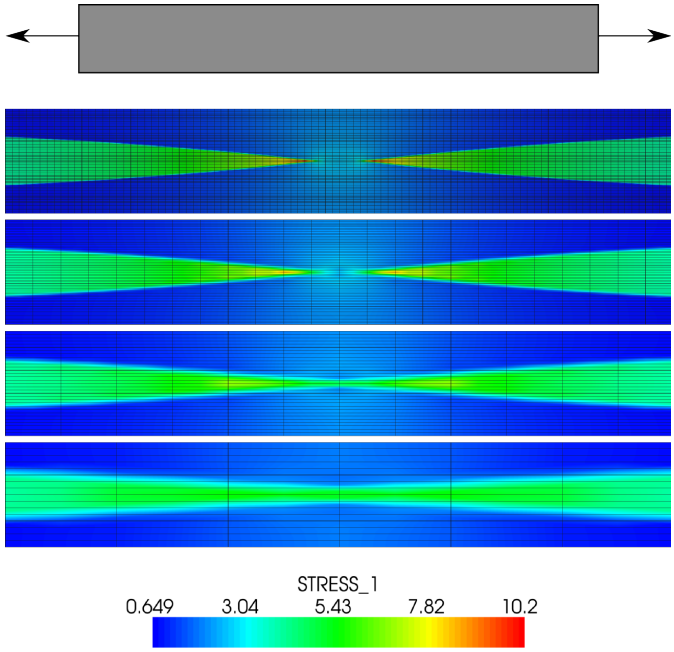

(a) $\max(||\sigma||) = 5.43, 6.72, 8.44, 10.2$

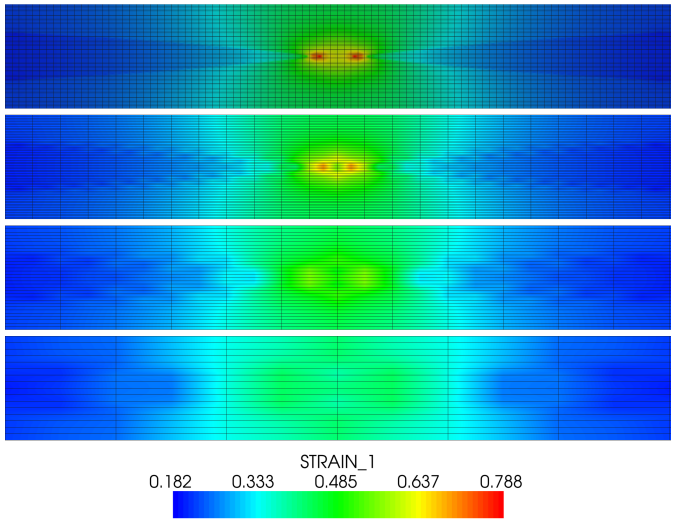

(b) $\max(||\varepsilon||) = 0.430, 0.559, 0.698, 0.788$

Figure 4.4: 2D model showing geometric singularity at a crossover point in lenticular yarns where $V_{y,f}$ is constant across the yarn at 0.7372 in all-yarn cells, graphic showing meshes of 512,2048,8192,32768 cells (bottom coarsest, top finest).

In Figure 4.5 the same problem is shown, where $V_{f,dr} = 0.75$, which means that $V_{y,f}$ at the yarn edges is 25% lower than in the center of the yarn. It can be seen that in this case (as in the case where $V_{f,dr} = 1$) the peak stress doesn't converge, but here maximum strain (which occurs in all-matrix elements away from the yarn tip) starts to

level off.

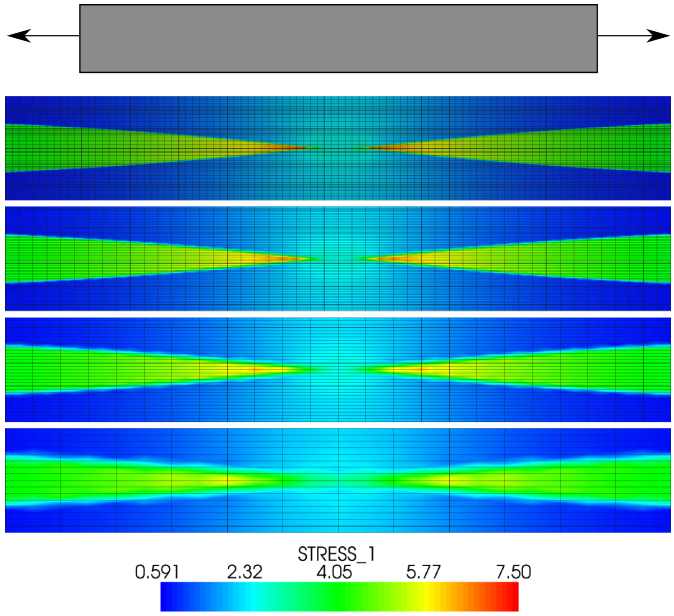

(a) $\max(||\sigma||) = 5.64, 6.09, 6.71, 7.5$

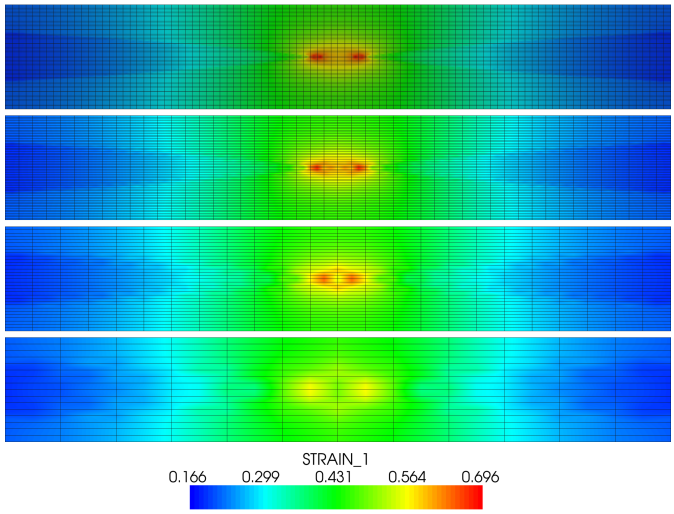

(b) $\max(||\varepsilon||) = 0.563, 0.645, 0.676, 0.696$

Figure 4.5: Identical model as the problem shown in Figure 4.4 but with 25% dropoff in $V_{y,f}$.

4.2 Comparison with conformal FE

The aim of comparing the AMR based method to a conformal meshing based method is to quantify the penalty paid in accuracy for the added robustness in using AMR. Additionally, it is necessary to establish whether the two methods are sensitive to the same geometric and mechanical aspects of the problem. Direct comparison is made somewhat more difficult by the fact that the meshing algorithm modifies geometry internally, i.e. it works to a minimum and maximum edge length which means that the resulting mesh does not exactly overlay the "analytical" geometry formulation used in TexGen. This can have the result that the FE program, when querying the textile model for yarn properties, can obtain matrix properties inside a yarn element. The comparison is performed using the TexGen integrated tetrahedral meshing algorithm on the same textile structure that was analysed in section 3.3 (see Figure 3.11). The conformal mesh is given in Figure 4.6.

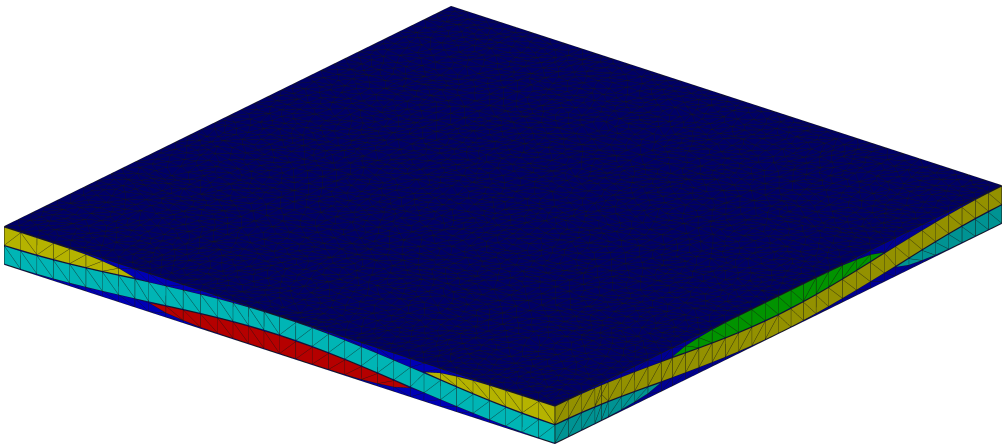

Figure 4.6: Tetrahedral mesh of a single layer plain weave generated using TexGen's internal tet-meshing algorithm

The stiffness convergence for the conformal tetrahedral mesh and the averaged hexahedral meshes are given in Figure 4.7(a). The AMR solution was obtained twice, once with refinement closer to uniform (refinement applied to the top 85% worst ranked elements), once with refinement set more selective (worst 50% refined). The convergence of V_f is given in Figure 4.7(b) since the direct lookup of $V_{y,f}$ in the integration point means that different meshes obtain different V_f values.

When looking at the strain distribution in Figure 4.8 it is seen that the sharp divides present in Figure 4.8(b) are smoothed out in the mixed-material models in Figure 4.8. Resulting in lower peak strain values in the averaged model.

Although the two methods converge to approximately the same V_f (within 0.2%) the RVE stiffness differs by about 1.7%. It is assumed that this is due to the characteristics of linear tetrahedral elements which are known to overestimate stiffness. It is also noted that the tetrahedral mesh contains elements of very poor aspect ratio, due to the high aspect ratio of the resin domain.

In addition, the strain peaks given in Figure 4.8(b) occur at a slightly different location than in Figure 4.8(c) and 4.8(d).

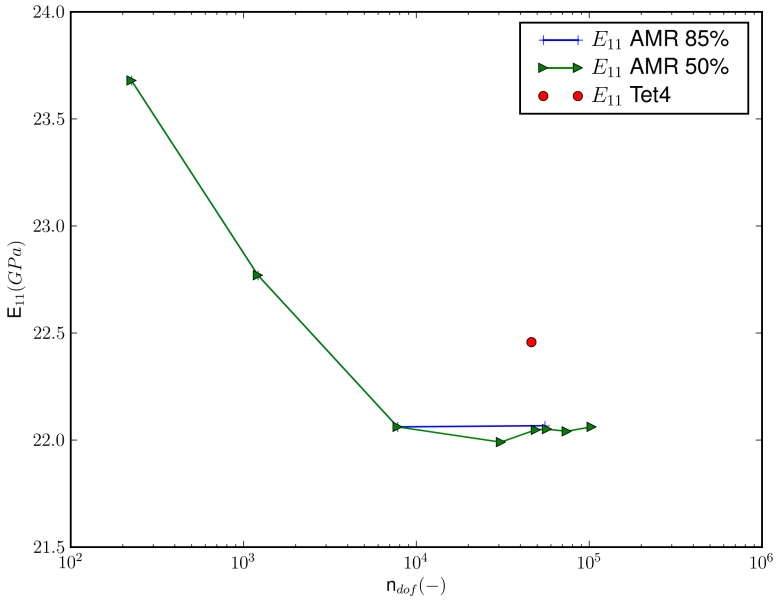

(a) E_{11} convergence upon mesh refinement

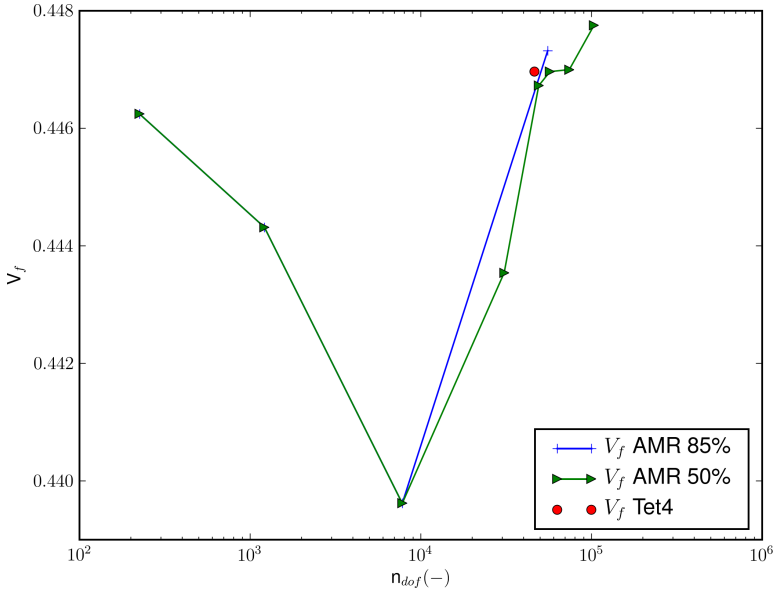

(b) V_f convergence upon mesh refinement

Figure 4.7: Stiffness and volume fraction convergence using AMR in comparison to a conformal linear tetrahedron mesh. It is seen here that for the very selective refinement strategy (refine top 50% error measures) V_f values don't fully converge, but remain in a narrow range of 0.2%.

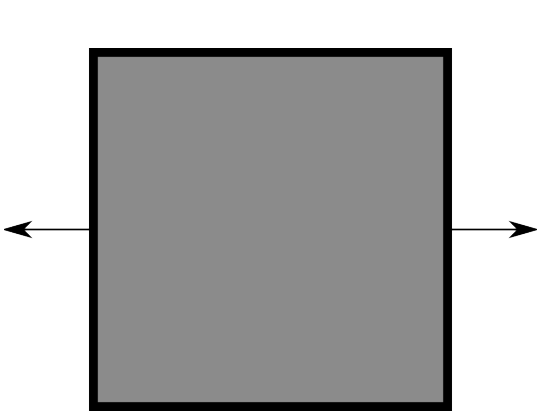

(a) Loading direction used in Figures 4.8(b),4.8(c),4.8(d).

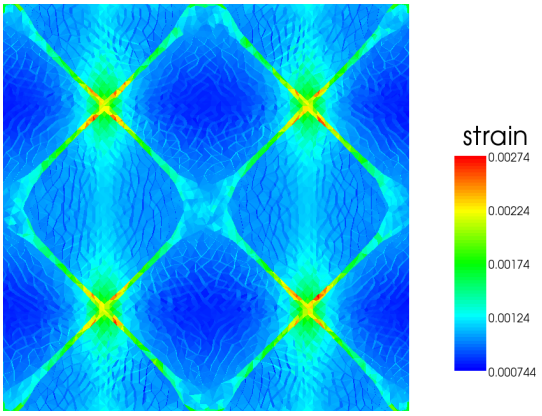

(b) Average element strain $||\varepsilon||$ on the midplane of a tetrahedral mesh of 74828 linear elements

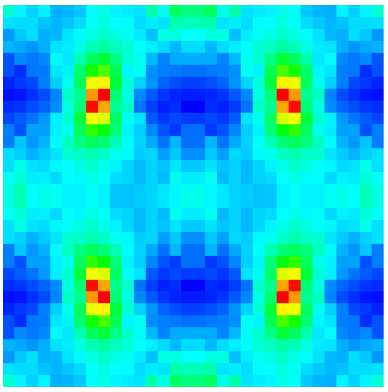

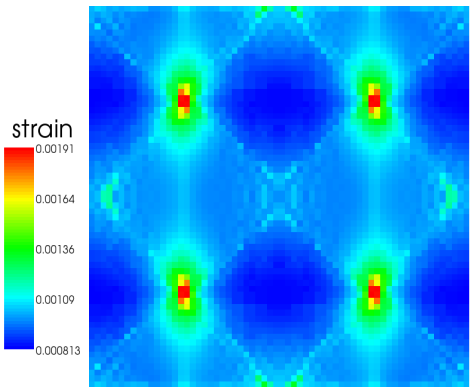

(c) Average element strain on the midplane of a hexahedral mesh of 17732 elements

(d) Average element strain on the midplane of a hexahedral mesh of 147940 elements

Figure 4.8: Comparison of strains in a tetrahedral mesh and hexahedral mesh, showing the averaging effect of material sampling.

4.3 Conclusions

In this chapter the behaviour of FE for typical textile composites based on both uniform and adaptive grid refinement was studied, the following characteristics are noted:

- Both AMR and uniform mesh refinement based methods converge in modelling macroscale stiffness terms.
- The sampling density inside the element can be used to speed up convergence of all stiffness terms.
- Stiffness terms that are more strongly dependent on the presence of a resin layer between the yarns converge slower.
- Local element stress and strain levels in mixed elements don't converge for typical lenticular yarn shapes in 2D or 3D analyses in the range of mesh refinement studied.
- The gradual transverse dropoff of the intra-yarn fibre volume fraction $V_{y,f}$ has the effect of a) dropping the stress concentration level b) making the predicted stress level at the singularity less strongly affected by mesh refinement.

4.3.1 Damage modelling

In the convergence behaviour the performance of the damage model is not considered. The reasons for this omission are twofold, firstly, the local stress terms are seen to converge very slowly if at all. This means that any damage model based on local stress values will show irregular results upon mesh refinement. Secondly, in the current implementation multiple materials exist within a single element, stress terms can be combined to obtain a nonlocal measure in a variety of different ways.

Due to implementation limitations the nonlocal stress measure and damage models were not available in the 2D calculations, making it impractical to obtain convergence characteristics, and impossible to obtain these values as a function of all possible influential parameters.

In the 3D results consistency is promoted by using the same damage model, mesh size and mesh refinement settings across all runs.

Chapter 5

Experiments and parametric analysis

In Chapter 3 the design and implementation of a method suitable for parametric analysis of textile composites was described.

In Chapter 4 the method was used to analyse selected example cases with the aim of comparing it to other methods and showing its behaviour in terms of performance and operation.

This chapter describes the use of the model on a physical textile composite and attempts to relate tensile testing, microscopy data and several parametric numerical studies.

The justification for performing such an experimental study, instead of analysing the large body of experimental data that has been published in literature, is that this allows for extensive microscopic data to be gathered for the *same* plaques that were mechanically tested. I.e. it ensures a *full* and *matching* set of mechanical and geometry data.

Since we are particularly interested in the effects of the internal textile geometry, a test material was chosen for which it is relatively easy to analyse and control the internal geometry. The textile was selected based on the following characteristics:

- Large tow dimensions:
  - Easy to examine using a microscope.
  - Possible to align manually during layup (control nesting).
- Relatively open weave structure:
  - Inter-yarn spacing allows alignment of adjacent layers during layup.
- Simple plain weave structure:

  - Since plaques with multiple layers are made the complexity of the models used is still substantial, in particular when taking into account relative phase shifting of the layers.

- In addition, the same material was used in the work of Crookston [1] from which additional validation data was obtained, this comparison is presented in Appendix A.

The current chapter aims to present a full numerical and experimental study of a single textile, the chapter is structured as follows:

- Experimental results from tensile experiments are presented in section 5.1.
- Microscopy samples are used to analyse the geometry of the textile reinforcement of the tensile specimens, this is discussed in section 5.2.
- A computation model is set up in terms of textile parameters (see Figure 3.11) according to the textile geometric variables found in section 5.2. The parametric analyses are described in section 5.3 and can be subdivided in the following categories:
  - Influence of yarn related variables, in yarn V_f distribution (section 5.3.2), yarn flattening (section 5.3.1) and inter-yarn spacing (section 5.3.3).
  - Influence of multi-layer variables like nesting and phase shifting (section 5.4).
- Conclusions are drawn in section 5.5.

5.1 Mechanical testing

5.1.1 Specimens

The validation material used for the manufacturing of specimens was Vetrotex RT600 glass textile (with a dry areal weight of $600 g/m^2$) combined with Reichhold Norpol 420-100 unsaturated polyester resin.

Two batches of specimens were made each with a different goal:

1. Controlled phase shifting
2. Low void content, high V_f (within the constraints posed by using less than 2 layers)

Controlled phase shifting The plaques made for controlled phase shifting were made out of two layers of textile, hand-layed and hand wetted. Hand lay-up was performed on a back-lit glass plate, the inter-yarn spacing allows the light to shine through and as such allows lining up of two (or more) layers of fabric.

To get a consistent surface quality on both sides of the composite a top glass plate was used and a vacuum was applied after wetting out the fabric. The result was a composite of which the nesting was indeed controlled (being either fully in- or fully out of phase), however, void content was very high (see Figure 5.1) , as was the thickness variation in the specimens. Specimens were cut using a diamond saw with no additional mechanical operations.

Low void content In order to make sure that void content and thickness variation are not overshadowing the influence of the factors under investigation a second batch of specimens was made using a RTM tool and both inlet pressure and an outlet vacuum to drive resin infusion.

Because the thickness between different layups of a 2-layer composite can vary quite significantly (due to nesting and compaction) a PTFE filler plate was used to allow reduction of the mould cavity height.

The result of this method was a set of specimens with much lower void content but with an arbitrary degree of phase shifting throughout the plaque (since the tool does not have a backlight and layers shift when the stack is being transferred from a layup table to the tool).

Another result of using a flexible filler material is a nonuniform thickness of the plaque. This has an effect on the calculated specimen V_f and for each specimen the volume

Figure 5.1: Tensile specimens made attempting to align to layers of plain weave fabric. It can be seen that the specimens have a high void content and are poorly wetted out.

fraction is calculated as follows:

$$\frac{n_l \cdot \rho_A}{t \cdot \rho_{glass}} \tag{5.1.1}$$

Where n_l is the number of layers, ρ_A is the areal weight of the textile, t is the laminate thickness and ρ_{glass} is the density of glass.

In this case dogbone shaped specimens were manufactured using water jet cutting. The guidelines in the ASTM-D3039-95 were used to manufacture the speciments. Due to poor surface quality of these specimens (caused by the water-jet) the sides were ground off to obtain a smooth surface, this caused the specimen dimensions (as recorded in Table 5.1) to deviate from the nominal values specified in the standard.

There were several plaques made but only two of sufficient quality, both of which were 2-layer plaques. They are referred to in graph legends as A and B. Specimen measurements are given in Table 5.1, along with the experimentally obtained moduli, these are given as an average over the first 10 or 20 readings to give an indication of the consistency in the initial part of the tensile test, which is assumed to show linear elastic behaviour.

plaque	specimen	t_1(mm)	t_2(mm)	w_1(mm)	w_2(mm)	V_f(-)	$E_{xx,20}$(MPa)	$E_{xx,10}$(MPa)
A	1	0.87	0.89	8.5	8.5	0.5244	24.421	24.859
A	2	0.94	0.97	8.55	8.56	0.4832	24.317	24.164
A	3	1.01	1.06	8.51	8.51	0.4459	21.979	21.919
A	4	1.08	1.14	8.6	8.59	0.4158	23.951	23.684
A	5	1.1	1.16	8.59	8.59	0.4084	21.702	21.766
A	6	1.09	1.14	8.49	8.49	0.4139	23.047	23.422
A	7	1.04	1.09	8.72	8.77	0.4333	22.595	23.598
A	8	0.98	1.04	8.59	8.53	0.4569	24.166	24.821
A	9	0.92	0.95	8.68	8.65	0.4936	25.483	25.782
A	11	0.96	0.89	8.72	8.96	0.4989	24.292	24.760
B	1	0.82	0.82	8.59	8.57	0.5628	30.670	30.793
B	2	0.85	0.89	8.51	8.5	0.5305	24.997	24.596
B	3	0.92	0.96	8.56	8.56	0.4909	26.486	26.900
B	5	0.98	1.04	8.62	8.6	0.4569	24.171	23.848
B	6	0.97	0.98	8.59	8.59	0.4733	23.593	24.437
B	7	0.99	0.95	8.65	8.64	0.4758	25.128	24.611
B	8	0.91	0.96	8.65	8.67	0.4936	28.579	28.952
B	9	0.86	0.89	8.49	8.51	0.5274	27.848	28.044
B	11	0.9	0.86	8.65	8.7	0.5244	28.635	29.192

Table 5.1: Moduli $E_{xx,20}$ and $E_{xx,10}$ measured as $\frac{\sigma_t - \sigma_0}{\varepsilon_t - \varepsilon_0}$ for $t = 20$ and $t = 10$ respectively

5.1.2 Tensile test results

Tensile tests were performed using an Instron 1195 testing machine, which was connected to a data logging PC recording data from both the load cell and the extensometer.

The results are obtained directly from the Instron binary datafile[1]. Stress-strain curves for specimen batches A and B are given in Figure 5.2. This data is used in section 5.3 in relation to modelling data, where comparisons are made with datasets of similar V_f.

[1]There is a specific note on using legacy binary output files to avoid rounding errors in Appendix D.2

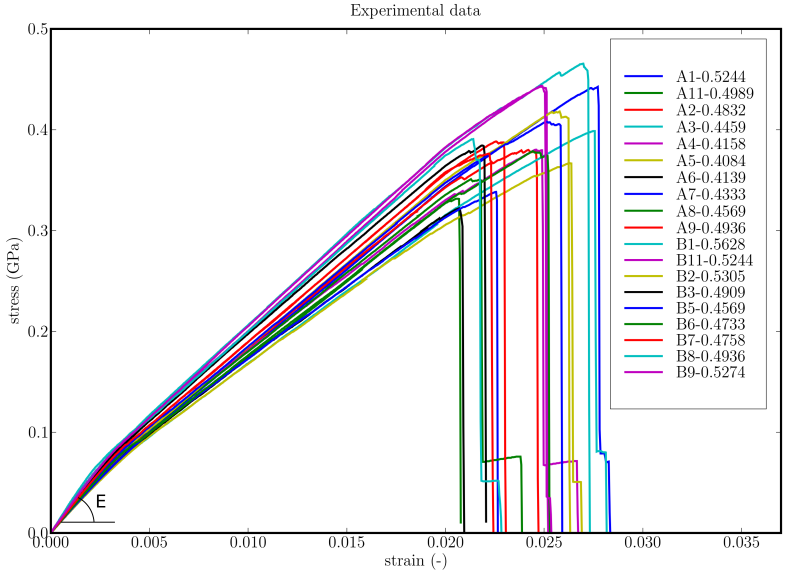

(a) Stresses calculated using specimen thickness as given in Table 5.1. The moduli calculated in 5.1 are computed from the first $10, 20$ load steps.

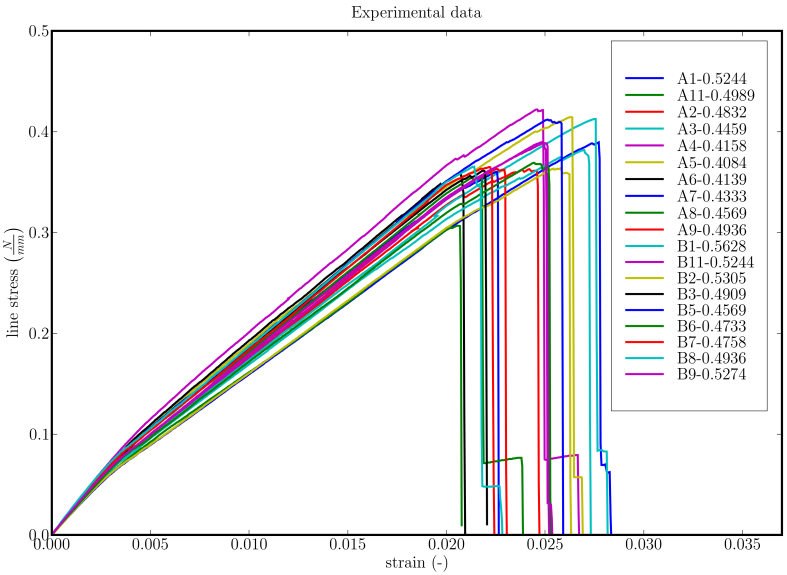

(b) Line stress (stresses in Figure 5.2(a) multiplied by thickness), eliminating the effects of thickness variability

Figure 5.2: Experimental data for 2 layer RT600 dogbone specimens, moulded using RTM and outlet vacuum, it can be seen that there is substantial variation in both the volume fraction and the initial stiffness of the specimen.

5.2 Microscopy

Microscopy has been used to form the geometric input for textile models used in the following sections. The material that was analysed was cut-off material of the same plaques as the tensile specimens (see section 5.1.1).

Since the samples analysed here are not the tensile specimens themselves there is no reason to analyse V_f or shape anomalies except in the *average* sense.

Hence, a method was chosen that would allow generation of a large number of yarn shapes.

Methodology The method of obtaining yarn shapes is as follows:

1. Produce a microscopy sample out of plaque offcuts:
   - Bond together a stack of offcuts.
   - Cut into specimen size pieces (about 25mm).
   - Cast into polyester resin.
   - Cut and polish the specimen surface.
2. Calculate a bilinear focus plane using microscope stage settings and focus parameters in 3 points on the sample surface[2].
3. Scan the surface using automatic stepping of the microscope stage.
4. Stitch images together to form a graphic image of the transverse yarns as seen in Figure 5.3.
5. Correct light-gradient originating from using a side mounted light on the stage.
6. Draw polyline outlines around yarns, also shown in Figure 5.3.
7. Write filled outlines to graphics files, outlines as seen in Figure 5.4 and 5.5.
8. Loop over all yarn shapes and add matrix formulation of graphics file to the weighted average.

An average yarn cross-section is obtained through this procedure which is shown in Figure 5.6. It can be seen here that the shape is closer to lenticular than it is to elliptical. The height-width ratio of the binary image is approximately 1 : 10, the aspect

[2]This is currently a standard method that is implemented in microscope stage controller software, for this work it was implemented as a stage controller user routine

ratio in the samples was in the range [1 : 8, 1 : 15] (disregarding all yarns for which only partial cross sections are scanned).

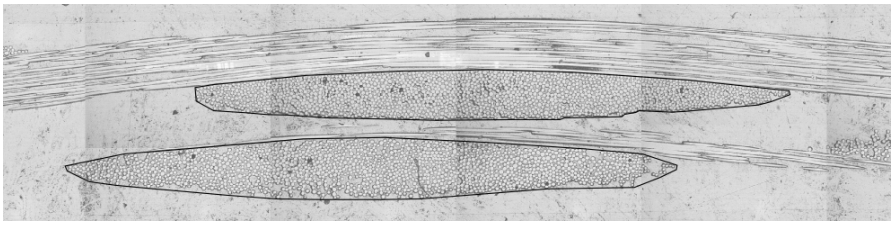

Figure 5.3: Stitched micrographs of yarns in a 2-layer plaque with polyline outline

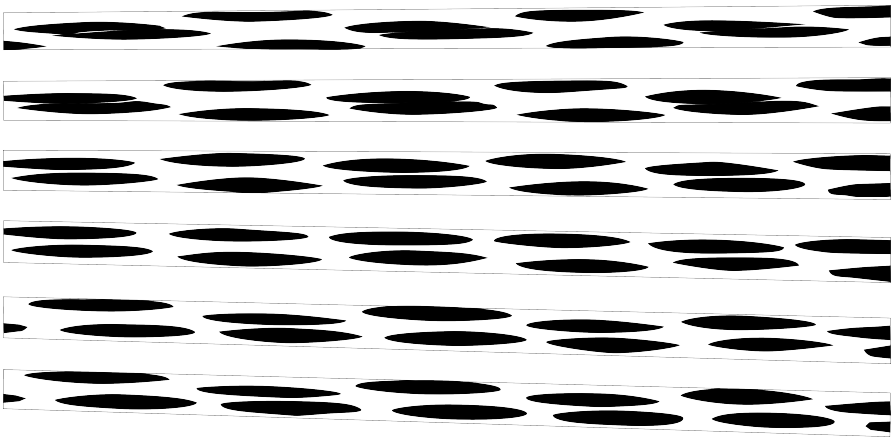

Figure 5.4: Bundle outlines as used for calculation of bundle metrics and matrix content (V_{md}, as defined in Equation 5.2.1). V_{md} per layer (%): $25.743, 18.247, 12.190, 14.126, 18.959, 12.689$ Averaged: 16.9 %

The yarn is assumed to be balanced, which makes it possible to calculate the V_{md} from only the area of the outlined yarns (the transverse yarns are assumed to have the same area). Matrix content for a balanced weave is calculated according to

$$V_{md} = 1 - \frac{2}{A_o/A_y} \tag{5.2.1}$$

where V_{md} the fraction of the total domain that is made up of matrix material (not including the resin in the yarns), A_o is the area of the composite outline, A_y is the area of the yarn outline.

Other yarn metrics that were obtained from the micrographs are given in Figure 5.7.

5.2.1 Conclusions regarding yarn geometry

- Yarn geometry is variable within fairly wide bounds, as an example, aspect ratio varies between 1 : 8 and 1 : 15, with an average of 1 : 10.

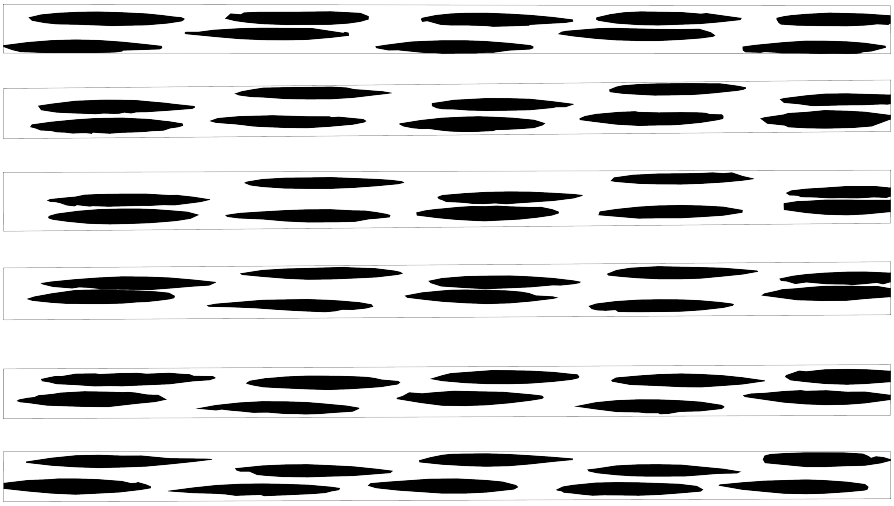

Figure 5.5: Bundle outlines as used for calculation of bundle metrics and matrix content. V_{md} per layer (%): $27.934, 32.328, 37.783, 36.230, 29.265, 28.028$ Averaged: 32.1 %

(a) Sum of all cross section displayed in grey-scale

(b) Binary image of all cross sections using a threshold level of 0.5 (where 1.0 is indicates a pixel covered by all 105 whole cross sections shown in Figures 5.4 and 5.5)

Figure 5.6: Average cross section as obtained from bundle outlines given in Figure 5.4 and 5.5

- Average yarn geometry is fairly consistent (i.e. averaging over any larger subset of yarn shapes results in a lenticular cross section), the lenticular base shape as used in TexGen is a good representation of the yarn shape present in the textile.

5.2.2 Limitations

It is noted here that there are a number of limitations to the data gathering strategy employed in this section.

- No attention is paid to combinations of yarn widths or correlation of the yarn width to other factors such as local specimen thickness or nesting. This means

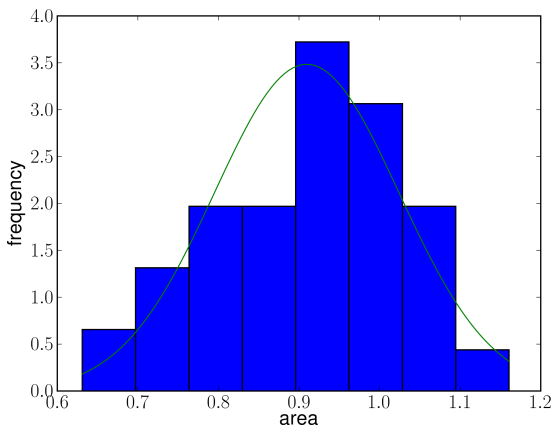

(a) Yarn area distribution, $\mu = 0.91mm^2$, $\sigma = 0.11mm^2$

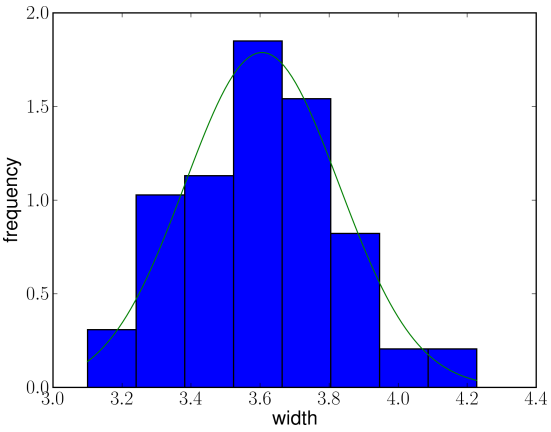

(b) Yarn width distribution, $\mu = 3.6mm$, $\sigma = 0.22mm$

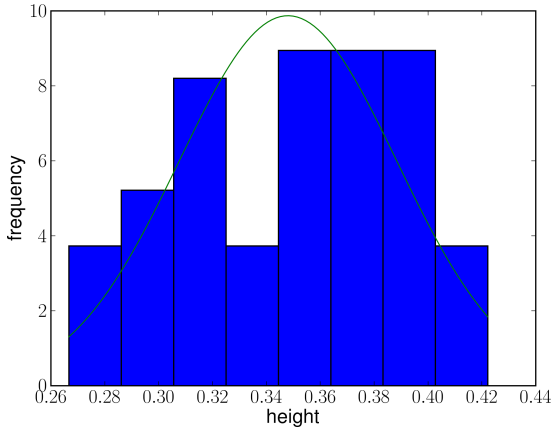

(c) Yarn height distribution, $\mu = 0.35mm$, $\sigma = 0.04mm$

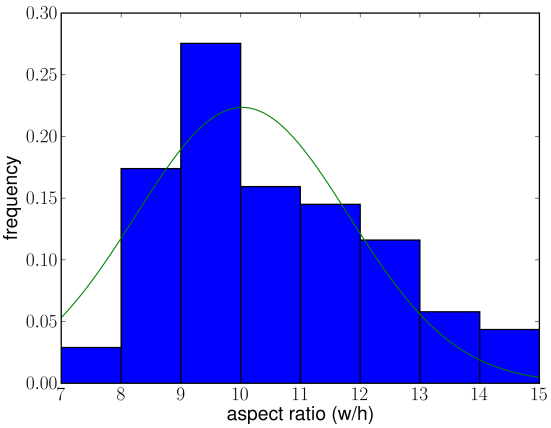

(d) Yarn shape aspect ratio distribution, $\mu = 10.02$, $\sigma = 1.79$

Figure 5.7: Yarn cross section area and cross section width are seen to be approximately normally distributed. The height distribution does not fit this pattern, which may be due to the fact that the height reading is strongly affected by twisting of the cross section.

that it is not known from the current data whether yarns vary in width very locally (due to some local settling mechanism) or over a longer section of the specimen (because the specimen is being flattened).

- The shape of a yarn section has not been correlated to a location along the yarn, predominantly because this requires interpretation of the image of the longitudinal yarn, which is difficult to obtain with sufficient accuracy.
- All yarn section cuts are assumed to be orthogonal to the yarn path.
- Strong conformance of the yarns to longitudinal yarns can change shape in an

anisotropic manner, which can have the effect (when averaged pixel-by-pixel as described above) of reducing the apparent tow width (as indicated in Figure 5.8).

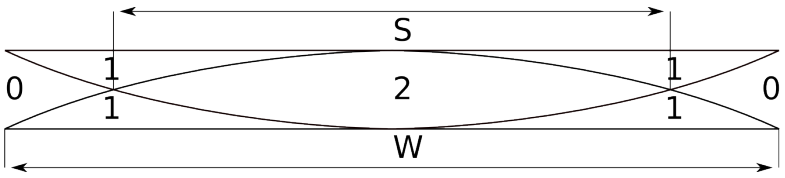

Figure 5.8: Pixel count in yarn domain when summing two opposite conforming yarns, where S is the apparent tow width and W is the actual tow width.

5.3 Parametric studies

This section describes a number of numerical parametric studies on textile structures representative of the textile used for tensile testing in section 5.1.

From the section describing the optical measurements and analysis of the samples there are a number of variables that warrant particular attention.

- Yarn properties
  - Horizontal inter-yarn spacing
  - Vertical inter-yarn spacing
  - Internal yarn fibre volume fraction distribution $V_{y,f}$ (this was also noted by Lomov et al in [43] as an important factor)
  - Flattening of the yarn where the yarn is touching the tool surface
- Multilayer properties
  - Nesting
  - Phase shifting of adjacent layers

The parametric studies are presented to see to what extent predicted 2D stress concentration factors have an effect on the 3D mechanical response.

In practice the yarn input variables have an influence on what damage mechanism is triggered first, and propagation of damage occurs subsequently. Plain weave textiles are interesting in this perspective since different modes can potentially appear first (depending on the geometric variables). This is shown in Figure 5.9 where the transverse yarn damage variable is given at 0.9 times damage initiation loading, showing both the crossover and the middle of the yarn as potential initiation points.

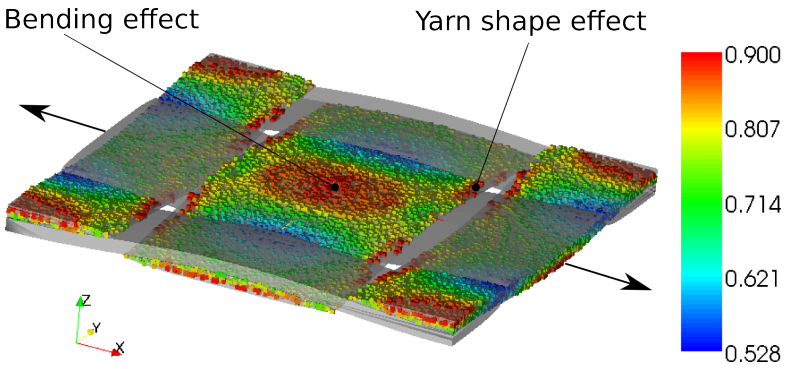

Figure 5.9: Transverse yarn damage plot for a single layer plain weave based composite in tension

Models in this section are described in terms of the parametric model introduced in section 3.3, Table 3.1. The parameter set used in this chapter is defined as a baseline with alterations, the baseline table is given in Table 5.2, the alterations are given in the section at hand. The baseline variable table was formed such that an expansion to two layers leads to yarn aspect ratios is the range observed in section 5.2.

length	8
γ_x	[0,0.25]
γ_y	[0,0.25]
h_n	1
numlayer	1
vgap	0.02
hgap	0.2
height	0.5
fibre_area	0.42
$V_{f,dr}$	1.0
f_f	0.1
rotate	[0,0]
domainsize	[1,1]
weavestyle	plain

Table 5.2: Geometric parameter set used for baseline single layer textile, variations discussed in this chapter are single or dual parameter alterations of this set. Parameter declarations are given in Table 3.1.

Computations Through this section the solver parameters are kept constant in an attempt to keep modelling variables from influencing the relative outcome of simulations.

The models are solved using 5 levels of refinement with a base mesh of $[4, 4, 1]$ cells for a single layer textile and $[4, 4, 2]$ cells for the nesting cases, where the first 3 levels are uniform refinement. At each refinement step the elements within the highest 85% error estimate readings are flagged for refinement. A maximum refinement level mismatch of 1 level is allowed, if the mesh does not satisfy this condition the coarse elements are refined.

The nonlocal feature size is set to $2.8mm$. A 2^3 gaussian integration rule is used using 8-node hexahedral elements using linear Lagrange shape functions.

In Petsc the solver settings `-ksp_type bcgs -pc_type sor` are used (biconjucate gradient solver using successive overrelaxation as preconditioner) with a error norm cutoff of $1e-6$. This was found to converge in all cases and to run faster than `gmres` (generalised minimum residual) in the cases considered.

Using these settings runtime for a single linear static analysis (or damage step) was about 5-10mins on a single AMD opteron 2.2 GHz core.

5.3.1 Flattening of yarns

When manufacturing textile composite parts using solid tools the preform conforms to the tool surface, resulting in local compression of the dry yarns. The deformation induced in the preform is complex and would require analysis with the appropriate dry fibre material models to predict, which is outside the scope of this work (refer to [11] for more information regarding dry textile modelling). Here, this mechanism is taken into account using two assumptions:

- The yarn cross section area is reduced by the overlap area between the tool and the undeformed yarn (see Figures 5.10(a) and 5.10(b)).
- The change in global V_f caused by reducing the yarn cross-sectional area is taken up by the average yarn $V_{y,f}$ such that the fibre area is constant along the yarn.

Implementation is done in TexGen by defining a parameter f_f which is defined as the maximum height of a yarn measured from its centreline, at the section where the undulation reaches the RVE surface (see Figure 5.10).

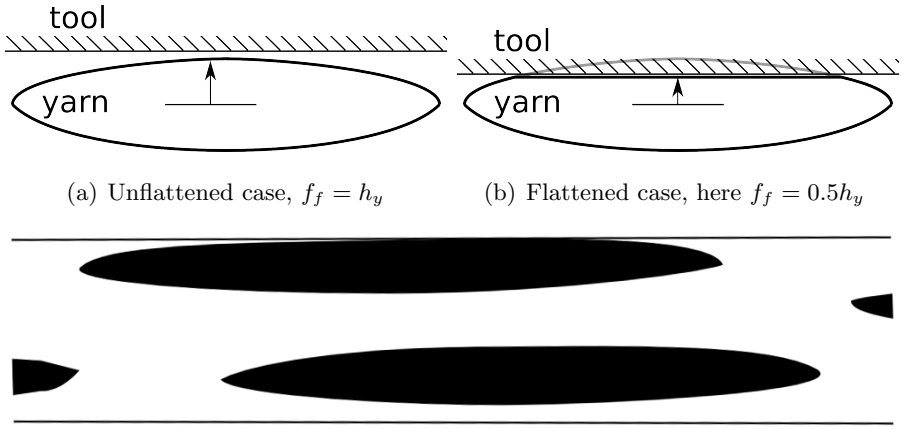

(a) Unflattened case, $f_f = h_y$ (b) Flattened case, here $f_f = 0.5h_y$

(c) Flattened yarn micrograph outline (sample from Figure 5.4)

Figure 5.10: Model representation of a yarn compressed by a tool surface, ↑ indicates the f_f parameter used to indicate yarn flattening

Modification of the yarn cross section in this manner reduces the cross sectional area of the yarn and raises $V_{y,f}$ in that section.

Local increases in $V_{y,f}$ are linked to both stiffness and strength through micromechanics (in this case in the form of the ICAN micromechanics models as described in section 3.2.2), it locally increases the stress level in sections of the yarn close to the tool surface (stiffness effect) and locally decreases strength in the same areas (strength effect).

When looking at the relation of strength to V_f as represented in Figure 3.7 it is expected that the strength effect will have a bigger impact. Whether or not this will result in a qualitative change in the damage progression sequence (start damage onset in a different position) in representative materials is the topic of the analysis in this section.

Three extreme cases are analysed, relating to high, medium and low values of f_f.

The effects of f_f on the geometry of a single layer (which is affected on both top and bottom surface) is shown in Figure 5.11. It can be seen that the flattening affects both the actual V_f as well as the location in the model where peak V_f is reached.

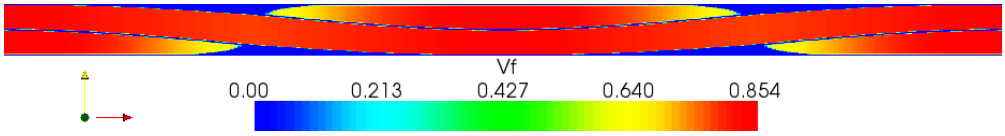

(a) $f_f = 0.07$

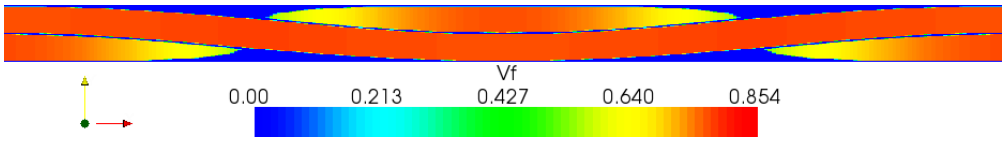

(b) $f_f = 0.09$

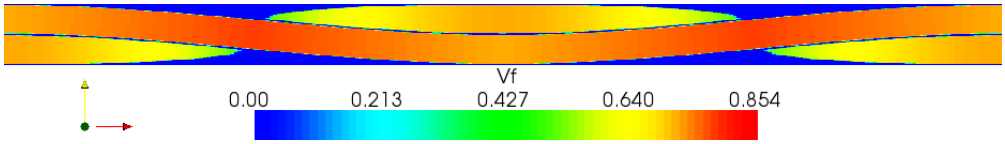

(c) $f_f = 0.11$

Figure 5.11: V_f plotted on the 2D grid for three levels of flattening $f_f = 0.07, 0.09, 0.11$, a quadratically distributed 15% sideways dropoff in $V_{y,f}$ is assumed ($V_{f,dr} = 0.85$)

When monitoring the transverse stress in the off-axis yarns (see Figure 5.12) it can be seen that an increase in σ_{xx} of about 45% exists for $f_f = 0.11$ to $f_f = 0.07$. Figure 5.11 shows that in this location the fibre density $V_{y,f}$ is also higher, leading to lower transverse strength. The combination of these two factors would suggest a significantly lower damage initiation load for the flattened composite than for the unflattened case. When looking at Figure 5.13 it can be seen that damage initiates at about 15% lower stress (see Figure 5.13(b)) in the flattened case. The fact that the effect is not very pronounced is most probably due to a much lower bending effect in the 3D 2-layer unit cell than in the 2D slice.

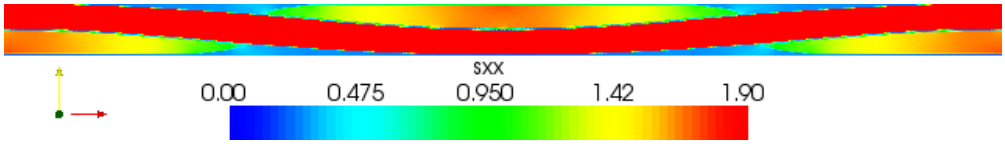

(a) $f_f = 0.07$

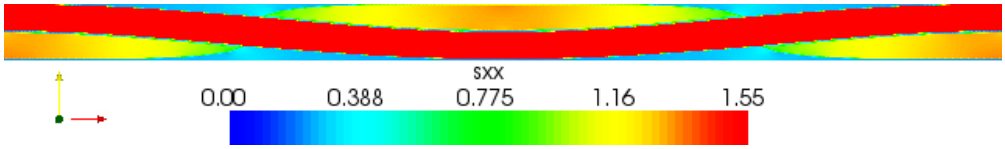

(b) $f_f = 0.09$

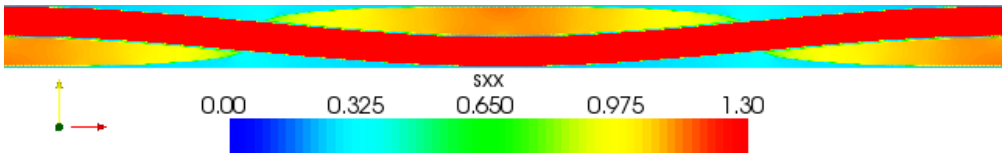

(c) $f_f = 0.11$

Figure 5.12: σ_{xx} plotted on the 2D grid for $f_f = 0.07, 0.09, 0.11$, the colour scale is adjusted to the σ_{xx} range that occurs in the transverse yarn, loading parallel to $x-$axis

Conclusions

In this section the effect of flattening of yarns, as happens in compressed preforms where rigid tooling surfaces are used, is investigated.

It is seen that using the current damage model this effect can account for a 15% change in strength, as well as a 13% variation in stiffness. The change in stiffness corresponds directly with the change in volume fraction. The strength variation is dominated by the assumption that local yarn volume fraction $V_{y,f}$ increases upon yarn compression, which lowers the transverse strength.

The measure in which $V_{y,f}$ drops off towards the side of the yarn is approached in this section by taking a 15% as maximum and 0% as minimum (higher values have been reported in literature, but this would lead to unrealistically high $V_{y,f}$ values in the middle of the yarn in the current model). No attempt was made to perform proper statistical analysis of $V_{y,f}$ dropoff on the specimens obtained. However, point checks of the micrographs show that it is present. Inspection of micrographs also shows that there is merit in investigating the effects of through yarn-thickness changes in $V_{y,f}$, see Figure 5.14.

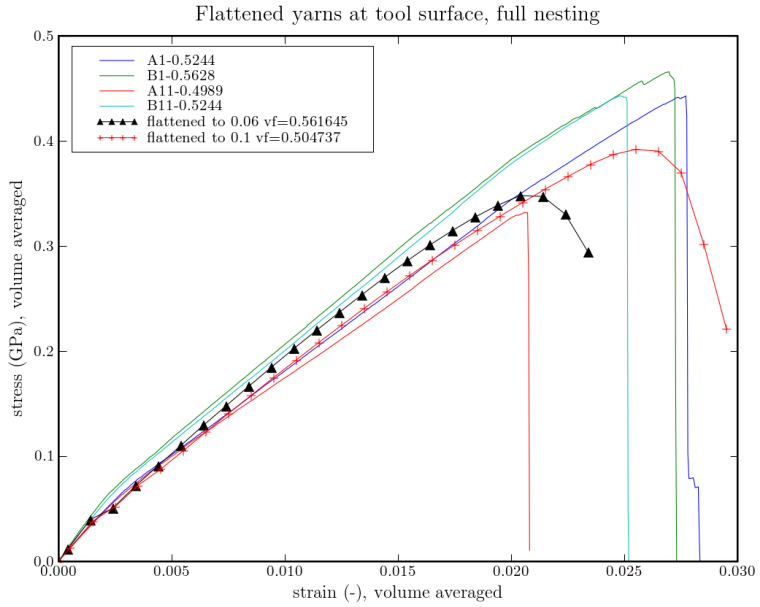

(a) Stress strain curve for yarns with $f_f = 0.06, 0.1$ in a 2-layer nested textile along with experimental results of specimens spanning the same V_f range

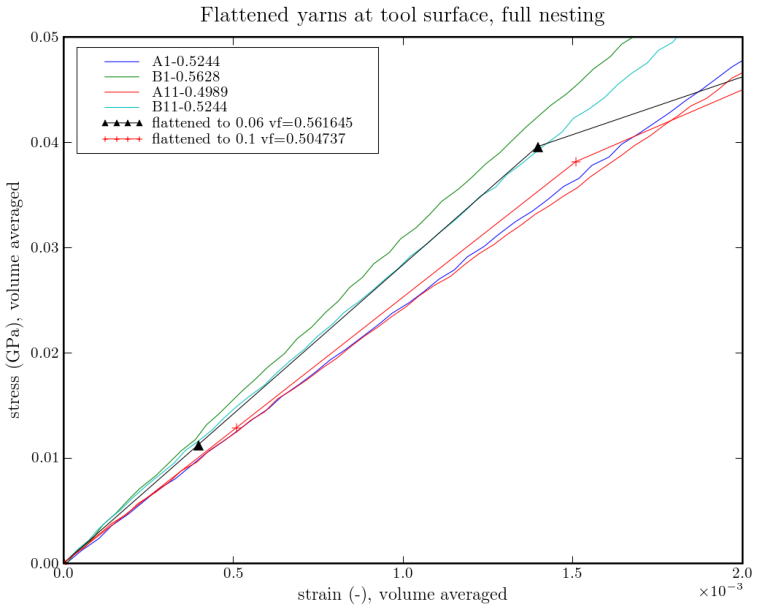

(b) Close-up showing the damage steps for the stress strain curve given in Figure 5.13(a)

Figure 5.13: The effect of flattening of yarns in 3D analysis. Computed V_f values are given, the higher V_f in the flattened case is due to the fact that the same fibre area yarns are inserted in a smaller RVE. Experimental curves for specimens (see Table 5.1) with similar V_f values are inserted from Figure 5.2.

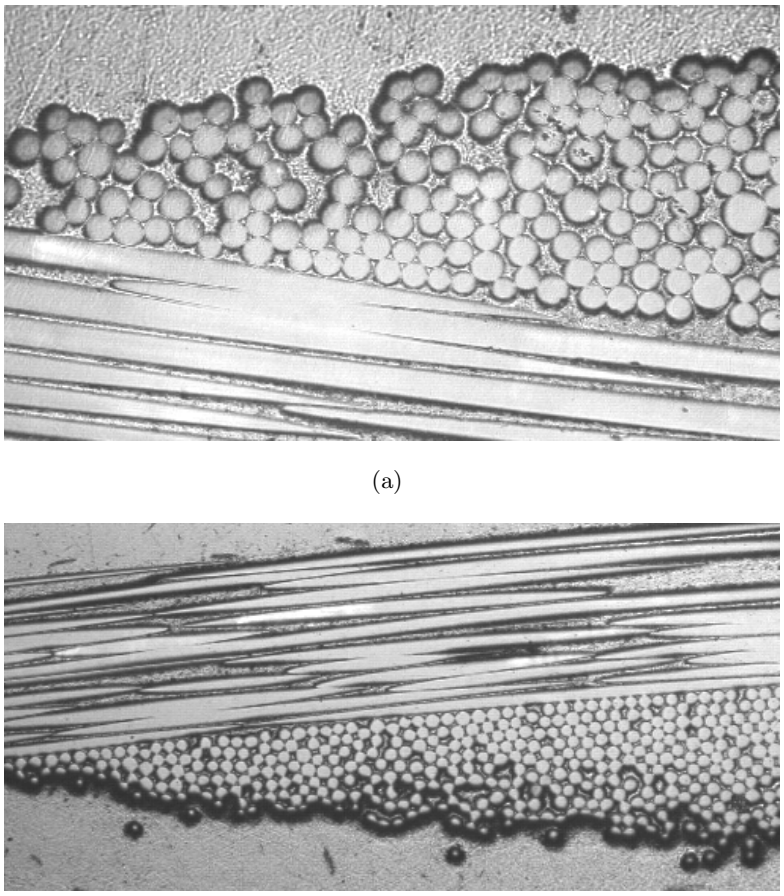

(a)

(b)

Figure 5.14: Micrographs showing near optimally dense stacking of fibres adjacent to a longitudinal yarn and increasingly loose stacking towards the free edge of the yarn

5.3.2 Yarn internal V_f distribution

Assumptions regarding internal V_f distribution of yarns can have a large impact on the predicted stress distribution in the textile geometry as well as affecting the local strength of a composite. The intra-yarn volume fraction $V_{y,f}$ is coupled to the stiffness and strength through micromechanics and, in the case of strength predictions, the relation is increasingly strong towards higher values of $V_{y,f}$, as was illustrated in Figure 3.7.

This phenomenon has been reported earlier by Koissin, Ivanov and Lomov [44]. It can be seen in Figure 5.15 that the current specimens also show a different $V_{y,f}$ nearer the side of the yarn than in the center.

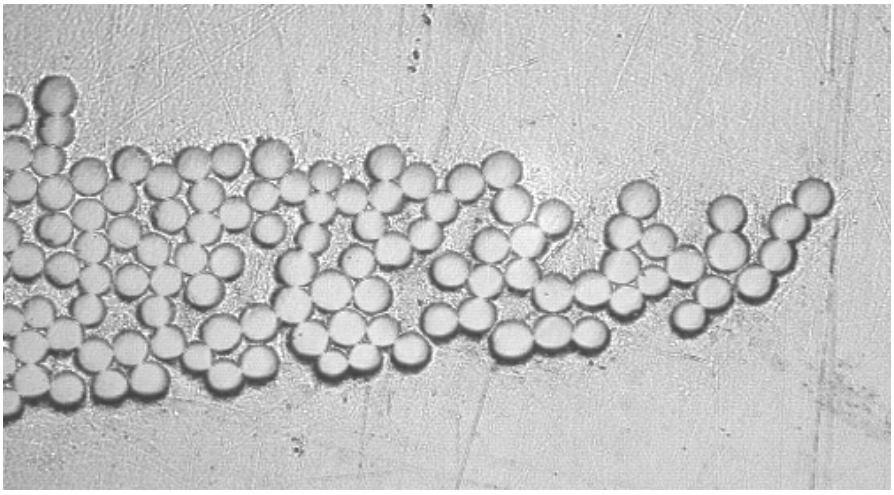

Figure 5.15: Micrograph of a tow cross section where inter-fibre spacing increases towards the tow end (i.e. $V_{y,f}$ drops off)

Because of the difficulty associated with systematic image analysis of such pictures, as well as the high picture resolution needed to obtain accurate results, the problem is handled by assuming a range (from 0% dropoff to 15% dropoff) and evaluating the effect this has on mechanical properties.

Damage initiation: The effects of different V_f distribution on the stress distribution is illustrated in 2D in Figure 5.16, which takes a slice from the textile model shown in Figure 5.16(a). The slice shows the point where the sides of transverse yarns meet as they cross over. It can be seen here that peak stress is distributed more evenly in the case of a larger $V_{f,dr}$. Coupled with higher local strength (since lower local V_f) this would lead to the prediction that, dependent on the assumed $V_{y,f}$ distribution, damage could initiate first in the middle of the transverse yarns ($V_{f,dr}$ higher) or in the transverse yarns at the crossover.

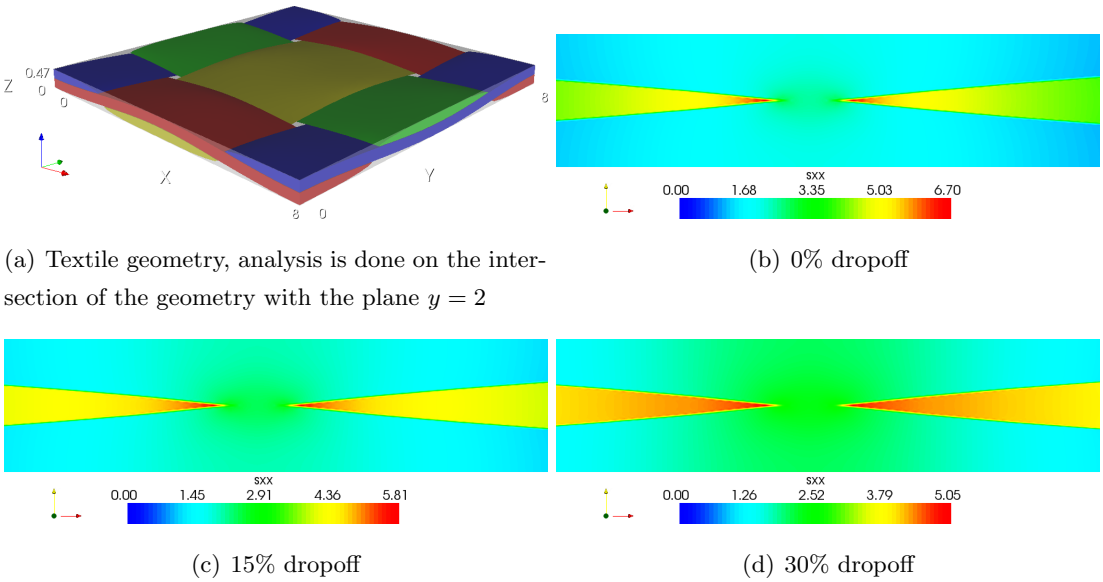

(a) Textile geometry, analysis is done on the intersection of the geometry with the plane $y = 2$

(b) 0% dropoff

(c) 15% dropoff

(d) 30% dropoff

Figure 5.16: 2D plane strain analysis of crossover geometries with different V_f distribution. The colour scale is adjusted to the stress range present in the yarn. It can be seen that the stress concentration factor is greatly lowered by having a sideways dropoff in V_f within the yarn. Loading direction parallel to the $x-$axis.

3D analysis of the composite confirms this effect (see Figure 5.18) but it is less pronounced than in the 2D analysis.

The point of damage initiation (see Figure 5.18) is seen to lie on the location indicated in Figure 5.16 as a concentration in transverse yarn stress (the point "connection" between two yarns).

Discussion This section shows that the effect of intra-yarn fibre volume fraction $V_{y,f}$ has a strong effect on predicted damage initiation and a significant effect on tensile strength.

This result shows in 3D failure analysis but originates from the combination of increasing local $V_{y,f}$ and the corresponding decrease in transverse strength. The decrease in transverse strength is based on stress concentration factors occurring in arrangements of cylindrical fibres with uniform inter-fibre spacing. As can be seen from the micrographs (Figures 5.14 and 5.15), this simplification is not quite representative of actual fibre arrangements.

In particular, it is observed that randomness in fibre arrangement is more likely to occur in more loosely stacked fibres, and that such randomness will also have a detrimental effect on transverse strength (since it will result in smaller minimum gap size between

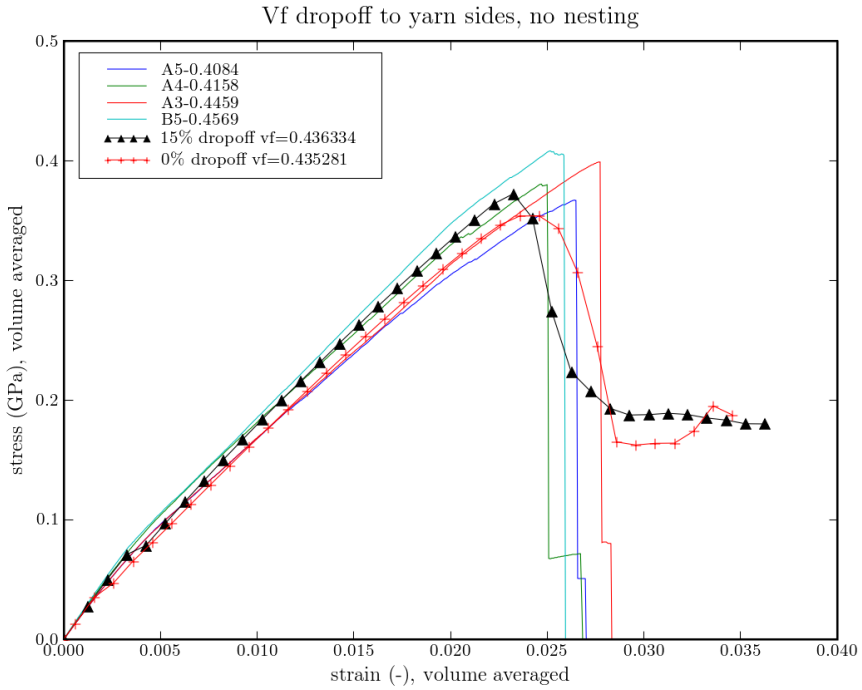

(a) $V_{f,dr} = 0\%$ shows a 5% decrease in strength compared to $V_{f,dr} = 15\%$

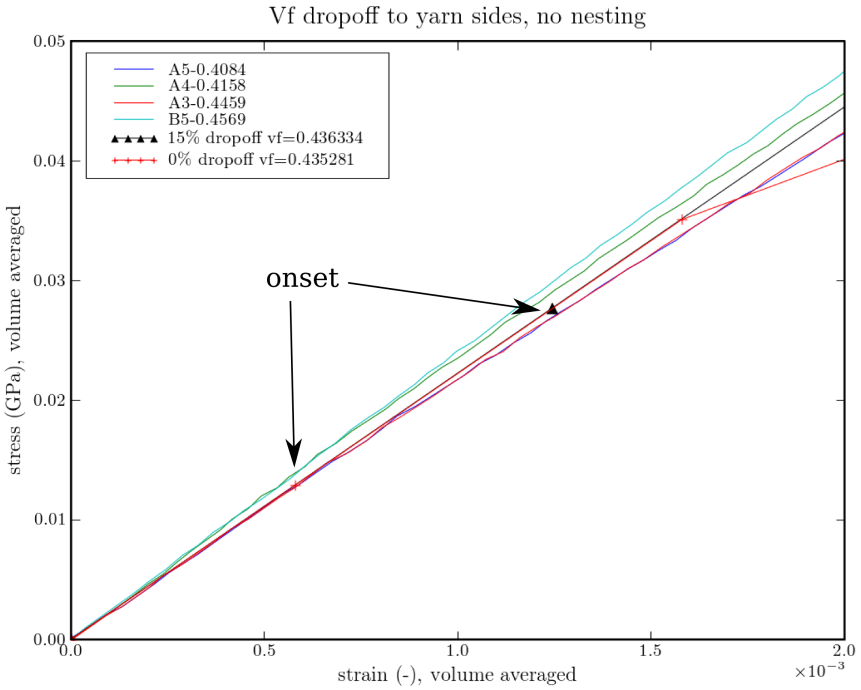

(b) $V_{f,dr} = 0\%$ relates to 50% earlier onset of damage

Figure 5.17: Effects of V_f dropoff on the stress strain response

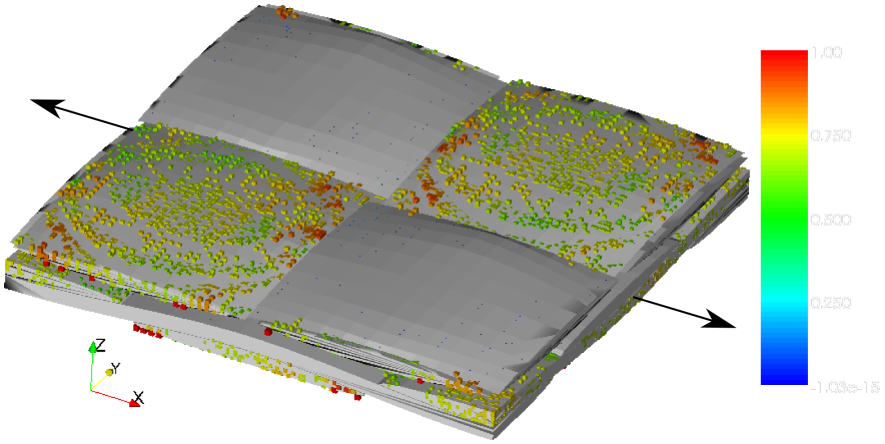

(a) $V_{f,dr} = 15\%$

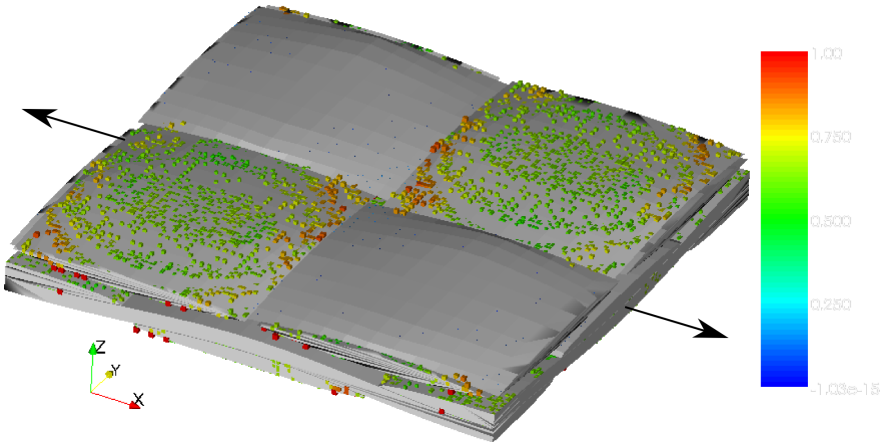

(b) $V_{f,dr} = 0\%$

Figure 5.18: Integration point damage (transverse tow damage mechanism) given for $V_{f,dr} = 0.85, 1.0$. Both plots show damage variable D ranging from 0 to 1 (first loadstep). It can be seen that in the $V_{f,dr} = 15\%$ case the area of high failure index is wider and the middle of the yarn is closer to initial damage.

the fibres, resulting in higher stress concentration factors).

No attempt has been made to incorporate the effect of higher randomness in loosely stacked fibres on mechanical properties into the simulations. Should this be done it could take the form of an addition to the micromechanics models.

5.3.3 Inter-yarn spacing

The inter-yarn spacing can be seen to have significant effect on the intensity of the stress concentration that dominates damage initiation in transverse yarns (interfering with the effect of V_f distribution as shown in section 5.3.2).

2D results are given for three values of g_h in Figure 5.19. The stress concentration factor seen in the 2D analysis is about 15% (increase in stress for the sharper yarns), relating to the same grid size and material sampling rate, as well as the same $V_{f,dr}$ (this is explicitly noted since in section 4.1.2 it is concluded that the stress level is strongly mesh size dependent).

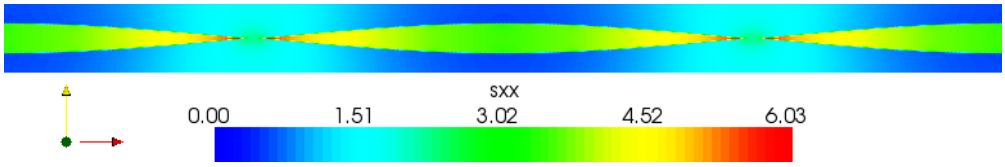

(a) $g_h = 0.1$

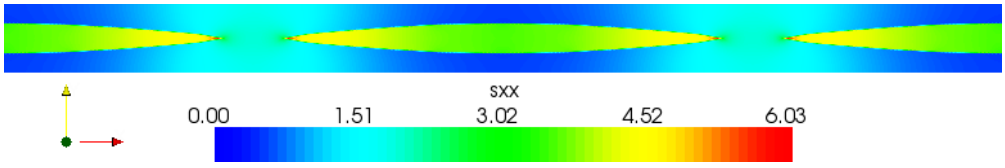

(b) $g_h = 0.5$

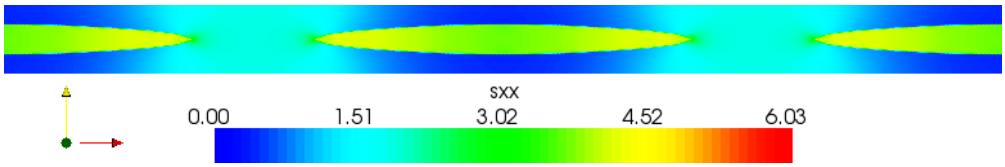

(c) $g_h = 1.0$

Figure 5.19: Stress concentration reduction as a function of increased inter-yarn spacing. σ_{11} is given for loading parallel to the $x-$axis.

3D analysis for the same textile (see Figure 5.20) shows that the sharper yarn shape gains about 6% in strength for a 12% increase in volume fraction.

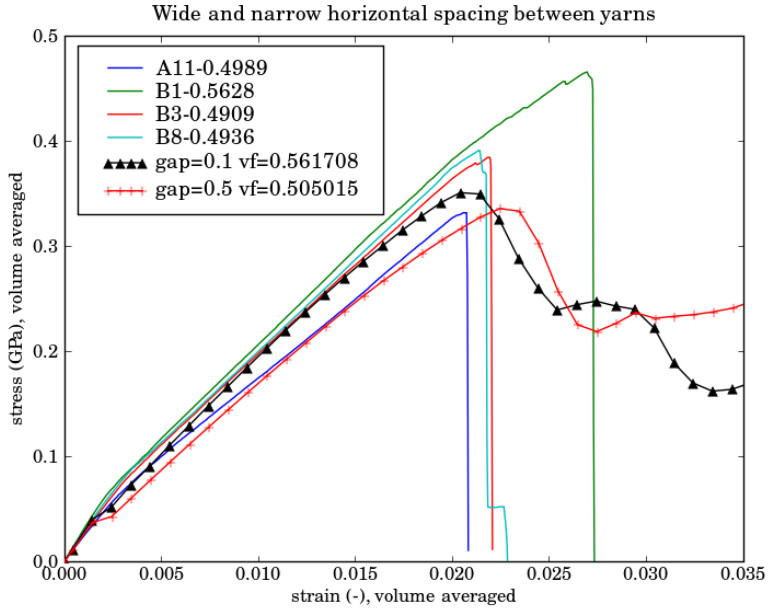

(a) Strength marginally higher in the low g_h scenario

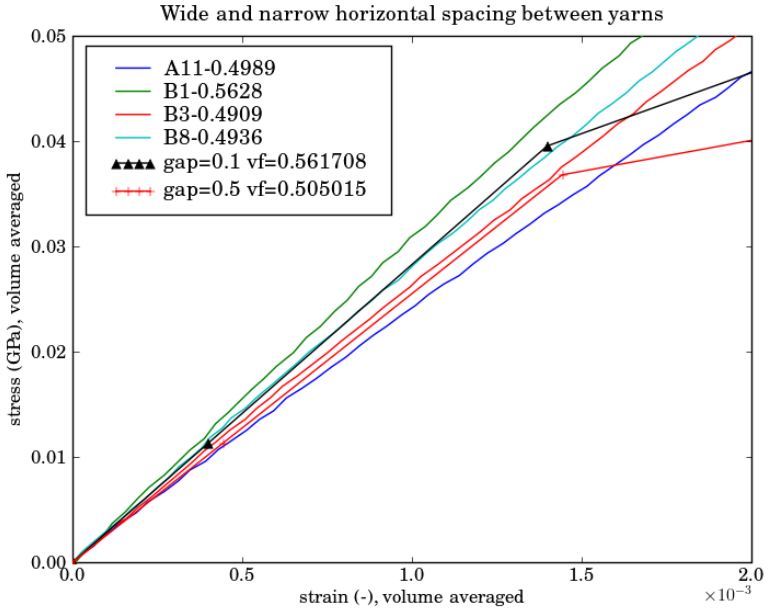

(b) Initial damage occurs at the same stress level for $g_h = 0.1, 0.5$

Figure 5.20: Two values of g_h analysed in 3D axial tension, the models are normalised by maximum $V_{y,f}$. For this reason there is a significant difference in V_f. The damage initiation point as well as failure are predicted at practically the same stress level.

5.4 Nesting and phase shifting

Nesting is the phenomenon that occurs when surface undulations of two layers interlock and the stack thickness becomes thinner than the summation of thicknesses of the individual layers. The degree to which this can occur is dependent on the phase shift between the two layers which is denoted by $\gamma = [\gamma_x, \gamma_y]$ being the phase shift in x and y direction respectively (given in terms of λ which is the undulation length in the textile at hand). In Figure 5.21 three configurations with different phase shifts are given.

From geometric inspection of textiles it follows that "simpler" textiles (such as plain weaves) have more scope for nesting than satin or twill woven textiles.

The effect that is illustrated in the results from a plane strain analysis presented in Figure 5.22, where stress (σ_{xx}) contours are given for two levels of nesting.

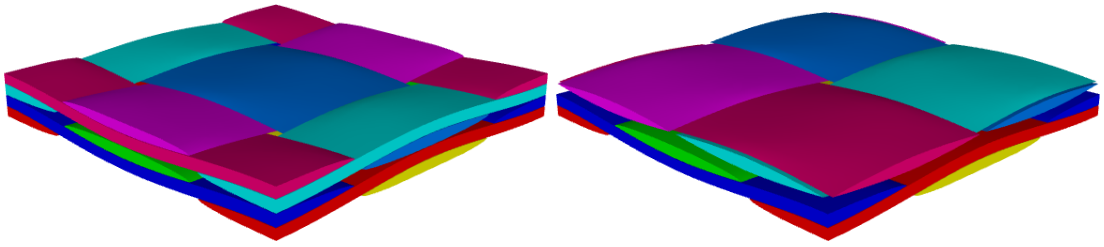

(a) $\gamma_x, \gamma_y = 0, 0$

(b) $\gamma_x, \gamma_y = 0.25, 0.25$

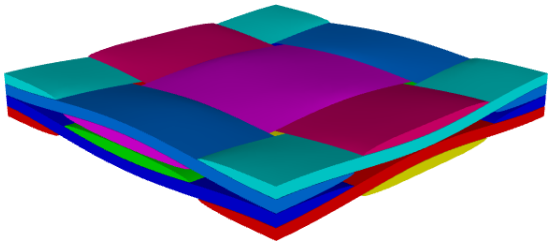

(c) $\gamma_x, \gamma_y = 0.5, 0$

Figure 5.21: Nested plain weave textile in 3 different relative layer configurations as given through the phase shift variables γ_x, γ_y as given in Table 3.1.

5.4.1 Bending effects

Bending effects related to nesting work in two ways:

1. Nesting affects the thickness of multilayer laminates which affects the bending stiffness
2. Waviness in yarns underlying the nesting can be synchronous or mirrored in adjacent layers. In the case of mirroring the out-of plane terms of two deforming layers

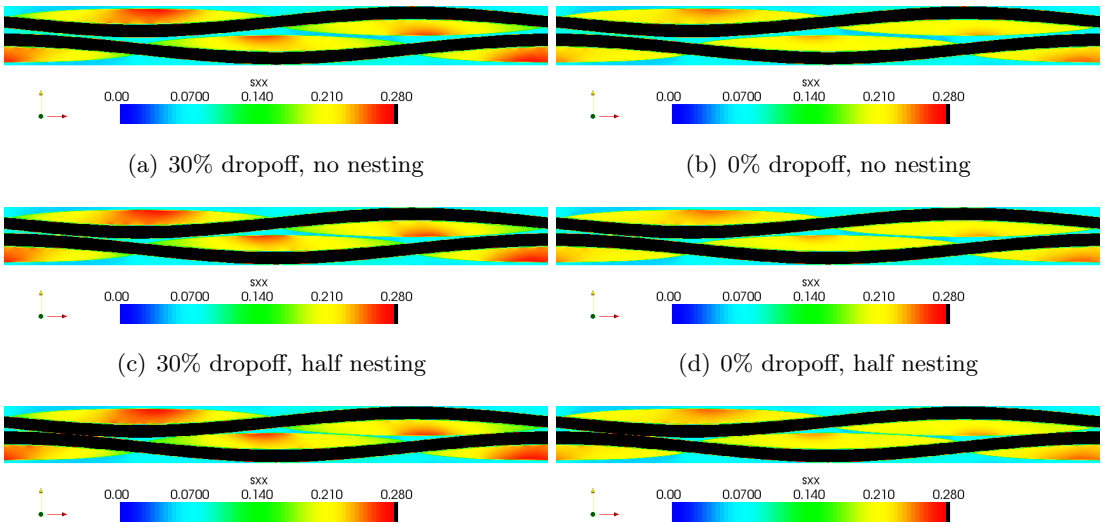

(a) 30% dropoff, no nesting

(b) 0% dropoff, no nesting

(c) 30% dropoff, half nesting

(d) 0% dropoff, half nesting

(e) 30% dropoff, full nesting

(f) 0% dropoff, full nesting

Figure 5.22: σ_{11} contours at a slice taken from geometry at $y = 1.5$, it can be seen that local stress intensity in the bundles rises as layers get closer together. The loading is applied parallel to the $x-$axis.

work cancel each other out, while in the synchronous case the resulting composite will be wavy (locally bent). This phenomenon was also observed by Ishikawa and Chou [88].

Bending effects diminish for larger stacks of textile layers; however, since the experiments related to this thesis were performed using 2-layer specimens, the effects are present. Table 5.3 gives the results of a factorial study on the relative strength of $V_{f,dr}$ and h_n (see Table 3.1), showing that the case of a 2-layer textile the effect of $V_{f,dr}$ is expected to be far stronger than the effect of h_n.

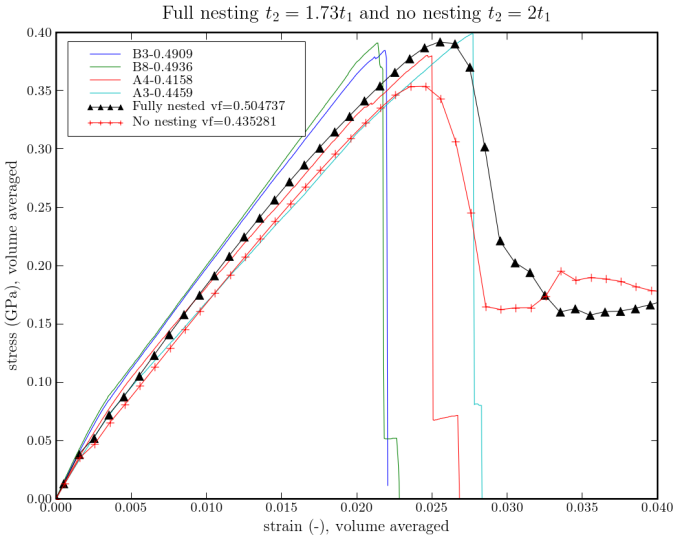

(a) Nested configuration showing about 10% higher tensile strength for 15% higher V_f

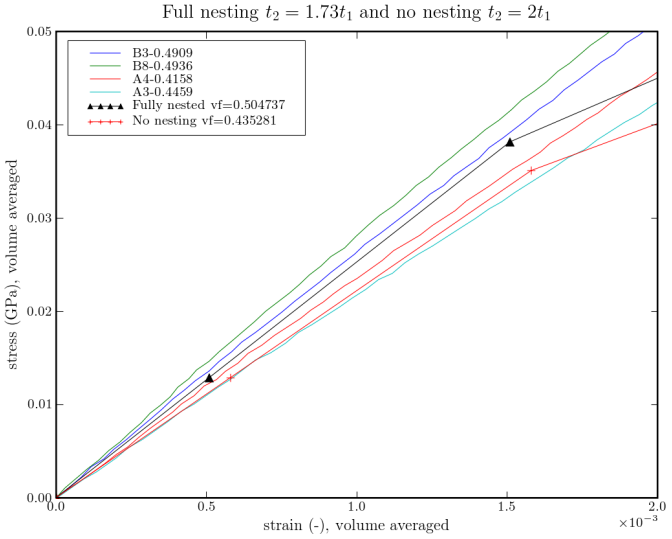

(b) Stiffness gain (17%) is approximately proportional to the gain in V_f

Figure 5.23: Difference between fully nested and unnested 2-layer composite, experimental data covering the same V_f range shown alongside. It is seen that nesting increases the V_f without increasing $V_{y,f}$. The difference stiffness and failure stress both coincide with the increase in V_f.

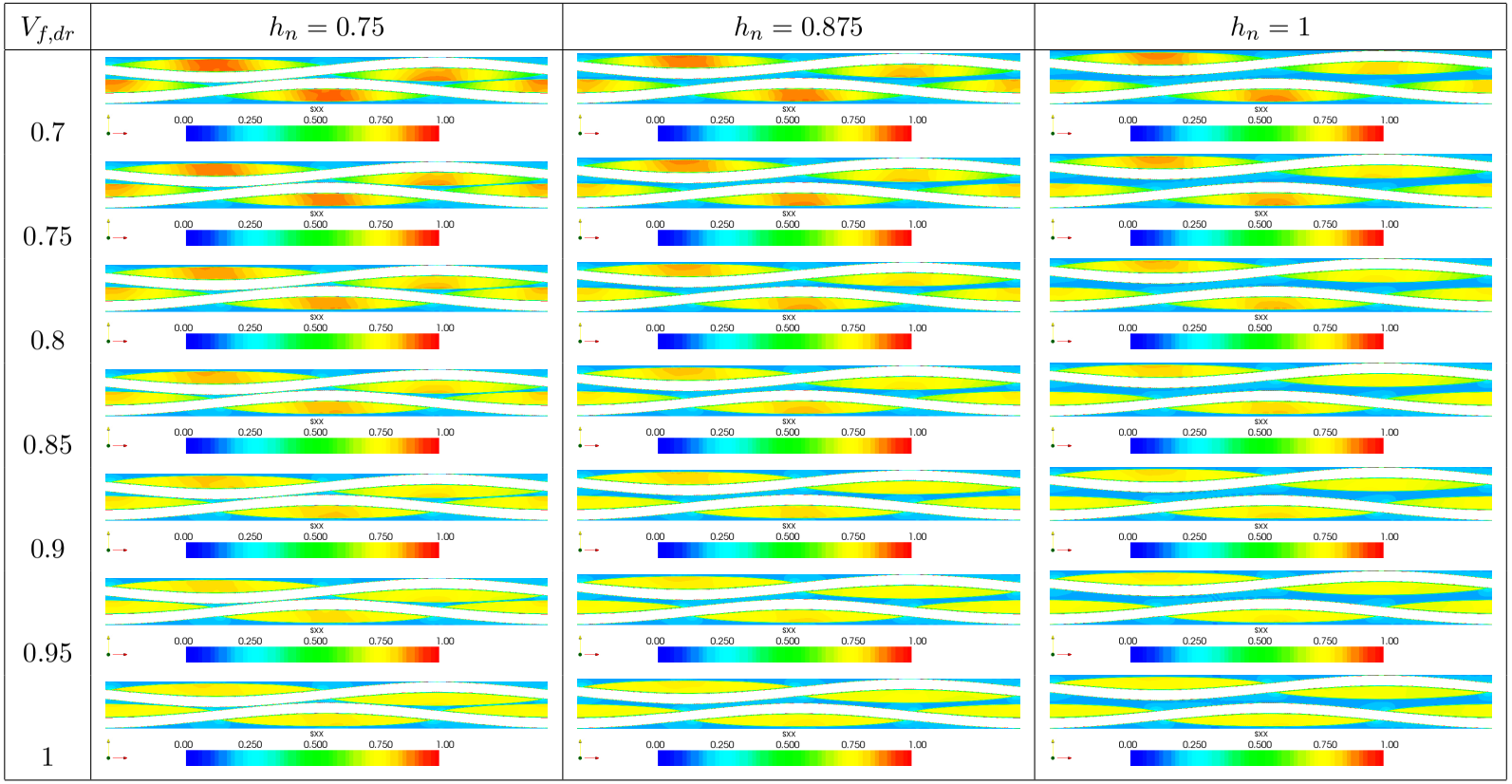

Table 5.3: Axial stress σ_{11} shown for a 2D plane strain analysis of different degrees of nesting in conjunction with different levels of $V_{f,dr}$, a textile model with $0.25, 0.25\lambda$ phase shift (see Figure 5.21(b)), slice taken at $y = 1.5$ (the plane on which the minimum distance between yarn surfaces of the 2 layers is smallest). It is shown here that the maximum transverse yarn stress is approximately 20% higher in the case of full nesting and 30% dropoff than with no dropoff and no nesting. It is noted that 30% is not a realistic value for $V_{f,dr}$, but also in a 20% range the effect of $V_{f,dr}$ is significantly stronger than the effect of h_n.

5.5 Conclusions

This chapter describes an attempt to match up experimental, geometric and computational results for one textile.

Since full statistical evaluation of such data is not within the scope of this thesis the goal of this study has been qualitative and can be summarised as follows:
Given a geometric variation of the textile structure as obtained through microscopy, does the model produce stiffness and strength predictions in a range similar to the experimental scatter? Parametric studies were done using the AMR based method devised and demonstrated in Chapters 3 and 4. In addition the phenomena were qualitatively analysed using 2D models.

- Within the constraints of the study presented (fixed level of refinement etc.) the computational results follow the test results closely.
- The variation of properties in the computational studies results in all cases in the expected qualitative change (as predicted from doing 2D analysis on key "slices" of the textile) in response with regards to strength and stiffness. I.e. 2D analysis indicates that higher values of $V_{f,dr}$ should result in higher strength values of the composite, 3D damage analysis replicates this.
- The point of damage initiation predicted by the model varies by too large a factor to accurately represent the material in testing. From the numerical studies in Chapter 4 it is shown that converged stress values cannot be obtained in 3D for the geometries under consideration. It appears that the use of a nonlocal stress measure does not solve this problem.

Chapter 6

Discussion and conclusions

6.1 Discussion

The research described in this thesis was set up to overcome or rather avoid a bottleneck in mesoscale mechanics modelling of textile composites. As indicated in the literature review there are a host of methods available to solve textile composites mechanics problems, some aimed at efficiently solving complex textiles over larger domains (Mosaic and Binary models), others aiming to obtain a good qualitative match with observed damage propagation (direct solution combined with conformal meshing of the full textile structure). The latter type of models tends to rely on automatic mesh generators (as found in commercial FE preprocessors) to obtain meshes that represent the textile structure.

The problem addressed in this thesis originates from the fact that for realistic textile geometries (i.e. textiles with realistically high V_f) such meshes are hard to obtain, and impossible to obtain in an automatic off-line manner without introducing artificial modifications to the textile geometry. Automatic modelling is deemed essential in parameter studies, stochastic analysis as well as multiscale modelling. Robust methods have been reported (AMR and Domain Superposition based) but not in conjunction with geometrically realistic and general textile models and damage models. This thesis describes implementation of an AMR based method in such a manner that the resulting system is fully automatic and could (computer hardware permitting) converge to arbitrary accuracy. This has been demonstrated on a parametrically defined single- and multilayer textile and satisfactory agreement between modelling and experiment has been achieved in predicting strength of a woven composite, loaded in the fibre direction. It was seen that although the stiffness behaviour of an RVE converges the local stress terms don't converge within reasonable computational cost, in particular when the problem con-

tains mixed-material elements (which is invariably the case). This was dealt with by introducing a nonlocal stress measure which was used as input to the damage model.

If left "untreated", for realistic yarn and matrix strength values, transverse yarn damage occurs prematurely in elements that contain integration points of both yarn and matrix type. It can therefore be concluded that a reasonable solution of the RVE can only be reached when the yarn has load-bearing capability after damage initiation, and that damage detection readings in such points cannot be trusted. It is left for later work to investigate whether a satisfactory treatment can be formulated for this issue.

When observing textile modelling methods in a more general sense, it can be seen that assumptions have to be made in a number of stages between obtaining key textile parameters and generating a numerical solution of the mechanical response. This is shown schematically in Figure 6.1.

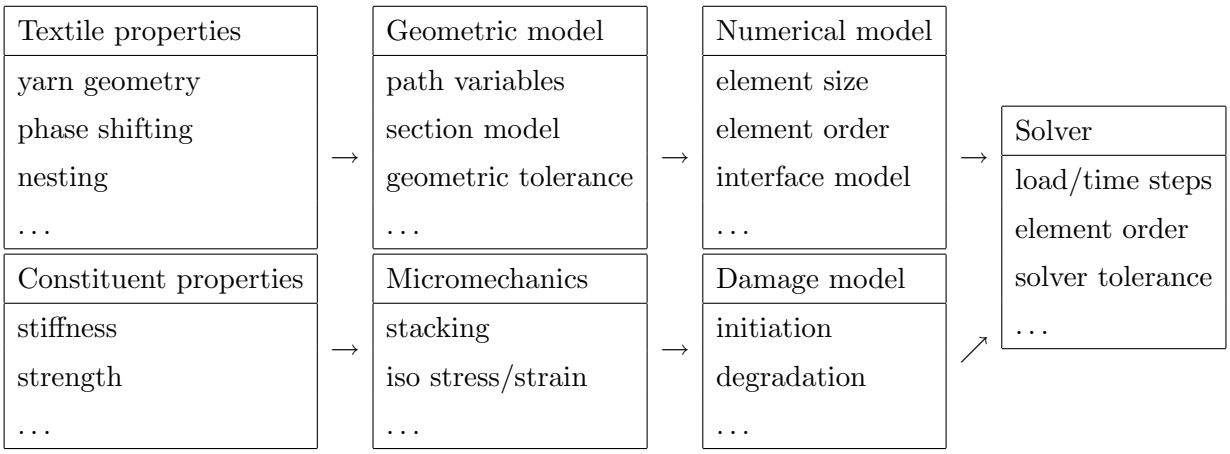

Figure 6.1: Physical and numerical parameters and assumptions which relate to the outcome of textile composites mechanics analyses.

The current method, in the scheme presented in Figure 6.1 puts emphasis on geometric accuracy and trails the detailed conformal meshing based methods such as the approach taken by Lomov et al [43] in accuracy of the analysis of local stresses in the RVE. However, also in the cases for which direct (conformal) geometric models can be constructed, tradeoffs of this type are made.

In the opinion of the author the current method's capability to generate large numbers of datasets automatically, in combination with TexGen features with regards to automatically constructing textile geometries would allow for a more systematic way of datamining the "design space" of textile variables and potentially decoupling the numerical and other modelling influences from the physical ones which are the object of study.

6.2 Conclusions

6.2.1 Modelling methodology

The current method is dependent on local (element) averaging of material properties to deal with all field variables that affect local stiffness (material type, $V_{y,f}$ and yarn orientation). The following can be concluded about the behaviour of such mixed-material elements in simulations:

1. Accuracy of the *global* RVE stiffness response can be improved efficiently by increasing the number of intra-element material sampling points (efficient because the lookup of properties is fast, scales linearly, and does not affect the FE solver time).

2. The *local* stiffness response inside the RVE can also be improved by increasing the number of intra-element material sampling points. As a result, the strain distribution in the RVE improves.

3. The stress distribution in elements which contain stiffness contributions from multiple materials does *not* converge as a function of either mesh refinement or intra-element material sampling. This holds for both the averaged case (sum stiffnesses and assign single D matrix to the element) and the gauss point case. There are a number of factors contributing to this:

    - The presence of a geometric singularity (sharp corner) in lenticular yarn shapes, this problem has been examined in literature (for FE analysis a region containing a crack tip) by using a nonlocal stress measure. This approach has been taken here as well.
    - A fairly arbitrary distribution of matrix/yarn material inside the cell, depending on the location, mesh refinement level and geometric parameters of the textile.

6.3 Recommendations for future work

- Additional validation and numerical testing of the nonlocal stress measure used to avoid problems relating to poor convergence of local stress terms. Although the damage model produced a reliable response based on nonlocal stress results when comparing to a small set of experiments (see Chapter 5), its performance as

a function of mesh refinement, geometric aspect ratio and resin-fibre stiffness ratio are unknown.

- Formulate and implement strain or energy based failure criteria for mixed-material elements. Possibly operating on nonlocal measures, possibly resolving geometric singularity issues by including microscale data (which does not have this singularity).

- The use of the current method in a nested manner, with the option of expanding the yarn into filaments for the cases where filaments are relatively large compared to other geometric features, meaning that it would not be valid to assume treat tows as homogeneous entities (such information could come from the filament modelling tool described by Sherburn in his thesis [11]).

- Performance optimisation of the current method, with particular focus on:

  - The effect of the treatment of boundary conditions on convergence in iterative solvers.
  - The use of AMG solvers.
  - The parallelisation of all aspects of the textile analysis, not just the matrix solution but also matrix assembly and material querying, in addition to formulating distributed memory versions of integration point data structures.

- Postprocessing of large numbers of complex datasets has not been a focal point in the current work, in particular the inclusion of simulation results in stochastic macroscale material parameters would be key to bringing the outcome of the current research into composite design practice.

- Explore the practical use of the current method as a substructuring method on matrix failure dominated cases and general geometries.

  As an example a notched specimen sample was analysed using a non-conformal tetrahedral mesh (see Figure 6.2). Although it is clear from earlier conclusions that the stress solution in this problem cannot be converged, the strain distribution (Figure 6.2(b)) looks good qualitatively as does the evolution of matrix damage (excluding the damage initiated in the corners of the modelled cutout).

  This shows that if a theoretically sound "treatment" of damage in mixed-material elements were devised, this would open up a large class of problems for analysis (any volume in which a textile geometry and a volume mesh can be defined, with no connectivity requirement between the two).

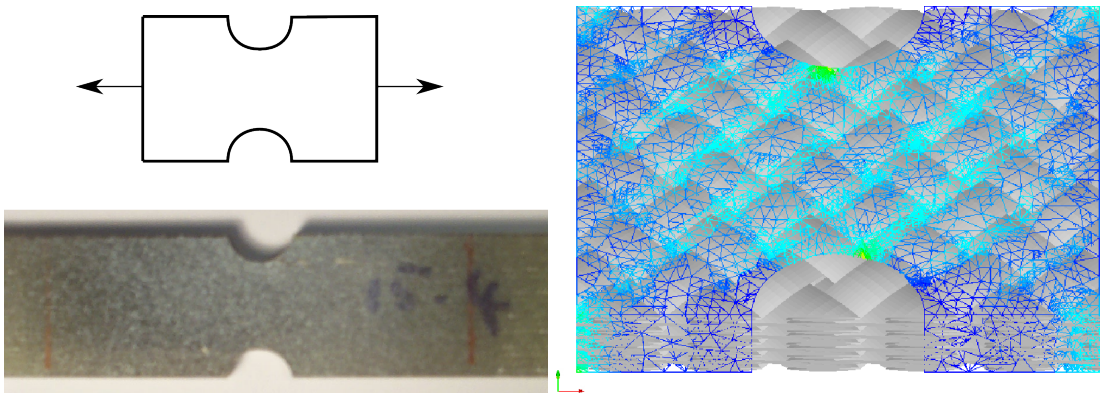

(a) Notched tensile specimen geometry and schematic drawing of the model and applied loading.

(b) Tetrahedral mesh showing the strain distribution along with the underlying TexGen textile geometry

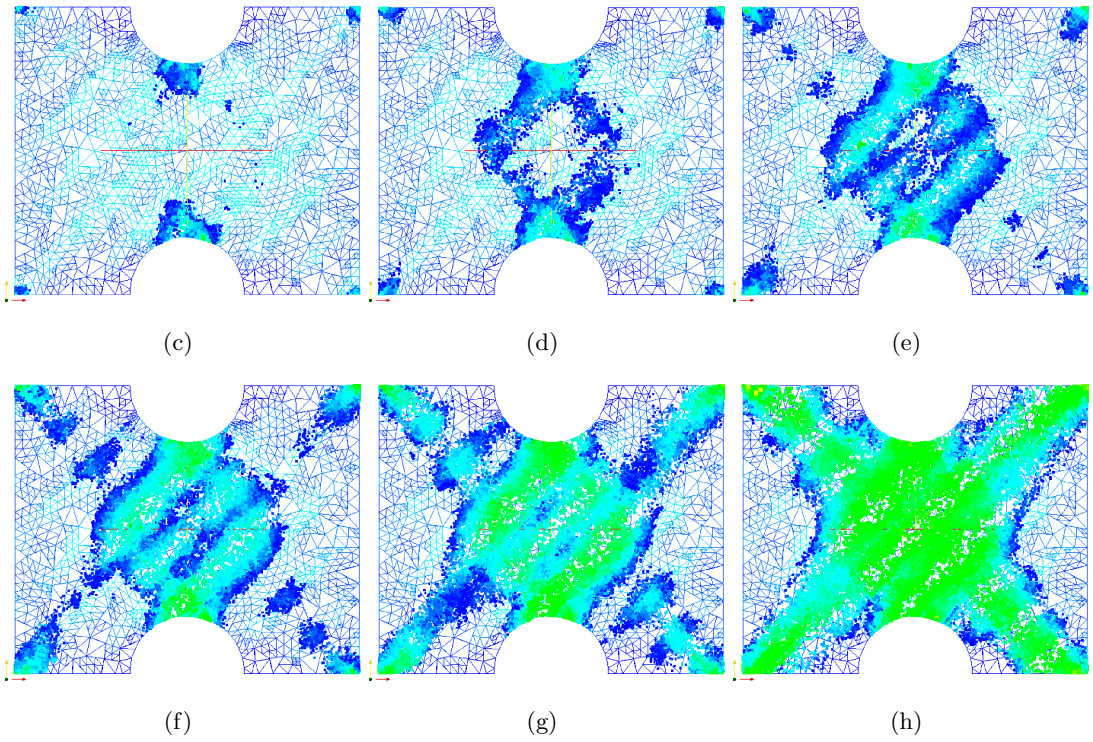

(c) (d) (e)

(f) (g) (h)

Figure 6.2: Example analysis where an 8-layer RT600 textile oriented in the bias direction is shown along with predicted evolution of the matrix damage variable D, only the gauss points in which $D > 1$ (damage is initiated) are shown.

6.4 Outlook

At the time of writing this thesis, composites are well established structural materials of which very large quantities are processed each year by the aerospace, automotive and the wind energy industry. In these industries it is commonplace to perform extensive

analysis and optimisation before first series production takes place.

This situation exists because the finite element simulation of laminate structures has gone from a specialist to a routine activity.

What this leads to is expansion of the overall simulation capability in a number of directions:

- Higher fidelity analysis
  - Additional physics (nonlinear, multiphysics etc)
  - Increased resolution
  - Multiscale modelling
- Increasingly wide optimisation scopes in design problems
- Stochastic modelling

All of these activities are aimed at reducing uncertainty in design, therefore allowing the designer to get closer to the limit, i.e. reduce the safety margin and still be confident of a well-performing design.

Such models have material data as a basis, which, in the case of textile composites, is effectively meso-scale data. This means that higher confidence in material data quickly results in improved designs of composite structures (i.e. lower cost of energy, higher vehicle safety etc).

It is in this light that fully automatic approaches to textile modelling can be seen to have value, since very large databases of textile properties can be generated allowing the use of statistical tools to discover interactions that may not be apparent and remove effects that are not intended.

Bibliography

[1] J. J. Crookston. *Prediction of elastic behaviour and initial failure of textile composites.* PhD thesis, University of Nottingham, United Kingdom, School of M3, 2004.

[2] J. J. Crookston, A. C. Long, and I. A. Jones. A summary review of mechanical properties prediction methods for textile reinforced polymer composites. *Proceedings of the Institution of Mechanical Engineers Part L (Journal of Materials: Design and Applications)*, 219(2):91–109, 2005.

[3] S. P. Timoshenko and J. M. Gere. *Mechanics of Materials.* Brooks-Cole, 1972.

[4] P. L. N. Murthy and C. C. Chamis. *ICAN Users and programmers manual.*

[5] S. W. Tsai and H. T. Hahn. *Introduction to Composite Materials.* Technomic Publishing Company, Inc., 1980.

[6] ANSYS Software Inc. Ansys. [Online; accessed 28-August-2008].

[7] MSC Software Inc. Msc nastran. [Online; accessed 28-August-2008].

[8] Hibbit, Karlsson, Sorensen, and HKS Inc. *Abaqus Standard*, 2007.

[9] J. Hofstee and F. van Keulen. Elastic stiffness analysis of a thermo-formed plain-weave fabric composite part II: analytical models. *Composites Science and Technology*, 60:1249–1261, June 2000.

[10] F. Peirce. The geometry of cloth structure. *Journal Textile Institute*, 28:45–96, 1937.

[11] Martin Sherburn. *Geometric and Mechanical Modelling of Textiles.* PhD thesis, University of Nottingham, Department of Mechanical Engineering, 2007.

[12] J. Hofstee, H. de Boer, and F. van Keulen. Elastic stiffness analysis of a thermo-formed plain-weave fabric composite: Part I: geometry. *Composites Science and Technology*, 60:1041–1053, May 2000.

[13] J. Hofstee and F. van Keulen. 3-D geometric modeling of a draped woven fabric. *Composite Structures*, 54:179–195, 00 2001.

[14] J. Hofstee, H. de Boer, and F. van Keulen. Elastic stiffness analysis of a thermoformed plain-weave fabric composite–part III: experimental verification. *Composites Science and Technology*, 62:401–418, 00 2002.

[15] J. W. S. Hearle and W. J. Shanahan. An energy method for calculations in fabric mechanics. *Journal Textile Institute*, 69(4):81–110, 1978.

[16] J. W. S. Hearle. Engineering design of textiles. *Indian Journal of Fibre and Textile Research*, 31(1):142–49, March 2006.

[17] Textiles Ltd. ScotCad. Scotweave technical weaver ^{TM}. [Online; accessed 28-August-2008].

[18] X. Tang, J. D. Whitcomb, A. D. Kelkar, and J. Tate. Progressive failure analysis of 2 x 2 braided composites exhibiting multiscale heterogeneity. *Composites Science and Technology*, 66:2580–2590, November 2006.

[19] J. Whitcomb and K. Srirengan. Effect of various approximations on predicted progressive failure in plain weave composites. *Composite Structures*, 34:13–20, January 1996.

[20] J. Whitcomb, K. Srirengan, and C. Chapman. Evaluation of homogenization for global/local stress analysis of textile composites. *Composite Structures*, 31:137–149, 1995.

[21] S. Lomov. Wisetex. [Online; accessed 22-August-2008].

[22] Martin Sherburn. Texgen v3, 2007. [Online; accessed 22-August-2008].

[23] P. Potluri, I. Parlak, R. Ramgulam, and T. V. Sagar. Analysis of tow deformations in textile preforms subjected to forming forces. *Composites Science and Technology*, 66:297–305, February 2006.

[24] P. Potluri, D. A. Perez Ciurezu, and R. B. Ramgulam. Measurement of meso-scale shear deformations for modelling textile composites. *Composites Part A: Applied Science and Manufacturing*, 37:303–314, February 2006.

[25] P. Potluri, A. Manan, M. Francke, and R. J. Day. Flexural and torsional behaviour of biaxial and triaxial braided composite structures. *Composite Structures*, 75:377–386, September 2006.

[26] P. Potluri and A. Manan. Mechanics of non-orthogonally interlaced textile composites. *Composites Part A: Applied Science and Manufacturing*, 38:1216–1226, April 2007.

[27] P. Potluri and V. S. Thammandra. Influence of uniaxial and biaxial tension on meso-scale geometry and strain fields in a woven composite. *Composite Structures*, 77:405–418, February 2007.

[28] T. S. Lundstrom. The permeability of non-crimp stitched fabrics. *Composites Part A: Applied Science and Manufacturing*, 31:1345–1353, December 2000.

[29] F. Desplentere, S. V. Lomov, D. L. Woerdeman, I. Verpoest, M. Wevers, and A. Bogdanovich. Micro-CT characterization of variability in 3D textile architecture. *Composites Science and Technology*, 65:1920–1930, October 2005.

[30] D. M. Blackketter, D. M. Walrath, and D. E. Hansen. Modeling damage in a plain weave fabric-reinforced composite material. *Journal of Composites Technology & Research*, 15(2):136–142, 1993.

[31] P. Potluri, D. A. Perez Ciurezu, and R. B. Ramgulam. Measurement of meso-scale shear deformations for modelling textile composites. *Composites Part A: Applied Science and Manufacturing*, 37:303–314, February 2006.

[32] S. C. Quek, A. M. Waas, K. W. Shahwan, and V. Agaram. Failure mechanics of triaxially braided carbon composites under combined bending-compression loading. *Composites Science and Technology*, 66:2548–2556, November 2006.

[33] S. C. Quek, A. M. Waas, K. W. Shahwan, and V. Agaram. Compressive response and failure of braided textile composites: Part 1–experiments. *International Journal of Non-Linear Mechanics*, 39:635–648, June 2004.

[34] S. C. Quek, A. M. Waas, J. Hoffman, and V. Agaram. The crushing response of braided and CSM glass reinforced composite tubes. *Composite Structures*, 52:103–112, April 2001.

[35] S. C. Quek, A. Waas, K. W. Shahwan, and V. Agaram. Compressive response and failure of braided textile composites: Part 2–computations. *International Journal of Non-Linear Mechanics*, 39:649–663, June 2004.

[36] S. C. Quek, A. M. Waas, K. W. Shahwan, and V. Agaram. Analysis of 2D triaxial flat braided textile composites. *International Journal of Mechanical Sciences*, 45:1077–1096, 00 2003.

[37] M. Zako, Y. Uetsuji, and T. Kurashiki. Finite element analysis of damaged woven fabric composite materials. *Composites Science and Technology*, 63:507–16, 2003.

[38] S. V. Lomov, A. V. Gusakov, G. Huysmans, A. Prodromou, and I. Verpoest. Textile geometry preprocessor for meso-mechanical models of woven composites. *Composites Science and Technology*, 60:2083–2095, August 2000.

[39] S. V. Lomov, E. B. Belov, T. Bischoff, S. B. Ghosh, T. Truong Chi, and I. Verpoest. Carbon composites based on multiaxial multiply stitched preforms. part 1. geometry of the preform. *Composites Part A: Applied Science and Manufacturing*, 33:1171–1183, September 2002.

[40] S. V. Lomov, R. S. Parnas, S. Bandyopadhyay Ghosh, I. Verpoest, and A. Nakai. Experimental and theoretical characterization of the geometry of two-dimensional braided fabrics. *Textile Research Journal*, 72(8):706–12, 2002.

[41] A. Willems, S. V. Lomov, I. Verpoest, and D. Vandepitte. Optical strain fields in shear and tensile testing of textile reinforcements. *Composites Science and Technology*, In Press, Accepted Manuscript.

[42] Ignaas Verpoest and Stepan V. Lomov. Virtual textile composites software wisetex: Integration with micro-mechanical, permeability and structural analysis. *Composites Science and Technology*, 65:2563–2574, December 2005.

[43] S. V. Lomov, D. S. Ivanov, I. Verpoest, M. Zako, T. Kurashiki, H. Nakai, and S. Hirosawa. Meso-FE modelling of textile composites: Road map, data flow and algorithms. *Composites Science and Technology*, 67:1870–1891, July 2007.

[44] V. Koissin, D. S. Ivanov, S. V. Lomov, and I. Verpoest. Fibre distribution inside yarns of textile composite: geometrical and FE modelling. In *Proceedings of TEXCOMP-8*, number T02, 18 October 2006 16.

[45] S. V. Lomov, D. S. Ivanov, T. C. Truong, I. Verpoest, F. Baudry, K. Vanden Bosche, and H. Xie. Experimental methodology of study of damage initiation and development in textile composites in uniaxial tensile test. *Composites Science and Technology*, In Press, Corrected Proof.

[46] L. Gorbatikh, D.S. Ivanov, S.V. Lomov, and I. Verpoest. On modelling of damage evolution in textile composites on meso-level via property degradation approach. *Composites Part A*, 38:2433–2442, 2007.

[47] M. F. Adams, H. H. Bayraktar, T. M. Keaveny, and P. Papadopoulos. Applications of algebraic multigrid to large-scale finite element analysis of whole bone

micro-mechanics on the IBM SP. In *ACM/IEEE Proceedings of SC2003: High Performance Networking and Computing*, 2003.

[48] Y. Gowayed and L. Yi. Mechanical behavior of textile composite materials using a hybrid finite element approach. *Polymer Composites*, 18(3):313–319, 1997.

[49] H. J. Kim and C. C. Swan. Voxel-based meshing and unit-cell analysis of textile composites. *International Journal for Numerical Methods in Engineering*, 56:977–1006, 2003.

[50] H. J. Kim and C. C. Swan. Algorithms for automated meshing and unit cell analysis of periodic composites with hierarchical tri-quadratic tetrahedral elements. *International Journal for Numerical Methods in Engineering*, 58:1683–1711, 2003.

[51] J. Xu, B.N. Cox, M.A. McGlockton, and W.C. Carter. A binary model of textile composites–ii. the elastic regime. *Acta metall. mater.*, 43(9):3511–3524, 1995.

[52] E.V. Iarve, E.G. Zhou, T.J. Whitney, D.H. Mollenhauer, and T. Breitzman. Independent mesh method based prediction of local and volume average fields in textile composites. In *Proceedings of the 49th AIAA/ASME/ASCE/AHS/ASC Conference on Structures, Structural Dynamics, and Materials, 7-10 April 2008, Schaumburg, IL.*

[53] A.E. Bogdanovic. Multi-scale modeling, stress and failure analyses of 3-d woven composites. *J Mater Sci*, 41:6547–6590, 2006.

[54] Q. Yang and B. Cox. Predicting local strains in textile composites using the binary model formulation. In *Proceedings of the 14th International Conference on Composite Materials, San Diego, USA, 2003.*

[55] G. Huysmans, I. Verpoest, and P.Van Houtte. A poly-inclusion approach for the elastic modelling of knitted fabric composites. *Acta Materials*, 60:3003–3013, 1998.

[56] libmesh:a C++ framework for the numerical simulation of partial differential equations on serial and parallel platforms. [Online; accessed 28-August-2008].

[57] S.W. Tsai and E.M. Wu. A general theory of strength for anisotropic materials. *Journal of Composite Materials*, 5:58–80, 1971.

[58] P. D. Soden, A. S. Kaddour, and M. J. HintonE. *Composites Science and Technology*, 64:589–604, March 2004.

[59] A. Puck and H. Schurmann. Failure analysis of frp laminates by means of physically based phenomenological models. *Composites Science and Technology*, 58, 1998.

[60] J. Kopp A. Puck and M. Knops. Guidelines for the determination of the parameters in puck action plane strength criterion. *Composites Science and Technology*, 62:371–378, 2002.

[61] S.T. Pinho, C.G. Davila, P.P Camanho, L. Iannucci, and P. Robinson. *Failure models and criteria for FRP under in-plane or three dimensional stress states including shear nonlinearity: NASA/TM-2005-213530.* National Aeronautics and Space Administration, 2005.

[62] Tomo Takeda, Satoru Takano, Yasuhide Shindo, and Fumio Narita. Deformation and progressive failure behavior of woven-fabric-reinforced glass/epoxy composite laminates under tensile loading at cryogenic temperatures. *Composites Science and Technology*, 65:1691–1702, September 2005.

[63] X. Tang, J. D. Whitcomb, A. D. Kelkar, and J. Tate. Progressive failure analysis of 2 x 2 braided composites exhibiting multiscale heterogeneity. *Composites Science and Technology*, 66:2580–90, November 2006.

[64] R.H.W. ten Thije, R. Akkermana, and J. Hutink. Large deformation simulation of anisotropic material using an updated lagrangian finite element method. *Computer Methods in Applied Mechanics and Engineering*, 196:3141–3150, 2007.

[65] T. I. Zohdi and P. Wriggers. A model for simulating the deterioration of structural-scale material responses of microheterogeneous solids. *Computer Methods in Applied Mechanics and Engineering*, 190(22-23):2803–2823, February 2001.

[66] V.G. Kouznetsova, M.G.D. Geers, and W.A.M. Brekelmans. Multi-scale second-order computational homogenization of multi-phase materials: a nested finite element solution strategy. *Computer Methods in Applied Mechanics and Engineering*, 193:5525–5550, December 2004.

[67] Q. Yu and J. Fish. Multiscale asymptotic homogenization for multiphysics problems with multiple spatial and temporal scales: a coupled thermo-viscoelastic example problem. *International Journal of Solids and Structures*, 39:6429–6452, December 2002.

[68] Jacob Fish and Kamlun Shek. Multiscale analysis of composite materials and structures. *Composites Science and Technology*, 60:2547–2556, September 2000.

[69] Jacob Fish and Qing Yu. Two-scale damage modeling of brittle composites. *Composites Science and Technology*, 61:2215–2222, 00 2001.

[70] K. Schloegel, G. Karypis, and V. Kumar. Dynamic repartitioning of adaptively refined meshes. *Supercomputing*, 1998.

[71] mpich2. MPICH2 is a high-performance and widely portable implementation of the Message Passing Interface (MPI) standard.[Online; accessed 28-August-2008].

[72] S. Balay, K. Buschelman, V. Eijkhout, W. D. Gropp, D. Kaushik, M. G. Knepley, L. Curfman McInnes, B. F. Smith, and H. Zhang. PETSc users manual. Technical Report ANL-95/11 - Revision 2.3.2, September 2006. see http://www.mcs.anl.gov/petsc.

[73] W. Bangerth, R. Hartmann, and G. Kanschat. *deal.II Differential Equations Analysis Library, Technical Reference.* http://www.dealii.org.

[74] J-C. Bauwens. Attempt to correlate the formation of free volume and the plastic deformation process in glassy polymers. *Polymer*, 21:699–705, June 1980.

[75] Adib A. Becker. *The Boundary Element Method in Engineering; A complete course.* McGraw-Hill book company, 1992.

[76] W. Ruijter. BEACON: Investigation of the applicability of BEACON as a BE add-on to an FE package for use in modelling textile preform based composites, internal report., 2004.

[77] V. Popov and H. Power. An o(N) taylor series multipole boundary element method for three-dimensional elasticity problems. *Engineering Analysis with Boundary Elements*, 25:7–18, 2001.

[78] N. Kamiya, H. Iwase, and E. Kita. Parallel computing for the combination method of BEM and FEM. *Engineering Analysis with Boundary Elements*, 18:223–229, 1996.

[79] F. Robitaille and R. Gauvin. Compaction of textile reinforcements for composites manufacturing. ii: compaction and relaxation of dry and h2o-saturated woven reinforcements. *Polymer Composites*, 19(5):543–557, 1998.

[80] C.C. Wong, A.C. Long, M. Sherburn, F. Robitaille, P. Harrison, and C.D. Rudd. Comparisons of novel and efficient approaches for permeability prediction based on the fabric architecture. *Composites Part A*, 37:847–857, 2006.

[81] J.J. Crookston, F. Robitaille, A.C. Long, I.A. Jones, and J.W. Ooi. A systematic study of the mechanical properties of textile composite unit cells based on geometric modelling. In *Proceedings of the 14th International Conference on Composite Materials (ICCM 14), San Diego, USA.*

[82] Free Software Foundation. Gnu general public license. [Online; accessed 28-August-2008].

[83] Guido Dhondt and Klaus Wittig. CALCULIX: A free software three-dimensional structural finite element program. [Online; accessed 28-August-2008].

[84] C. C. Chamis. Mechanics of composite materials: past, present and future. *J Compos Technol Res*, 11:3–14, 1989.

[85] L. E. Asp, L. A. Berglund, and R. Talreja. A criterion for crack initiation in glassy polymers subjected to a composite-like stress state. *Composites Science and Technology*, 1996.

[86] M. G. A. Tijssens and E. van der Giessen. A possible mechanism for cross-tie fibril generation in crazing of amorphous polymers. *Polymer*, 43:831–838, February 2002.

[87] D. W. Kelly, J. P. Gago, O. C. Zienkiewicz, and I. Babuska. A posteriori error analysis and adaptive processes in the finite element method: Part I error analysis. *Int. J. Num. Meth. Engng.*, 19:1593–1619, 1983.

[88] T. Ishikawa and T.W. Chou. Stiffness and strength behaviour of woven fabric composites. *Journal of Materials Science*, 17:3211–3220, 1982.

[89] W. Ruijter, J.J. Crookston, A.C. Long, and I.A. Jones. Modelling of composite materials using fem and adaptive meshing. In *Proceedings of the 12th European Conference on Composite Materials (ECCM 12), 29th August-1st September 2006, Biarritz, France.*

[90] J.J. Crookston, W. Ruijter, A.C. Long, and I.A. Jones. Modelling mechanical performance including damage development for textile composites using a grid-based finite element method with adaptive mesh refinement. In *Proceedings of the 8th International Conference on Textile Composites (TexComp 8), 16-18th Oct 2006, Paper T09, Nottingham, UK.*

[91] W. Ruijter, J. Crookston, A. Long, and I.A. Jones. Computational meso-scale analysis of textile composites using adaptive finite element analysis. In *Proceedings of the 47th AIAA/ASME/ASCE/AHS/ASC Structures, Structural Dynamics and Materials (SDM 47) Conference, 1-5th June 2006, Newport, RI, USA.*

Appendix A

Additional validation

In addition to the cases described in Chapter 5, validation analyses were also performed against a set of bias direction tensile test cases documented in the PhD work of Jonathan Crookston (see [1]).

This work is documented here rather than in Chapter 5 because no related geometric analysis was performed. In addition, tensile specimens were cut from 8-layer plaques, so any effects caused by out-of-plane bending in the cases considered in Chapter 5 would not be present in the experiments shown here.

These cases are documented in [89] and [90], where it was seen that the behaviour can be described with the same damage model but that the results are sensitive to the number of layers modelled (size of the RVE) and slight variations in the material degradation settings. The smallest RVE considered is shown in Figure A.1.

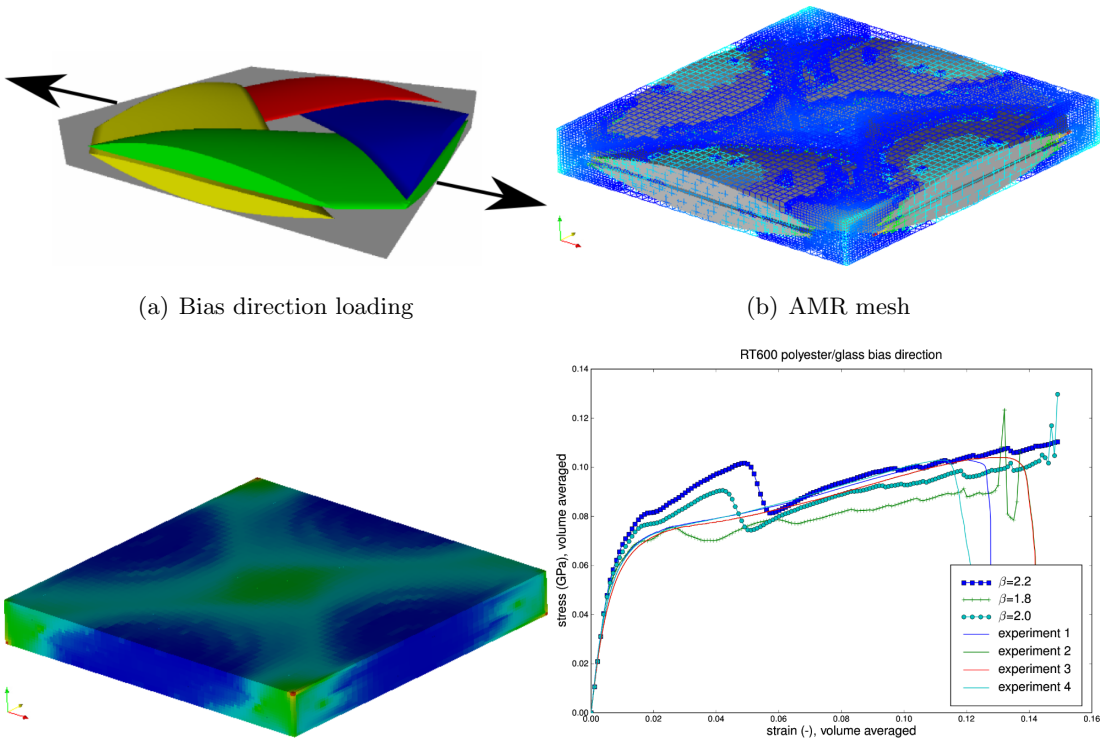

(a) Bias direction loading

(b) AMR mesh

(c) Strain distribution

(d) Stress strain curve for various damage variable settings

Figure A.1: RT600 textile loaded in the bias direction experiments and modelling. It is shown that the result in this case is particularly sensitive to the variables in the damage model with regards to the load-bearing capability of the matrix material after initial damage. Reproduced from [91].

The damage variable D is tracked for the various loading stages, this is shown in Figure A.2 from a top view perspective (this is why the damage pattern is not symmetric).

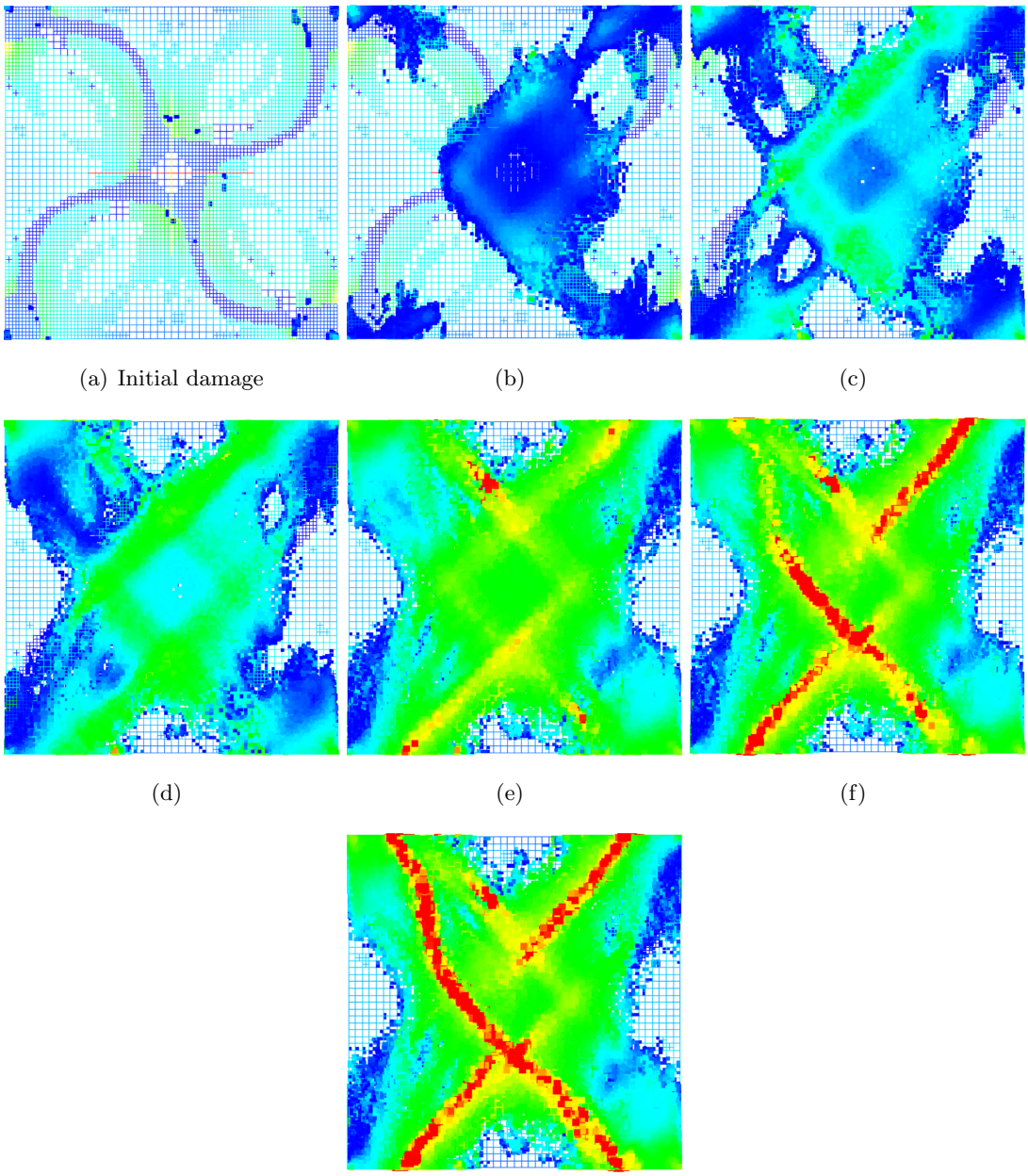

(a) Initial damage (b) (c)

(d) (e) (f)

(g) Final failure

Figure A.2: Damage variable D normalised so that red indicates fully damaged material.

Appendix B

Querying textile models using the TexGen API

Modelling methods described in this thesis are dependent on efficient interrogation of textiles for local properties such as yarn orientation and $V_{y,f}$. This is done through the TexGen API which can be accessed from C++.

An example is given here where a grid of `mpoints`^{3} points is generated for each cell and added to a point list for querying in TexGen through the `GetPointInformation` call.

Note that any code examples given here use the LibMesh API for the handling of meshes. Not all code is reprinted here, only key components of the mechanical analysis tool and textile composite preprocessing tool are printed.

```
points.resize(mesh.n_active_elem()*mpoints*mpoints*mpoints);

MeshBase::element_iterator el = mesh.active_elements_begin();

MeshBase::element_iterator el_end = mesh.active_elements_end();

for(; el!=el_end ; el++){

  Elem* elem = (*el);

  for(unsigned int j=0;j<mpoints;++j){

    for(unsigned int k=0;k<mpoints;++k){

      for(unsigned int l=0;l<mpoints;++l){

        const Node nd0 = (*elem->get_node(0));
```

```
            const Node nd6 = (*elem->get_node(6));

            float mp = (float) mpoints;

            points[i++] = TexGen::XYZ(
                nd0(0) + (1./(2.*mp)+(1.0/mp)*j)*(nd6(0)-nd0(0)),
                nd0(1) + (1./(2.*mp)+(1.0/mp)*k)*(nd6(1)-nd0(1)),
                nd0(2) + (1./(2.*mp)+(1.0/mp)*l)*(nd6(2)-nd0(2))
                );

        }

    }

  }

}

textile->GetPointInformation(points, point_info);
```

A test running this algorithm on a plain weave textile shows that scaling of CPU time with the number of points looked up is linear (see Figure B.1).

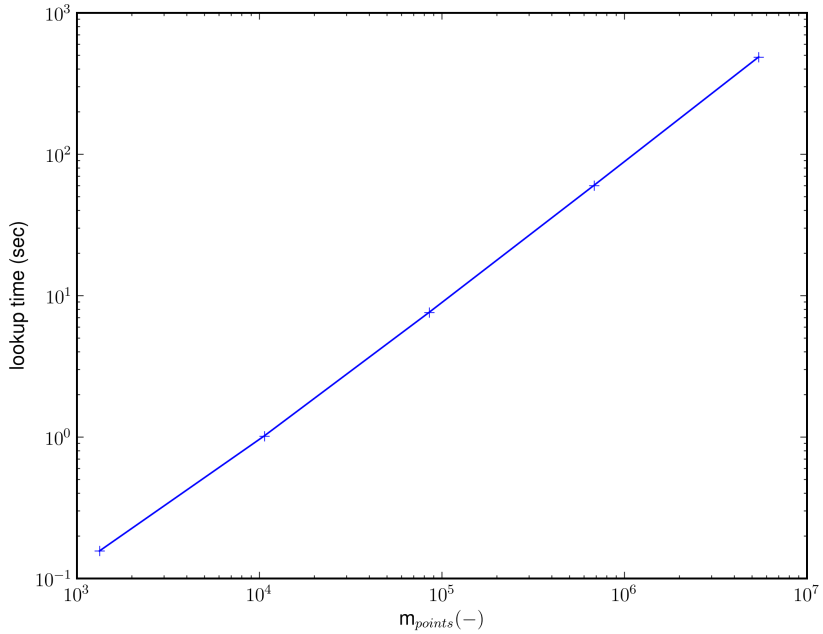

Figure B.1: CPU time needed for lookup of n_{points} points in a plain weave textile. The graph shows linear scaling, the test was run on one core of a AMD64 athlon 2.2 Ghz dual core machine. The meshes used are 1^3 to 16^3 with material sampling 11^3.

Appendix C

Analysis of textile composites in Abaqus/CalculiX

In this appendix the usage of CalculiX (the input format of which is compatible with Abaqus) is described for elastostatic analysis of textile composites using non-conformal meshing (for information on CalculiX, refer to [83]). What has been developed is a basic preprocessor that can produce a structured mesh with locally averaged properties for each element according to the local textile structure. This method is used for the 2D and 3D analyses in Chapter 4 and 5. The reason for the use of Abaqus/CalculiX is the wide range of phenomena for which there are adequate models implemented in these packages. This drastically shortens the development time if models like plasticity, thermal-mechanical coupling are needed.

The input format for Abaqus is described in the Abaqus User Manual [8], this section is about generation of grid averaged FE models.

In Appendix B it is shown how textile models can be interrogated inside C++ programs, this data is used .

C.1 Property averaging

This is used to produce FE input decks for uniform meshes. The code shown in Listing C.2 shows material property averaging implemented on all terms of the rotated material stiffness matrix D, which is written to Abaqus in the following format:

```
*MATERIAL,NAME=5
*ELASTIC,TYPE=ANISOTROPIC
91.4953,5.08156,10.6616,5.08439,5.55388,10.6617,0,0
```

```
0,3.44129,0.420121,-0.00249254,0.00691614,0,3.44417,0
0,0,0.00469318,0,2.55389
*EXPANSION,TYPE=ANISO
0.000376759,0.000428713,0.000428711,0,-2.73873e-07,0
```

Listing C.1: Program listing showing property averaging for $mpoint^3$ sized stencil.

```
for(unsigned int j=0;j<n_points;++j){

  unsigned int nid = n_points*i_elem+j;

  int material = point_info[nid].iYarnIndex;

  const double vf = point_info[nid].dVolumeFraction;

  tangent = point_info[nid].YarnTangent;

  DenseVector<Real> D_point(21);

  D_point.zero();

  DenseMatrix<Real> alph(3,3);

  alph.zero();

  double alpha[3];

  if(material==-1){

    double e[3],g[3],nu[3];

    for(unsigned int k=0;k<3;++k){

      e[k] = Ematrix;

      g[k] = Ematrix/(2*(1+numatrix));

      nu[k] = numatrix;

    }

    micromech->get_matrix_thermal_expansion(alpha);
```

```
    for(unsigned int k=0;k<3;++k)alph(k,k) = alpha[k];

    fill_storage(D_point,e,g,nu);

  }else{

    is_matrix = false;

    elem_vf += vf;

    TexGen::XYZ y,z;

    make_carth_set(tangent,y,z);

    double e[3],g[3],nu[3];

    micromech->set_fibre_volume_fraction(vf);

    micromech->get_elastic_moduli(e,g,nu);

    micromech->get_thermal_expansion( alpha);

    DenseVector<Real> dfull(21);

    dfull.zero();

    double unrot[3][3][3][3];

    fill_storage(dfull,e,g,nu);

    fill_tensor(unrot,dfull);

    DenseMatrix<Real> R(3,3);

    for(unsigned int k=0;k<3;++k)alph(k,k) = alpha[k];

    // get rotation matrix
    for(unsigned int k=0;k<3;++k){

      R(k,0) = tangent[k];
```

```
      R(k,1) = y[k];

      R(k,2) = z[k];

    }

    alph.left_multiply(R);

    alph.right_multiply_transpose(R);

    // get transformed D matrix
    for(unsigned int i=0;i<21;++i){
      // this is taken from Calculix code,
      // since we are trying to write
      // ccx input it is good to already
      // have the appropriate ordering in use
      const unsigned int j1 = t_l[i][0];

      const unsigned int j2 = t_l[i][1];

      const unsigned int j3 = t_l[i][2];

      const unsigned int j4 = t_l[i][3];

      for(unsigned int j=0;j<3;++j)

        for(unsigned int k=0;k<3;++k)

          for(unsigned int l=0;l<3;++l)

            for(unsigned int m=0;m<3;++m)

              D_point(i)+=R(j1,j)*R(j2,k)*R(j3,l)*R(j4,m)*
                unrot[j][k][l][m];
    }

  }

 D.add(1./(float)n_points, D_point);

 Alpha.add(1./(float)n_points, alph);
```

```
}
```

C.2 Periodic boundary conditions

Here an algorithm is given that formulates periodic boundary conditions for textiles bounded by rectangular domains. The method returns the `*EQUATION` terms that are used in the Calculix input deck.

Listing C.2: Program listing showing property averaging for $mpoint^3$ sized stencil.

```
struct eqn{

  int bot;

  int top;

  int d;

};

bool compare_eqn(eqn first, eqn second){

  return first.bot< second.bot;

}

std::string get_periodic_bcs(Mesh& mesh, CTextile* textile){

    TexGen::XYZ bot, top;

  // get the domain limits

  std::stringstream perbcs;

  const CDomain* domain = textile->GetDomain();

  ((CDomainPlanes*)domain)->GetBoxLimits(bot,top);

  BoundaryMesh bounds(3);

  mesh.boundary_info->sync(bounds);

  std::vector<eqn> ceqns;

  for(unsigned int dir=0;dir<3;++dir){
```

```
    std::vector<Node> nd0,nd1;
    for(unsigned int i=0;i<mesh.n_nodes();++i){
      Node& nd = mesh.node(i);
      if(nd(dir)<bot[dir]+TOL){
        nd0.push_back(nd);
      }else if(nd(dir)>top[dir]-TOL){
        nd1.push_back(nd);
      }
    }
    sort(nd0.begin(),nd0.end());
    sort(nd1.begin(),nd1.end());
    // we want to add the equation top = bot +d or bot-top+d=0
    for(unsigned int i=0;i<nd0.size();++i){
      eqn a;
      a.bot = nd0[i].id()+1;
      a.top = nd1[i].id()+1;
      a.d = mesh.n_nodes()+dir+1;
      ceqns.push_back(a);
    }
  }
  sort(ceqns.begin(), ceqns.end(), compare_eqn);
```

```
  for(unsigned int i=0;i<ceqns.size();++i){

    for(unsigned int k=1;k<=3;++k){

      if(i>0 && ceqns[i].bot!=ceqns[i-1].bot){

        perbcs<<"*EQUATION\n3"<<std::endl;

        perbcs<<ceqns[i].bot<<","<<k<<",1,"<<ceqns[i].top
          <<","<<k<<",-1,"<<ceqns[i].d<<","<<k<<",1" <<std::endl;

      }

    }

  }

  return perbcs.str();

}
```

C.3 Implementation of a parametric textile model using TexGen

The concept of the parametric textile model is described in 3.3, here the implementation using the TexGen python interface is given.

The input argument for the textile generation is a parameter structure written as follows (no representative values):

```
tex_param = {
  'length'     : 4.05, \
  'height'     : 0.5, \
  'vgap'       : 0.02,\
  'hgap'       : 0.1,\
  'fibre_area'  : 0.25,\
  'vf_dropoff'  : 0.85,\
  'numlayer'    : 2,\
  'rel_z_offset'  : 0.87,\
  'x_gamma'    : 0.25,\
  'y_gamma'    : 0.25,\
  'flat_value'  : 0.19,\
  'rotate'     : [0,0],\
  'domainsize'  : [0.8,0.8],\
  'weavestyle'  : 'plain'}
```

The last lines of the textile generator show that only textiles without interference are returned. This is done because in that case properties looked up in a point inside the overlapping region will be dependent on the yarn ordering, and hence result in spurious output (like $E_{11} \neq E_{22}$ for a balanced weave).

```
def make_textile(t_par):

  length = t_par['length']

  height = t_par['height']

  rot = t_par['rotate']

  style = t_par['weavestyle']

  if style=='plain':

    weave_pattern = [[0,0],[1,1]]
```

```
elif style=='5satin':

  weave_pattern = [[0,0],[1,2],[2,4],[3,1],[4,3]]

else:

  sys.exit('no valid weave style specified')

tex = CTextileWeave2D(len(weave_pattern),
  len(weave_pattern),length*0.5,height)

tex.SetGapSize(t_par['vgap']);

for i in weave_pattern:

  tex.SwapPosition(i[0], i[1]);

tex.SetYarnWidths(length*.5-t_par['hgap']);

tex.SetYarnHeights(height*.5-0.01);

fdist = CFibreDistribution1DQuad(t_par['vf_dropoff'])

yarns = tex.GetYarns()

addyarns = []

y_size = len(yarns)

z_offset = 0

# iterate over the number of added layers
for i in range(t_par['numlayer']-1):

  # compute how far to translate the yarns

  z_offset += height*t_par['rel_z_offset']

  trans = XYZ(t_par['x_gamma'][i+1]*length,
        t_par['y_gamma'][i+1]*length,
        z_offset);
```

```
    tex2 = CTextileWeave2D(tex)

    tex2.Translate(trans)

    tex2.Rotate(WXYZ(rot[i+1]*PI,0,0))

    addyarns.append(tex2.GetYarns())

    if i == t_par['numlayer']-2:

      tex2.FlattenYarns(t_par['flat_value'],1);

# now flatten the bottom layer
if t_par['numlayer']==1:

    tex.FlattenYarns(t_par['flat_value'],0)

else:

    tex.FlattenYarns(t_par['flat_value'],-1)

print t_par['x_gamma'][0],t_par['y_gamma'][0]

trans = XYZ(t_par['x_gamma'][0]*length,
      t_par['y_gamma'][0]*length,
      0);

tex.Translate(trans)

tex.Rotate(WXYZ(rot[0]*PI,0,0))

# then add yarns from the other layers
for i in addyarns:

    for j in range(len(i)):

      yarns.append(i[j])

# loop over all the old and new (translated) yarns to assign a fibre
# distribution
nyarns = []
```

```
for yarn in yarns:

  yarn.AssignFibreDistribution(fdist)

  yarn.SetFibreArea(t_par['fibre_area']*1e-6)

  yarn.SetResolution(t_par['section_resolution'])

  nyarns.append(yarn)


tex.DeleteYarns()

for i in nyarns:

  tex.AddYarn(i)


zflat = (t_par['height']/4-t_par['flat_value'])-0.5*t_par['vgap']

tex.Translate(XYZ(0,0,-zflat))

bot = XYZ(0,0,0)

top = XYZ(length*t_par['domainsize'][0],
  length*t_par['domainsize'][1],
  height*(1+(t_par['numlayer']-1)*t_par['rel_z_offset'])-2*zflat)

domain=CDomainPlanes(bot,top)

tex.AssignDomain(domain)

np = tex.DetectInterference()

if np>0:

  print 'textile geometry contains interference'

  return 1

else:
```

```
    return tex
```

Appendix D

Testing

It is noticed that the Instron machine used to perform tensile tests as used in Chapter 5 has a cycle of high-low stress measurement which results in a noisy signal when looking at the derivative of the stress strain curve.

This is shown in Figure D.1, where the tangent modulus is computed over $1, 2, 4$ and 8 samples. The local modulus $\frac{d\sigma}{d\varepsilon}$ is shown to reduce from early in the stress strain domain. This corresponds to the global modulus $\frac{\sigma_i - \sigma_0}{\varepsilon_i - \varepsilon_0}$ as seen in Figure D.2.

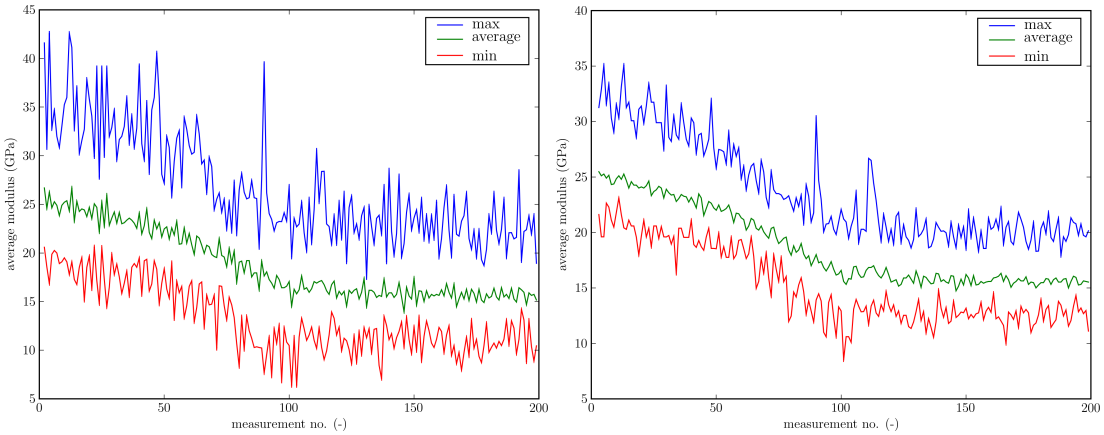

(a) $\frac{\sigma_i - \sigma_{i-1}}{\varepsilon_i - \varepsilon_{i-1}}$

(b) $\frac{\sigma_i - \sigma_{i-2}}{\varepsilon_i - \varepsilon_{i-2}}$

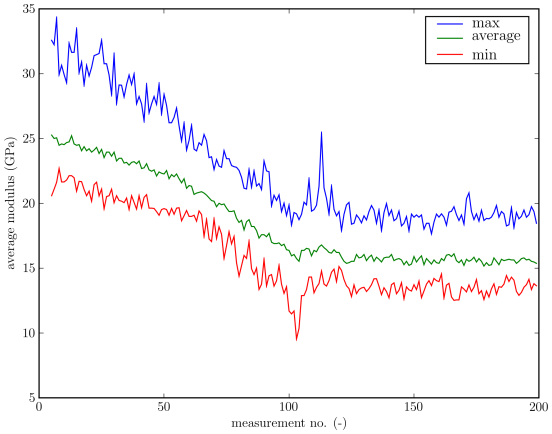

(c) $\frac{\sigma_i - \sigma_{i-4}}{\varepsilon_i - \varepsilon_{i-4}}$

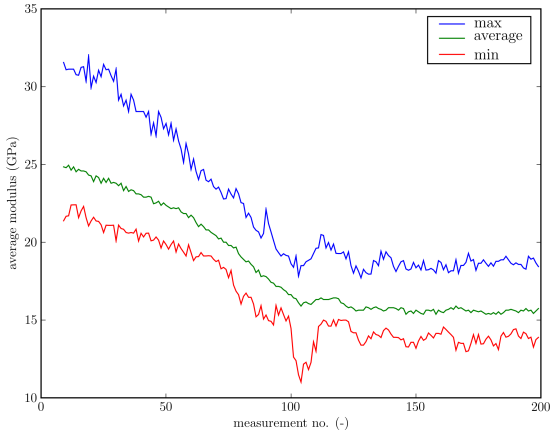

(d) $\frac{\sigma_i - \sigma_{i-8}}{\varepsilon_i - \varepsilon_{i-8}}$

Figure D.1: Different measures of $\frac{d\sigma}{d\varepsilon}$ throughout the experiments, the max, min and average values are for the specimens given in Table 5.1.

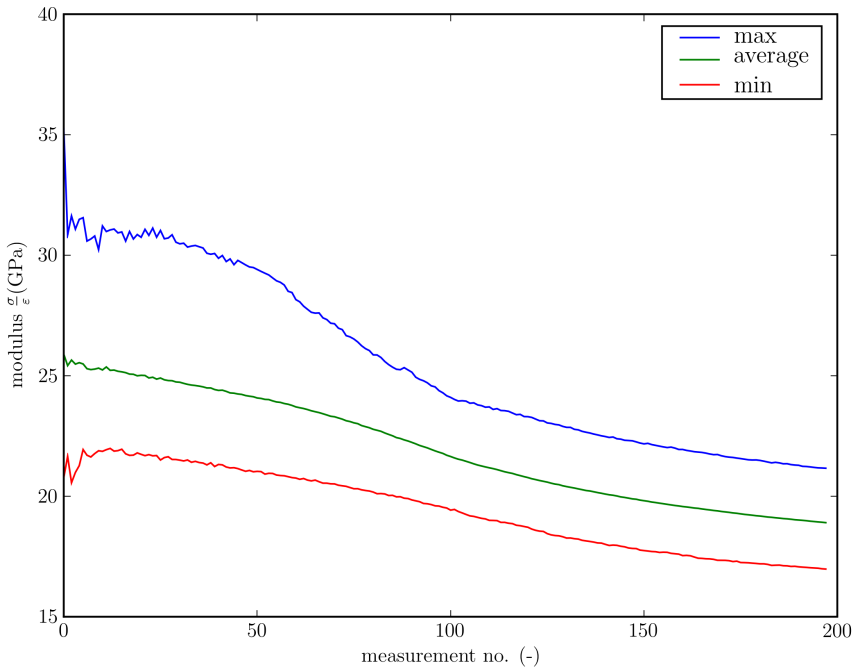

Figure D.2: Average, maximum and minimum elastic modulus as obtained from specimens as given in Table 5.1.

D.1 Extensometer slippage

In tensile testing an extensometer is used to record specimen elongation up to 2% strain. There are some cases where the outputs from the extensometer show sharp reverse steps (see Figure D.3) occurring generally between $\varepsilon > 0.015$ to the cutout strain of the extensometer $\varepsilon = 0.02$. This is attributed to slippage of the extensometer on the specimen.

A simple correction algorithm is applied, essentially assuming the previous strain step to hold during the "slipped" strain increment. This is implemented in the data reader described in D.2.

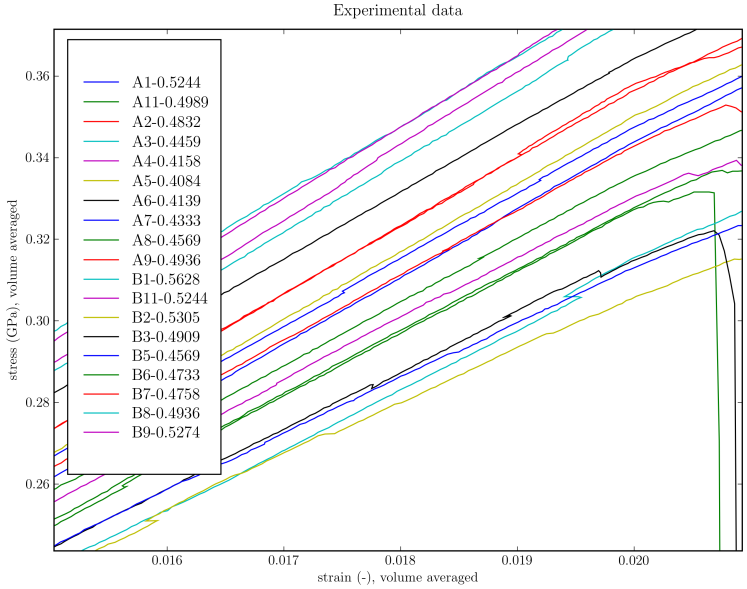

Figure D.3: Negative strain steps attributed to extensometer slippage, only occurs for $\varepsilon > 0.015$

D.2 Analysis of tensile testing data from Instron

This section documents the use of legacy instron binary datafiles. The tensile testing machine has an accompanying set of software that converts binary data into ASCII but this software was written with such focus on preserving disc space that values are rounded off quite severely.

The dataset reader is given here for convenience.

```
#! /usr/bin/env python
from pylab import *
import Numeric as N
import array
import os

thick_width = {\
  'A1':(.87,.89,8.5,8.5), \
  'B9':(0.86,0.89,8.49,8.51),\
  'A8':(0.98,1.04,8.59,8.53),\
  'B1':(0.82,0.82,8.59,8.57),\
  'B3':(0.92,0.96,8.56,8.56),\
  'B11':(0.9,0.86,8.65,8.7),\
  'A11':(0.96,0.89,8.72,8.96),\
  'A4':(1.08,1.14,8.6,8.59),\
  'A7':(1.04,1.09,8.72,8.77),\
  'B5':(0.98,1.04,8.62,8.6),\
  'B8':(0.91,0.96,8.65,8.67),\
  'A9':(0.92,0.95,8.68,8.65),\
  'B7':(0.99,0.95,8.65,8.64),\
  'A5':(1.1,1.16,8.59,8.59),\
  'A6':(1.09,1.14,8.49,8.49),\
  'B2':(0.85,0.89,8.51,8.50),\
  'B6':(0.97,0.98,8.59,8.59),\
  'A2':(0.94,0.97,8.55,8.56),\
  'A3':(1.01,1.06,8.51,8.51),\
  'L5':(1.47,1.4,10.175,10.17)\
  ,'L14':(1.49,1.54,10.15,10.11)\
  ,'S8':(1.23,1.225,10.17,10.01)\
  ,'L17':(1.54,1.51,10.13,10.1)\
  ,'L9':(1.29,1.3,10.1,10.02)\
  ,'S18':(1.14,1.155,10.135,10.15)\
  ,'L20':(1.31,1.31,10.05,10.19)\
```

```
  ,'S13':(1.27,1.21,10.15,10.02)\
  ,'L6':(1.405,1.38,10.13,10.16)\
  ,'S1':(1.16,1.2,10.44,10.12)\
  ,'S3':(1.21,1.26,10.13,10.13)\
  ,'L4':(1.42,1.385,10.15,10.18)\
  ,'S2':(1.23,1.21,10.13,10.14)\
  ,'L12':(1.44,1.45,10.17,10.165)\
  ,'S4':(1.18,1.21,10.05,10.15)\
  ,'S20':(1.24,1.255,10.13,10.04)\
  ,'S14':(1.235,1.14,10.14,10.2)\
  ,'Z1':(1.26,1.25,10.16,10.16)}

keys = thick_width.keys()
keys.sort()
for i in keys:
  line = i[0]+' & '+i[1:]
  for j in range(4):
    line += ' & '+str(thick_width[i][j])
  print line,'\\\\'



gauge_length = 0.05
area = 0.01 * 0.0014
rho_glass = 2600
nlayer = 2
areal_density = 600
ddir = os.getenv("HOME")+"/svn/temp/experiments/data/"
def get_plot_data(instron_strain_switch_correction=False,\
  correct_neg_strain=False,linestress=False):
  files ={ddir+'S1.MRD':['L5','L14','S8','L17','L9','P12'],\
    ddir+'S2.MRD':['S18','L20','S13','L6','S1','S3','L4','S2','P12','P12'],\
    ddir+'S3.MRD':['L12','S4','S20','S14','P14','P1243'], \
    ddir+'S4.MRD':['A1','B9','A8','B1','B3','B11','A11','A4','A7'],\
    ddir+'S5.MRD':['B5','B8','A9','B7','A5','A6','B2','B6','A2','A3'],\
    ddir+'VALIDATE.MRD':['Z1','P12']}
  alldata = {}
  res = {}
  for file in files:
    data = [[]]
    count = 0
    allline = ''
    for line in open(file,'rb'):
```

```
    allline += line
  binvalues = array.array('f')
  binvalues.fromstring(allline)
  starts = []
  # this bit is based on the finding that a
  # set of data is always preceded
  # by exactly 12 zeros, so we check if
  # the number itself is zero, then if
  # the ones around are and around those aren't,
  # then we record where the
  # block is in the starts[] array
  for i in range(len(binvalues)):
    if binvalues[i] ==0.0:
      try:
        if binvalues[i-1] != 0.0 and binvalues[i+12] != 0.0:
          count = 0
          for j in range(12):
            count += (binvalues[i+j]==0.0)
          if count ==12:
            starts.append(i+12)
      except:
        print "out of range"
  x, y = [], []
  nlabel = 0
  for i in range(len(starts)):
    x = [binvalues[j] for j in range(starts[i], \
      max(starts[(i+1)%len(starts)],\
      len(binvalues)),2)]
    y = [binvalues[j+1] for j in range(starts[i],\
      max(starts[(i+1)%len(starts)],\
      len(binvalues)),2)]
    count = 0
    for j in range(len(x)):
      if abs(x[j])>3 or abs(y[j])>1e5:
        count = j
        break
      if (j>10 and x[j]<x[j-1]-0.002):
        count = j
        break
    if count>200: # if a serious number of samples present in the set
      xcor = 0
      xnew = []
```

```
        for j in range(len(x)):
          if j>0:
            if correct_neg_strain:
              # if there is a negative strain jump
              if x[j]<x[j-1]:
                # shift the next strains
                xcor += x[j-1]-x[j]
          xnew.append(x[j]+xcor)
        # insert datasets with origin at [0,0]
        spec =  files[file][nlabel]
        # convert from inches to meters
        x = [j*0.0254/gauge_length for j in xnew]
        if instron_strain_switch_correction:
          for k in range(len(x)):
            if x[k]>0.02:
              x[k] = x[k-1]+(x[300]-x[150])/150
        try:
          width = average(thick_width[spec][2:4])
          thickness =  average(thick_width[spec][0:2])
          if linestress:
            area = width
          else:
            area = width*thickness
          vf = (nlayer*areal_density)/(thickness*rho_glass)
        except:
          area = 1e12
          vf = 0
        y = [j*4.448222/area*1e-3 for j in y]
        dt = ([k-x[0] for k in x[0:count]],\
          [j-y[0] for j in y[0:count]])
        res[files[file][nlabel]+' '+file] = (dt,vf)
        nlabel+=1
    return res
```

Appendix E

Tabulated 2D and 3D stiffness data

E.1 Constituent data

Material data for various fibres and resins. The specimens described in Chapter 5 are made using Vetrotex RT600, consisting of E-glass fibres (see Table E.1). The matrix material was Reichhold Norpol 420-100 resin, used with Akzo-Nobel NL49P 1% cobalt accelerator. The curing process was initiated using Butanox M50 catalyst.

	HTA	T300	E-glass	MTM44-1	polylite
E1 (GPa)	238	231	73	3.3	3.7
E2 (GPa)	28	14.5	73		
nu12 (-)	0.23	0.23	0.22	0.38	0.26
nu23 (-)	0.3	0.3	0.22		
St (GPa)			2		0.07
Sc (GPa)			2		0.07

Table E.1: Constituent property table

E.2 3D stiffness data

3D stiffness data is generated using methodology described in appendix C. Tables are generated to show behaviour of stiffness terms as a function of textile architecture (see Figure E.1), mesh anisotropy (see Table E.5), constituent properties and inter-yarn spacing (see Table E.3 where results for larger spacing are listed).

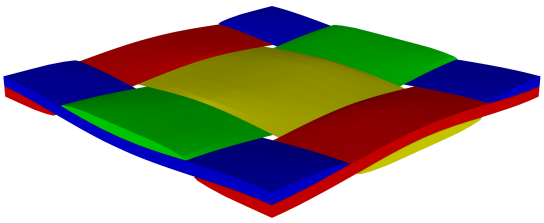

(a) Baseline plain weave, relates to Table E.2

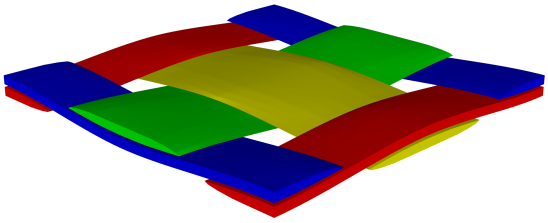

(b) Plain weave with large inter-yarn spacing, relates to Table E.3

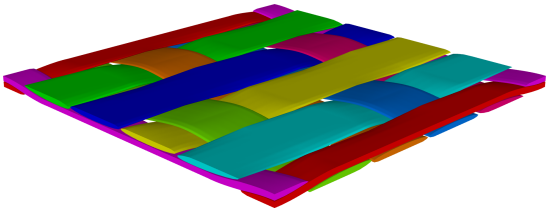

(c) Five harness satin weave, relates to Table E.4

Figure E.1: Textiles used for the generation of 3D stiffness data tables.

fibre	level	mpoints	E33	Vf	E22	E11	G13	nu12	nu13	nn	nu21	nu23	G23	nu32	G12	nu31
HTA.in	1	1	3.447	0	3.697	3.697	2.68	0.2598	0.2601	27	0.2598	0.2601	2.68	0.2425	2.935	0.2425
HTA.in	1	2	14.16	0.7108	91.04	91.04	13.23	0.03333	0.3538	27	0.03333	0.3537	13.23	0.05501	17.26	0.05501
HTA.in	1	3	9.975	0.4214	55.66	55.66	8.898	0.04021	0.3466	27	0.04021	0.3466	8.898	0.06211	11.46	0.06211
HTA.in	1	4	11.6	0.5333	69.32	69.32	10.59	0.03667	0.3504	27	0.03667	0.3504	10.59	0.05862	13.71	0.05862
HTA.in	1	5	10.13	0.4323	56.95	56.95	9.073	0.0397	0.3477	27	0.0397	0.3477	9.073	0.06184	11.67	0.06184
HTA.in	1	6	10.92	0.487	63.65	63.65	9.888	0.03792	0.3492	27	0.03792	0.3492	9.888	0.05993	12.77	0.05993
HTA.in	2	1	15.17	0.7108	88.3	88.13	13.41	0.04947	0.3468	125	0.04956	0.3468	13.32	0.05957	17.27	0.05967
HTA.in	2	2	11.8	0.5333	68.31	68.25	10.18	0.05155	0.3436	125	0.0516	0.3436	10.11	0.05934	13.72	0.05938
HTA.in	2	3	11.08	0.487	62.88	62.83	9.497	0.05133	0.3428	125	0.05137	0.3429	9.437	0.06043	12.77	0.06047
HTA.in	2	4	10.73	0.458	59.41	59.36	9.181	0.05157	0.3425	125	0.05161	0.3426	9.124	0.06188	12.19	0.06192
HTA.in	2	5	10.63	0.4564	59.23	59.19	9.079	0.05159	0.3424	125	0.05163	0.3425	9.023	0.06148	12.16	0.06152
HTA.in	2	6	10.39	0.4477	58.19	58.15	8.828	0.05197	0.3422	125	0.05201	0.3423	8.775	0.06114	11.99	0.06117
HTA.in	3	1	10.56	0.5333	66.66	66.64	8.174	0.06692	0.34	729	0.06695	0.34	8.165	0.05386	13.36	0.05388
HTA.in	3	2	10.1	0.458	58.26	58.24	7.948	0.06404	0.3375	729	0.06406	0.3375	7.939	0.0585	11.61	0.05851
HTA.in	3	3	9.837	0.4477	57.3	57.29	7.737	0.063	0.3379	729	0.06301	0.3379	7.729	0.05802	11.5	0.05802
HTA.in	3	4	9.896	0.4465	57.15	57.14	7.813	0.06322	0.3383	729	0.06323	0.3383	7.804	0.05859	11.47	0.05859
HTA.in	3	5	9.962	0.4463	57.13	57.12	7.894	0.06302	0.3383	729	0.06303	0.3383	7.885	0.059	11.45	0.05901
HTA.in	3	6	9.972	0.4468	57.18	57.17	7.905	0.06288	0.3383	729	0.06289	0.3383	7.897	0.059	11.48	0.05901
HTA.in	4	1	9.425	0.458	56.92	57.08	7.023	0.07064	0.3333	4933	0.07044	0.3328	7.023	0.05511	11.18	0.05503
HTA.in	4	2	9.407	0.4465	56.57	56.72	7.126	0.06938	0.3368	4933	0.06921	0.3364	7.124	0.05593	11.2	0.05587
HTA.in	4	3	9.5	0.4468	56.62	56.76	7.219	0.06911	0.3365	4933	0.06895	0.336	7.217	0.05639	11.18	0.05632
HTA.in	4	4	9.515	0.4483	56.81	56.95	7.23	0.06901	0.3366	4933	0.06884	0.3361	7.229	0.05629	11.22	0.05623
HTA.in	4	5	9.508	0.4482	56.81	56.95	7.227	0.06895	0.3366	4933	0.06878	0.3361	7.226	0.05625	11.22	0.05619
HTA.in	4	6	9.51	0.4479	56.78	56.92	7.228	0.069	0.3365	4933	0.06883	0.3361	7.226	0.0563	11.21	0.05623
HTA.in	5	1	8.856	0.4465	55.97	56.18	6.506	0.07264	0.3358	3.617e4	0.07237	0.3353	6.506	0.05304	11.01	0.05294
HTA.in	5	2	9.119	0.4483	56.54	56.74	6.767	0.07202	0.3361	3.617e4	0.07176	0.3356	6.767	0.05412	11.1	0.05402
HTA.in	5	3	9.136	0.4479	56.52	56.72	6.788	0.07192	0.3361	3.617e4	0.07167	0.3355	6.788	0.05424	11.09	0.05413
HTA.in	5	4	9.137	0.4476	56.49	56.69	6.792	0.07191	0.3361	3.617e4	0.07165	0.3356	6.792	0.05428	11.09	0.05418
HTA.in	5	5	9.149	0.448	56.54	56.74	6.802	0.07187	0.3361	3.617e4	0.07161	0.3356	6.801	0.0543	11.1	0.0542
HTA.in	5	6	9.147	0.4478	56.52	56.72	6.802	0.07187	0.3361	3.617e4	0.07161	0.3356	6.801	0.05431	11.09	0.05421
glass.in	1	1	3.447	0	3.697	3.697	2.68	0.2598	0.2601	27	0.2598	0.2601	2.68	0.2425	2.935	0.2425
glass.in	1	2	17.58	0.7108	35.64	35.64	13.51	0.1192	0.2726	27	0.1192	0.2726	13.51	0.1345	14.8	0.1345
glass.in	1	3	11.9	0.4214	22.7	22.7	9.106	0.1294	0.2737	27	0.1294	0.2737	9.106	0.1435	9.988	0.1435
glass.in	1	4	14.11	0.5333	27.7	27.7	10.82	0.1244	0.2733	27	0.1244	0.2733	10.82	0.1391	11.85	0.1391
glass.in	1	5	12.11	0.4323	23.18	23.18	9.271	0.1287	0.2738	27	0.1287	0.2738	9.271	0.1431	10.16	0.1431
glass.in	1	6	13.19	0.487	25.63	25.63	10.1	0.1261	0.2735	27	0.1261	0.2735	10.1	0.1408	11.07	0.1408
glass.in	2	1	18.79	0.7108	35.51	35.49	14.57	0.1218	0.2716	125	0.1219	0.2716	14.56	0.1437	14.81	0.1438
glass.in	2	2	14.15	0.5333	27.67	27.66	10.84	0.1266	0.2732	125	0.1266	0.2732	10.83	0.1397	11.86	0.1398
glass.in	2	3	13.17	0.487	25.6	25.59	10.07	0.1281	0.2737	125	0.1282	0.2737	10.06	0.1408	11.08	0.1408
glass.in	2	4	12.7	0.458	24.3	24.3	9.716	0.1293	0.2738	125	0.1293	0.2738	9.709	0.1431	10.59	0.1431
glass.in	2	5	12.56	0.4564	24.23	24.23	9.594	0.1294	0.274	125	0.1294	0.274	9.587	0.142	10.57	0.142

fibre	level	mpoints	E33	Vf	E22	E11	G13	nu12	nu13	nn	nu21	nu23	G23	nu32	G12	nu31
glass.in	2	6	12.22	0.4477	23.85	23.84	9.315	0.1298	0.2743	125	0.1299	0.2743	9.308	0.1406	10.43	0.1406
glass.in	3	1	12.08	0.5333	27.44	27.44	8.584	0.1279	0.2726	729	0.1279	0.2726	8.583	0.12	11.56	0.1201
glass.in	3	2	11.61	0.458	24	24	8.386	0.129	0.2709	729	0.129	0.2709	8.385	0.131	10.12	0.131
glass.in	3	3	11.25	0.4477	23.62	23.62	8.139	0.1297	0.2719	729	0.1297	0.2719	8.138	0.1295	10.03	0.1295
glass.in	3	4	11.35	0.4465	23.57	23.57	8.222	0.1297	0.2717	729	0.1297	0.2717	8.221	0.1309	10	0.1309
glass.in	3	5	11.46	0.4463	23.55	23.55	8.318	0.1296	0.2714	729	0.1296	0.2714	8.317	0.1321	9.992	0.1321
glass.in	3	6	11.47	0.4468	23.57	23.57	8.335	0.1296	0.2715	729	0.1296	0.2715	8.334	0.1321	10.01	0.1321
glass.in	4	1	10.52	0.458	23.65	23.68	7.315	0.1288	0.2697	4933	0.1287	0.2695	7.316	0.1198	9.789	0.1198
glass.in	4	2	10.55	0.4465	23.42	23.44	7.441	0.13	0.272	4933	0.1299	0.2718	7.441	0.1224	9.795	0.1224
glass.in	4	3	10.69	0.4468	23.41	23.43	7.551	0.1298	0.2713	4933	0.1296	0.2712	7.55	0.1239	9.779	0.1238
glass.in	4	4	10.71	0.4483	23.48	23.5	7.561	0.1297	0.2714	4933	0.1296	0.2712	7.561	0.1237	9.807	0.1237
glass.in	4	5	10.7	0.4482	23.48	23.5	7.558	0.1297	0.2714	4933	0.1296	0.2713	7.558	0.1236	9.813	0.1236
glass.in	4	6	10.71	0.4479	23.47	23.49	7.558	0.1297	0.2714	4933	0.1296	0.2712	7.558	0.1237	9.802	0.1237
glass.in	5	1	9.662	0.4465	23.26	23.29	6.73	0.1299	0.2736	3.617e4	0.1297	0.2734	6.73	0.1136	9.647	0.1135
glass.in	5	2	10.07	0.4483	23.4	23.44	7.029	0.1298	0.2726	3.617e4	0.1296	0.2724	7.028	0.1172	9.715	0.1171
glass.in	5	3	10.1	0.4479	23.39	23.43	7.054	0.1299	0.2725	3.617e4	0.1297	0.2723	7.053	0.1176	9.713	0.1175
glass.in	5	4	10.11	0.4476	23.38	23.41	7.059	0.1299	0.2725	3.617e4	0.1297	0.2723	7.058	0.1177	9.71	0.1176
glass.in	5	5	10.13	0.448	23.4	23.43	7.07	0.1299	0.2725	3.617e4	0.1297	0.2723	7.069	0.1178	9.717	0.1177
glass.in	5	6	10.12	0.4478	23.39	23.42	7.069	0.1299	0.2725	3.617e4	0.1297	0.2723	7.069	0.1178	9.714	0.1178

Table E.2: Fixed variables:`matrix=polylite.in analysis=mechanical nx=1 ny=1 nz=1 file=vfsingle_0.tg3 matsampling=gauss`

level	mpoints	E33	Vf	E22	E11	G13	nu12	nu13	nn	nu21	nu23	G23	nu32	G12	nu31
3	1	7.763	0.3498	20.22	20.22	5.377	0.1505	0.2691	729	0.1505	0.2691	5.377	0.1033	9.968	0.1033
3	2	9.779	0.3438	19.62	19.62	6.996	0.1461	0.2601	729	0.1461	0.2601	6.996	0.1297	9.45	0.1297
3	3	9.684	0.3439	19.69	19.69	6.947	0.1467	0.2611	729	0.1467	0.2611	6.946	0.1284	9.592	0.1284
3	4	9.694	0.338	19.39	19.39	6.977	0.1468	0.2609	729	0.1468	0.2609	6.976	0.1304	9.442	0.1304
3	5	9.656	0.3376	19.37	19.37	6.944	0.1468	0.2608	729	0.1468	0.2608	6.943	0.13	9.433	0.13
3	6	9.613	0.3361	19.32	19.32	6.919	0.1471	0.2611	729	0.1471	0.2611	6.918	0.1299	9.426	0.1299
4	1	7.957	0.3438	19.08	19.08	5.561	0.1451	0.2662	4913	0.1451	0.2662	5.561	0.111	8.981	0.111
4	2	8.365	0.338	19.07	19.07	5.9	0.1462	0.265	4913	0.1462	0.265	5.9	0.1162	9.109	0.1162
4	3	8.376	0.3361	19.02	19.02	5.913	0.1464	0.265	4913	0.1464	0.265	5.913	0.1167	9.105	0.1167
4	4	8.435	0.3366	19.02	19.02	5.953	0.1463	0.2645	4913	0.1463	0.2645	5.953	0.1173	9.09	0.1173
4	5	8.454	0.3377	19.08	19.08	5.968	0.1463	0.2645	4913	0.1463	0.2645	5.968	0.1172	9.126	0.1172
4	6	8.45	0.3373	19.07	19.07	5.966	0.1463	0.2646	4913	0.1463	0.2646	5.966	0.1172	9.123	0.1172
5	1	7.336	0.338	18.81	18.82	5.113	0.1465	0.2719	3.6e4	0.1464	0.2719	5.112	0.106	8.982	0.106
5	2	7.628	0.3366	18.86	18.87	5.337	0.1467	0.27	3.6e4	0.1467	0.27	5.337	0.1092	9.001	0.1091
5	3	7.672	0.3373	18.92	18.92	5.371	0.1467	0.2698	3.6e4	0.1467	0.2698	5.371	0.1094	9.035	0.1094
5	4	7.693	0.3374	18.93	18.93	5.386	0.1467	0.2697	3.6e4	0.1466	0.2696	5.385	0.1096	9.037	0.1096
5	5	7.696	0.3373	18.92	18.93	5.388	0.1467	0.2696	3.6e4	0.1466	0.2696	5.388	0.1097	9.036	0.1096
5	6	7.699	0.3374	18.93	18.94	5.391	0.1467	0.2696	3.6e4	0.1466	0.2696	5.39	0.1096	9.041	0.1096

Table E.3: Fixed variables:`fibre=glass.in matrix=polylite.in analysis=mechanical nx=1 ny=1 nz=1 file=vfsingle_vg_0.tg3 matsampling=gauss`

level	mpoints	E33	Vf	E22	E11	G13	nu12	nu13	nn	nu21	nu23	G23	nu32	G12	nu31
2	1	12.88	0.5741	68.83	68.84	9.033	0.05379	0.4113	405	0.05379	0.4113	9.034	0.07695	11.54	0.07695
2	2	12.77	0.545	68.83	68.83	9.551	0.05016	0.424	405	0.05017	0.424	9.536	0.07865	11.69	0.07865
2	3	12.51	0.5262	66.74	66.74	9.33	0.0505	0.4264	405	0.0505	0.4264	9.319	0.07993	11.37	0.07993
2	4	12.07	0.4963	63.17	63.18	8.941	0.05154	0.4314	405	0.05154	0.4314	8.932	0.0824	10.86	0.08238
2	5	12.13	0.5011	63.74	63.75	9.016	0.0512	0.4313	405	0.05119	0.4313	9.006	0.08211	10.95	0.08209
2	6	12.14	0.5015	63.82	63.83	9.025	0.05125	0.4309	405	0.05124	0.4309	9.015	0.082	10.97	0.08199
3	1	12.25	0.545	66.69	66.69	8.342	0.06056	0.4236	2601	0.06056	0.4236	8.339	0.07781	11.09	0.07781
3	2	11.69	0.4963	62.09	62.09	8.081	0.06088	0.4319	2601	0.06088	0.4318	8.079	0.08131	10.54	0.08131
3	3	11.82	0.5015	62.87	62.87	8.248	0.06025	0.4308	2601	0.06026	0.4308	8.245	0.08099	10.67	0.08099
3	4	11.97	0.51	63.94	63.93	8.4	0.05982	0.4293	2601	0.05982	0.4293	8.397	0.08038	10.81	0.08038
3	5	12.06	0.517	64.8	64.8	8.488	0.05927	0.4288	2601	0.05928	0.4288	8.485	0.07982	10.96	0.07982
3	6	11.91	0.5066	63.53	63.53	8.353	0.05983	0.43	2601	0.05983	0.43	8.351	0.08065	10.77	0.08065
4	1	10.8	0.4963	60.85	60.85	6.414	0.06567	0.4418	1.851e4	0.06567	0.4418	6.414	0.07839	10.13	0.07839
4	2	11.47	0.51	63.35	63.35	7.442	0.06411	0.4341	1.851e4	0.06411	0.4341	7.442	0.07863	10.58	0.07863
4	3	11.41	0.5066	62.97	62.97	7.39	0.0641	0.4351	1.851e4	0.0641	0.435	7.39	0.07882	10.54	0.07882
4	4	11.48	0.5092	63.33	63.33	7.468	0.06384	0.4343	1.851e4	0.06384	0.4343	7.468	0.0787	10.59	0.0787
4	5	11.44	0.507	63.06	63.06	7.434	0.064	0.4347	1.851e4	0.064	0.4347	7.434	0.07885	10.55	0.07885
4	6	11.48	0.509	63.31	63.31	7.474	0.06382	0.4343	1.851e4	0.06382	0.4343	7.473	0.07873	10.59	0.07873

Table E.4: Fixed variables:`fibre=HTA.in matrix=MTM44-1.in analysis=mechanical nx=2 ny=2 nz=1 file=five_harness4_0.tg3 matsampling=gauss`

level	mpoints	E33	Vf	E22	E11	G13	nu12	nu13	nn	nu21	nu23	G23	nu32	G12	nu31
1	1	18.83	0.7109	35.49	35.53	14.61	0.1217	0.2716	135	0.1216	0.2715	14.58	0.1441	14.81	0.144
1	2	13.65	0.4664	24.05	25.15	10.57	0.1316	0.272	135	0.1259	0.2732	10.51	0.155	10.65	0.1476
1	3	13.24	0.4473	23.7	23.45	10.24	0.1278	0.2735	135	0.1291	0.2679	9.985	0.1496	10.09	0.1544
1	4	13.2	0.4454	23.54	23.64	10.22	0.1293	0.2732	135	0.1287	0.2703	10.04	0.1516	10.15	0.1526
1	5	13.35	0.452	23.88	23.97	10.33	0.1293	0.273	135	0.1287	0.2712	10.2	0.1516	10.31	0.152
1	6	13.32	0.4504	23.74	23.91	10.31	0.1294	0.273	135	0.1284	0.2705	10.14	0.1517	10.25	0.1521
2	1	11.18	0.4664	22.47	24.16	7.867	0.1353	0.2627	765	0.1259	0.2657	7.519	0.1322	10.16	0.1216
2	2	12.11	0.4454	23.26	23.42	8.916	0.1285	0.2701	765	0.1276	0.2654	8.555	0.1382	9.729	0.1397
2	3	12.11	0.4504	23.59	23.72	8.9	0.1289	0.2702	765	0.1282	0.2676	8.633	0.1373	9.91	0.1379
2	4	12.14	0.4505	23.64	23.73	8.933	0.1289	0.2701	765	0.1284	0.2684	8.706	0.1379	9.947	0.1382
2	5	12.09	0.4471	23.53	23.57	8.911	0.1291	0.2704	765	0.1289	0.2686	8.688	0.138	9.915	0.1387
2	6	12.09	0.4467	23.5	23.56	8.916	0.1293	0.2703	765	0.129	0.2687	8.695	0.1382	9.91	0.1387
3	1	10.42	0.4454	22.43	22.97	7.264	0.1289	0.2693	5049	0.1258	0.2637	7.045	0.1226	9.312	0.1222
3	2	10.92	0.4505	23.52	23.61	7.684	0.1293	0.2705	5049	0.1288	0.2698	7.605	0.1253	9.779	0.1251
3	3	10.96	0.4467	23.41	23.44	7.761	0.1297	0.2708	5049	0.1296	0.2701	7.67	0.1264	9.751	0.1266
3	4	10.97	0.4469	23.43	23.44	7.761	0.1296	0.2707	5049	0.1296	0.27	7.677	0.1264	9.755	0.1267
3	5	11	0.4481	23.48	23.49	7.782	0.1295	0.2706	5049	0.1294	0.2699	7.698	0.1265	9.769	0.1267
3	6	11.01	0.4482	23.49	23.5	7.794	0.1294	0.2706	5049	0.1294	0.2699	7.707	0.1265	9.771	0.1269
4	1	9.888	0.4505	23.26	23.39	6.856	0.1295	0.2718	3.646e4	0.1288	0.2719	6.836	0.1156	9.656	0.1149
4	2	10.21	0.4469	23.37	23.38	7.127	0.1299	0.2722	3.646e4	0.1298	0.2718	7.091	0.1188	9.696	0.1189
4	3	10.29	0.4482	23.44	23.44	7.179	0.1297	0.2719	3.646e4	0.1297	0.2716	7.141	0.1193	9.712	0.1194
4	4	10.3	0.4479	23.43	23.43	7.185	0.1297	0.2719	3.646e4	0.1297	0.2716	7.146	0.1194	9.707	0.1195
4	5	10.3	0.4477	23.42	23.42	7.187	0.1297	0.2719	3.646e4	0.1297	0.2716	7.149	0.1194	9.708	0.1196
4	6	10.31	0.4479	23.43	23.43	7.191	0.1297	0.2719	3.646e4	0.1297	0.2716	7.153	0.1195	9.709	0.1196

Table E.5: Fixed variables:`fibre=glass.in matrix=polylite.in analysis=mechanical nx=2 ny=4 nz=1 file=vfsingle_0.tg3 matsampling=gauss`